

LIBRARY Michigan State University



RETURNING MATERIALS:
Place in book drop to
remove this checkout from
your record. FINES will
be charged if book is
returned after the date
stamped below.

NOV 2 8 2007

SURFACE SUBSTRATE EFFECTS ON KINETICS AND MECHANISMS

OF ELECTRODE REACTIONS

Ву

Hsue-Yang Liu

A DISSERTATION

Submitted to

Michigan State University
in partial fulfillment of the requirements

for the degree of

DOCTOR OF PHILOSOPHY

Department of Chemistry

ABSTRACT

SURFACE SUBSTRATE EFFECTS ON KINETICS AND MECHANISMS OF ELECTRODE REACTIONS

Ву

Hsue-Yang Liu

The double layer structure at the polycrystalline lead-aqueous interface has been studied by measuring the differential capacitance. The mixed electrolyte method was employed to study the specific adsorption of anions at the lead-aqueous interface from the measurement of the differential capacitance. The Hurwitz-Parsons analysis and other relative methods were employed to calculate the surface concentrations of the specifically adsorbed anions. Furthermore, the Frumkin isotherm was utilized to evaluate the free energy of specific adsorption and the interaction parameter g. The effect of the electrode pretreatment on the adsorbabilities of anions at the polycrystalline lead was also examined.

The kinetics of a number of mechanistically simple transitionmetal complexes have been examined at gallium, polycrystalline lead,
and mercury surfaces in order to explore the dependence of electrode
kinetics on the nature of the electrode material. Surprisingly, there
were significant differences in the rate constants corrected for the
ionic double layer effect between these surfaces. This indicated

the presence of "specific substrate" effects on electrode reactions.

The enthalpies and entropies of activation for the electroreduction of a number of Cr(III) complexes and Eu(III) at the lead-aqueous interface have been determined with a nonisothermal cell arrangement. The resulting small or even negative values of double layer corrected activation entropies at the lead surface suggest the occurrence of nonadiabatic electron-transfer processes. On the same grounds, the Marcus theory has been shown not to be adequate in the present case.

A series of cobalt porphyrins were employed to examine the electrocatalysis of oxygen reduction at pyrolytic graphite surfaces. A rotating ring-disc electrode was extensively used to evaluate the reaction pathway and subsequent reaction mechanisms of oxygen reduction at porphyrin-modified graphite surfaces. The "bulk" and "surface" redox properties of the Co(III/II) couple of the cobalt porphyrins were also examined by using cyclic voltammetry. Unlike monomeric porphyrins, the dicobalt cofacial porphyrin linked by four-atom bridge showed a remarkable enhancement of the electrocatalysis of the four-electron reduction of dioxygen to water.

EDUCATIONAL GENEALOGY

- M. J. Weaver
 - D. Inman
- J. O. Bockris
- H. J. T. Ellingham
 - A. J. Allmand
 - W. H. Nernst
 - W. Ostwald
 - C. Schmidt
 - J. Lirbig
 - J. L. Gay-Lussac
 - C. L. Berthollett

- C. G. Enke
- H. Laitinen
- I. Kolthoff
- N. Schoorl
- C. L. DeBruyn
- A. Franchimont
 - A. Wurtz
 - J. Dumas
 - L. Thenard
 - L. Vauquelin
- A. F. de Fourcroy

Jean Bucquet

A. Lavoisier

To My Parents

ACKNOWLEDGEMENTS

The author wishes to express his sincere appreciation to Professor M. J. Weaver for his inspiration, guidance, patience, and support during the course of this investigation and the preparation of this thesis.

Helpfull suggestions by Professor C. G. Enke are deeply appreciated.

The appreciation is also extended to Dr. D. Larkin for providing several essentially valuable suggestions.

He is also grateful to Ed. Schindler, Jane Farmer, and Joe Hupp for their suggestions and friendship which were invaluable to the completion of this degree.

Special thanks are given to his wife Huifen for her understanding and encouragement.

Above all, he would like to thank his family for their faith and encouragement which made all of this possible.

TABLE OF CONTENTS

Chapter		Page
LIST OF	TABLES	ix
LIST OF	FIGURES	хi
PART I		
CHAPTER	I. INTRODUCTION	1
CHAPTER	II. BACKGROUND	5
1.	Thermodynamics and Kinetics of Electrode Reactions	6
2.	The Structure of the Electrical Double Layer	10
3.	Theoretical Treatment of Heterogeneous Electron-Transfer Reactions	19
4.	Double Layer Effect on Electrode Kinetics	27
5.	Activation Parameters of Electrode Kinetics	31
CHAPTER	III. EXPERIMENTAL	37
1.	General Apparatus	38
2.	Reagents	39
3.	Electrochemical Techniques	41
	a. Cyclic Voltammetry	41
	b. DC and Pulse Polarography	45
	c. Rotating-Disk Voltammetry	45
	d. Capacitance Measurements	46
	i. AC Bridge	46
	ii. "Phase-Detection" Technique	46

Chap	ter																							Page
	4.	Elec	trode	e F	ret	rea	t me	ent			•	•				•	•	•	•	•	•	•		47
CHAF	PTER	IV.	DOU!												_					•	•	•		49
	1.	Intr	oduc	tio	n.			•							•	•			•	•	•	•	•	50
	2.		acter ace				-					-	_	•	•	•			•	•		•	•	51
	3.	Resu	ılts				•	•		•		• •		•	•	•	•	•	•			•		54
			Capac spec												es	•	•	•	•	•		•	•	54
			Time Capa		•											•	•	•					•	57
			Spec [.] Capa													•	•	•		•	•	•	•	62
			i.						ptio								•	•	•	•		•	•	62
			ii.	_					ptio									•	•		•	•	•	76
			iii.						f ti														•	76
			iv.	S	pec rom	ifi ide	c /	Ads Azi	orp de,	tio an	n	of Chl	Th	io	cy le.	ana •	a te	· •					•	84
	4.	Disc	ussi	on.	•		•	•						•		•		•			•		•	84
CHAP	TER		ELECT GALLT														•	•	•	•	•	•	•	96
Α.			stant on-M														•	•	•		•	•	•	97
	1.	Intr	oduct	tio	n.		•	•		•				•	•	•								97
	2.	Resu	ılts .				•										•				•			99
		a.	The I	Pre	tre	a tn	ent	t D	epei	nde	nc	е.		•	•	•			•		•	•		99
			The / Elect and / Inter	tro Amn	n E ine	lec Co	tro	ore lex	duci es a	tio at	n th	of e l	Cr ea.	(I d-	II Aq) ue	Aqι							102

Chap	oter			Page
		c.	Double Layer Corrected Rate Constants	105
		d.	Rate Constants of Some Cr(III) Complexes Measured at a Hanging Gallium Drop	112
			Electrode	112
	3.	Dis	cussion	113
		a.	Surface Contaminants	113
		b.	Reaction Mechanism	119
		с.	The Dependence of Outer-Sphere Electrode Kinetics on the Electrode Material	121
В.	Eva	luat	ion of Activation Parameters	124
	1.	Resi	ults	124
	2.	Disc	cussion	131
PAR	T II			
CHAI	PTER	VI.	ELECTROCATALYSIS OF OXYGEN REDUCTION	138
	1.	Int	roduction	139
	2.	Exp	erimental	148
		a.	Materials	148
		b.	Rotating Ring-Disc Electrode (RRDE)	149
		c.	Instrumentation	150
		d.	Porphyrin-Modified Graphite Surfaces	155
	3.	Res	ults	156
		a.	Characterization of the PG/Pt RRDE	156
		b.	Oxygen Reduction at the "Blank" Pyrolytic Graphite Surface	164
		c.	Redox Properties of the Cobalt Porphyrins	164
		d.	Oxygen Reduction at the Porphyrin- Modified Graphite Surfaces	177
	4.	Dis	cussion	189
		a.	An Attempt to Assign the Surface Redox Waves of the Attached Cobalt Porphyrins	189

Chapter	P	age
	b. Electrocatalysis of Oxygen Reduction at the Monomeric Porphyrin-Modified Surfaces	191
	c. Electrocatalysis of Oxygen Reduction at the Dimeric Porphyrin-Modified Surface	193
CHAPTER	VII. CONCLUSION AND SUGGESTIONS FOR FUTURE WORK	201
1.	Conclusion	202
2.	Suggestions for Future Work	204
REFERENC	CES	207

LIST OF TABLES

	Page
Standard Free Energy of Adsorption ΔG_a^o	
for Several Anions at Lead, Mercury, and	
Silver Electrodes	85
The Pretreatment Dependence of the Measured	
Rate Constants at Lead Electrodes for a	
Number of Transition-Metal Complexes	100
Summary of Rate Constants for the Electro-	
reduction of Several Transition-Metal Com-	
plexes at Lead and Mercury Electrodes	106
Rate Constants for the Electroreduction of	
Some Cr(III) Complexes Measured at Lead	
and Mercury Electrodes in 0.5 M NaClO ₄	
and 40 mM La(C10 ₄) ₃	110
Rate Constants for the Electroreduction of	
a Number of Cr(III) Complexes Measured at	
Mercury, Gallium, and Lead Electrodes	114
Activation Parameters for the Electrore-	
duction of Various Trivalent Metal Complexes	
at Mercury- and Lead-Aqueous Interfaces	125
	for Several Anions at Lead, Mercury, and Silver Electrodes

Table		Page
6.1	"Bulk" and "Surface" Redox Potentials for	
	the $Co^{2+/3+}$ Couple of Cobalt Porphyrins	169
6.2	Kinetics Parameters for Oxygen Reduction at	
	Porphyrin-Modified Surfaces	187

LIST OF FIGURES

Figure		Page
2.1	The electrode-solution interfacial struc-	
	ture including the specifically adsorbed	
	anions	. 13
2.2	Equivalent electric circuit of polycrystalline	
	electrode models: (a) Model I; (b) Model II	. 16
2.3	Proposed reaction sites for Cr(III) aquo	
	and ammine complexes at the electrode-aqueous	
	interface	. 22
2.4	Free energy profile for simple electro-	
	chemical reaction	. 29
3.1	Schematic diagram of an electrochemical	
	cell	43
3.2	Single amplifier potentiostat	43
4.1	Typical cyclic voltammogram for polycrystal-	
	line lead electrode (prepared by method D)	
	at 0.1 V sec^{-1} in 0.5 M $NaC10_4$	53
4.2	Differential capacitance vs. electrode po-	
	tential for polycrystalline lead in the	
	following conditions: (a)method (A) in	
	10 mM KF at 210 Hz extracted from Ref 64:	

Figure		Page
	(b)method (D) in 10 mM NaF at 200 Hz;	
	(▽) method (D) in 10 mM NaF at 50 Hz;	
	(Δ) method (D) in 10 mM NaF at 10 Hz; $^{\prime}\Delta$;	
	method (D) in 0.2 M NaF at 200 Hz; (●)	
	method (D) in 0.2 M NaF at 1000 Hz	56
4.3	Differential capacitance at 1000 Hz vs.	
	electrode potential for polycrystalline	
	lead prepared by method (D) in the various	
	concentrations of NaClO ₄ : (x) 10 mM, (o)	
	50 mM, (△) 0.5 M, (♦) 1.0 M, (▽) 5.0 M	59
4.4	Time dependence of the differential capaci-	
	tance at 1000 Hz for polycrystalline lead	
	in 0.1 M NaClO ₄	61
4.5	Differential capacitance at 200 Hz vs. elec-	
	trode potential for polycrystalline lead	
	prepared by method (D) in mixed NaF/NaI	
	electrolytes at an ionic strength of 0.2.	
	Key to iodide concentrations: (x) 0; (o)	
	2 mM; (△) 4 mM; (♦) 10 mM; (▽) 25 mM	64
4.6	The concentration of specifically adsorbed	
	iodide plotted against electrode charge for	
	polycrystalline lead prepared by method (D)	
	in mixed NaF/NaI electrolytes at an ionic	
	strength of 0.2 (at 200 Hz). Key to iodide	
	concentration: (a) 1 mM: (\wedge) 10 mM: (\Diamond)	

69

25 mM; (▽) 63 mM. .

Figure		Page
4.7	Differential capacitance at 210 Hz vs.	
	electrode potential for polycrystalline lead	
	prepared by method (A) in mixed KF/KI elec-	
	trolytes at an ionic strength of 0.2. Key	
	to iodide concentrations: (x) 0; (o) 1 mM;	
	(\triangle) 4 mM; (∇) 10 mM; (\square) 25 mM; (\diamondsuit) 70 mM.	
	This figure was extracted from Reference	
	78	. 71
4.8	The concentration of specifically adsorbed	
	anions (bulk anion concentration 10 mM)	
	plotted against electrode charge for poly-	
	crystalline lead in fluoride electrolytes	
	unless otherwise noted in the following	
	conditions: (a)method (A) for iodide at	
	210 Hz obtained by analyzing the corresponding	
	capacitance curves in Ref. 78; (b)method	
	(B) for iodide at 1000 Hz; (c)method (D)	
	for iodide at 200 Hz; (d)method (D) for	
	iodide at 1000 Hz; (e)method (D) for iodide	
	(in perchlorate electrolytes) at 1000 Hz;	

method (D) for thiocyanate at 1000 Hz

73

(x) method (D) for chloride at 1000 Hz;

(o) method (D) for azide at 1000 Hz; (∇)

method (D) for bromide at 1000 Hz; (Δ)

Figure		Page
4.9	Differential capacitance at 1000 Hz vs.	
	electrode potential for polycrystalline lead	
	prepared by method (D) in mixed NaF/NaI	
	electrolytes at an ionic strength of 0.2.	
	Key to iodide concentrations: (x) 0;	
	(o) 1 mM; (△) 10 mM; (♦) 25 mM; (▽) 65 mM	. 75
4.10	Differential capacitance at 1000 Hz vs.	
	electrode potential for polycrystalline lead	
	prepared by method (B) in mixed NaF/NaI	
	electrolytes at an ionic strength of 0.2.	
	Key to iodide concentrations: (x) 0; (o)	
	1 mM; (Δ) 10 mM; (♦) 25 mM; (∇) 65 mM	. 78
4.11	Differential capacitance at 1000 Hz vs.	
	electrode potential for polycrystalline lead	
	prepared by method (D) in mixed NaClO ₄ /NaI	
	electrolytes at an ionic strength of 0.5.	
	Key to iodide concentrations: (x) 0; (o)	
	1 mM; (Δ) 10 mM; (♦) 25 mM; (∇) 65 mM	. 80
4.12	$\ln(\frac{C_b(1-\theta)}{\theta})$ vs. θ for specific adsorption of	
	iodide for polycrystalline lead prepared by	
	method (D) at 200 Hz in mixed NaF/NaI	
	electrolytes at an ionic strength of 0.2.	
	Key to various electrode charges (o) 1.0;	
	(x) 0.0; (Δ) -1.0 μC/cm ²	. 83

Figure		Page
4.13	Differential capacitance at 1000 Hz vs.	
	electrode potential for polycrystalline lead	
	prepared by method (D) in (o) 0.5 NaF and	
	(x) 0.5 Na C10 ₄	. 91
5.1	Log k _{app} , where k _{app} is the measured rate	
	constant, vs. electrode potential at mercury	
	(closed symbols) and polycrystalline lead	
	prepared by method (D) (open symbols) in	
	0.5 M NaClO ₄ except for Cr(NH ₃) ₅ NCS ²⁺	
	in 40 mM La(C10 ₄) ₃ for a number of transition-	
	metal complexes as follows: (o) $Cr(OH_2)_6^{3+}$; (∇)	
	$Cr(NH_3)_6^{3+}$; (Δ) $Cr(NH_3)_5C1^{2+}$; (\Box) $Cr(OH_2)_5SCN^{2+}$;	٠
	(\$) Cr(OH ₂) ₅ C1 ²⁺ ; (\$\rightarrow\$) Cr(NH ₃) ₅ NCS ²⁺ ; (\$\rightarrow\$)	
	$Cr(NH_3)_5OH_2^{3+}; (D) Cr(OH_2)_5N_3^{2+}; (d) Cr(NH_3)_5N_3^{2+};$	
	(x) $Cr(OH_2)_5F^{2+}$; (+) $Cr(OH_2)_5OSO_3^{1+}$. 104
5.2	Differential electrode capacitance C against	
	electrode potential E for (a) polycrystalline	
	silver. (b) silver containing a monolayer	
	of upd lead. (c) as in (b) but with addi-	
	tional ca. two monolayers of bulk lead deposit.	
	(d) polycrystalline lead. Lead layer prepared	
	as indicated in Ref. 108. Electrolyte was 0.5	
	M NaClO $_4$, pH 3.5; for (b) and (c) additionally	
	contained 0.6 uM Pb ⁺²	. 117

Figure		Page
5.3	Differential capacitance at 1000 Hz vs.	
	electrode potential for polycrystalline lead	
	prepared by method (D) in 0.5 M NaClO ₄ at	
	various temperatures: (x) 5.5°C; (o) 16.5°C;	
	(♦) 25.5°C; (▽) 36.2°C	 129
6.1	Structures of cobalt porphyrins	 143
6.2	Diagram of a Rotating Ring-Disc Electrode	
	(RRDE)	 147
6.3	Schematic diagram for the connection of	
	the "modified" bipotentiostat	 152
6.4	Schematic diagram for the operation of	
	the "modified" bipotentiostat	 154
6.5	RRDE voltammogram for $Fe(CN)_6^{-3/-4}$ couple	
	at the PG/Pt electrode. The potential of	
	the Pt ring was held at 0.7 V vs. SCE. The	
	scan rate of the cyclic voltammogram was	
	0.1 V sec ⁻¹	 158
6.6	Plot of the limiting disk current i_{ℓ} vs.	
	the square root of rotation rate $(\omega^{1/2})$ for	
	the reduction of $Fe(CN)_6^{3-}$ (1.4 mM) on the	
	PG/Pt electrode	 161
6.7	Cyclic voltammogram at the "blank" graphite	
	electrode of the RRDE at 0.1 V/sec in 0.5 M	
	HTFA	 163

Figure		Page
6.8	Cyclic voltammograms for the reduction of	
	oxygen in 0.5 M HTFA at 0.1 V/sec on (a)	
	the "blank" graphite disk electrode; (b) the	
	platinum ring electrode; (c) the monomeric	
	porphyrin-modified surface; (d) the dimeric	
	porphyrin-modified surface	166
6.9	Cyclic voltammogram for the "bulk" redox	
	reaction of $Co^{3+/2+}$ of Co-Co-4 on the graphite	
	disk electrode in 0.1 M TBAP dichloromethane	
	at 0.2 V/sec	168
6.10-6.13	Cyclic voltammograms for the "surface" re-	
	dox reactions of $Co^{3+/2+}$ (?) at the PG disk	
	electrode in 0.5 M HTFA aqueous solution de-	
	aerated with nitrogen at 0.2 V/sec. The por-	
	phyrins under consideration are indicated in	
	the corresponding figures	-176
6.14-6.20	Disc (upper-i _D) and ring (lower-i _R) currents	
	for the reduction of oxygen in 0.5 M HTFA	
	on the PG/Pt electrode (ω = 600 rpm). Scan	
	rate for the corresponding cyclic voltammogram	
	for oxygen reduction at the PG disk electrode	
	is at 0.1 V/sec except Figure 6.19 at 0.2	
	V/sec	-186
6.21	Proposed mechanism for four-electron reduction	
	of oxygen molecule at the dimeric porphyrin-	
	modified graphite surface	196

Figure		Page
6.22	Proposed configuration for Co-O-O-Co	
	complexes	 199

CHAPTER I

INTRODUCTION

The investigation of homogeneous electron-transfer reactions l-ll in terms of experimental measurements as well as theoretical interpretation has long been an interesting subject and has successfully progressed to a certain extent. There are many ways with which the kinetics of electron-transfer reactions can be affected, such as Coulombic interactions, solvent reorganization energy, frequency factors, and electron and nuclear tunneling. Thus in order to investigate the elementary electron-transfer processes, it is desirable to choose suitable chemical systems with which individual factors that control electrochemical reactivity can hopefully be separated. Such tactics have been extensively undertaken in the study of homogeneous reactions. 6,10,11

Solid electrodes have successfully shown their usefulness in industrial practical applications, such as in the areas of batteries, fuel cells, or electrocatalysts. Thus, in order to improve their potentiality for the practical applications, it is essential to understand their fundamental properties, such as the electrodesolution interfacial structure and the thermodynamics and kinetics of electrode reactions.

Although similar kinetic concepts apply to both homogeneous and heterogeneous redox reactions, the measurement and interpretation of heterogeneous electron-transfer reaction kinetics are still very scarce and incomplete. The application of electrochemical methods to the study of the energetics of electron-transfer reactions offers several advantages over the study of homogeneous processes.

In homogeneous reactions, both of the reactants have to be activated to reach the appropriate configuration 12,13 in order to allow electron-transfer to occur. With electrochemical reactions, however, only one reactant is required to be activated; the energy of the electrons within the electrode can be conveniently altered by an external source, the applied electrode potential. Therefore, the driving force for electrode reactions can be obtained by simply altering the applied electrode potential (i.e., overpotential). In contrast, the thermodynamics of homogeneous reactions can only be altered by changing the temperature or pressure.

A fundamental question in electrochemical kinetics concerns the various ways in which the chemical nature of the electrode material may influence the energetics of electron-transfer reactions. This has been carefully examined at several solid electrodes 14 (Au, Ag, and Pt) and liquid mercury electrodes for a number of mechanistically simple transition-metal complexes. In this work, the polycrystalline lead electrode was chosen for study, mainly because it possesses a fairly negative polarizable potential region compared with Au, Ag, or Pt. Therefore, the interference of the adsorption of anions on the study of electrode kinetics is insignificant compared with other well-studied solid electrodes. In addition, polycrystalline lead or lead oxide are the most common electrode materials being used in battery technology. Gallium is another common liquid metal other than mercury whose electrode-solution interfacial structure has been well studied and is shown to be markedly different from that at mercury. Therefore, it is interesting as well as important to compare electrode kinetics at gallium and mercury surfaces.

First of all, it is obvious that the ionic double-layer structure at the electrode-solution interface will be dependent on the chemical nature of the electrode material. Thus, it is important to understand the fundamental properties of this double-layer structure at which electrochemical reactions occur. Valuable information of this type can be obtained from the measurements of differential capacitance. In this work, the measurement of the differential double-layer capacitance was performed at the lead-aqueous interface in order to evaluate the effect of the ionic double-layer on the corresponding kinetics of electrode reactions.

It has been shown that the ionic double-layer effect can account for the observed difference in the electroactivity between different electrode-solution interfaces. However, the comparison of electrode kinetics at polycrystalline lead, gallium, and mercury electrodes in this study indicates that the ionic double-layer effect cannot entirely explain the difference in the electroactivities.

Contrary to homogeneous reactions, temperature is not usually employed as a variable for heterogeneous reactions. The experimental accessibility of electrochemical activation parameters from the measurements of the dependence of temperature upon the rate constants has been questioned. 15,16 Nevertheless, it has been shown 17 that the so-called "ideal" activation parameters determined at a constant Galvani potential can be obtained by utilizing a non-isothermal cell that is described in Chapter II. The evaluation of such activation parameters provides a means to examine enthalpic and entropic contributions to the energetics of heterogeneous electron transfer.

CHAPTER II

BACKGROUND

The main purpose of this work is to examine to what extent the nature of the electrode material will affect electrode kinetics. It is essential to understand the thermodynamics of electrode interfaces in order to properly interpret the corresponding electrode kinetics. As mentioned in Chapter I, the electrode-solution interfacial structure is expected to be different from one electrode to another. It is useful to understand some fundamental concepts of the double-layer theory in order to characterize the electrodesolution interfacial. At the same time, the measurement of specific adsorption of anions provides a means to investigate the intrinsic property of the interfacial structure. Then, the theoretical treatment of the elementary electron-transfer processes will be discussed. Since the ionic double-layer structure greatly depends on the chemical composition of the electrode, in order to compare electrode kinetics at different electrode surfaces, it is necessary to consider the corresponding ionic double-layer effect. Furthermore, the evaluation of activation enthalpy and entropy can provide insight into the properties of the transition state for the elementary electron-transfer reactions.

1. Thermodynamics and Kinetics of Electrode Reactions

A simple electrode reaction can be expressed as

$$0x + ne^{-}$$
 (electrode, ϕ_m) $\stackrel{?}{\sim}$ Red (2.1)

where 0x and Red are the oxidized and reduced species of a redox couple, n is the number of electrons involved, and ϕ_m is the absolute potential difference (Galvani potential) between the electrode and solution. The thermodynamics of the redox couple can be described in terms of the overall electrochemical free energy of reaction $\Delta \overline{G}^\circ$ expressed as

$$\Delta \overline{G}^{\circ} = \Delta G^{\circ} - nF_{\phi_{m}}$$
 (2.2)

where ΔG° and nF_{φ_m} are the chemical and electrical components of $\Delta \overline{G}^{\circ}$ respectively. Generally, the chemical reaction rates can be altered by the applied electrical driving force nF_{φ_m} . The Galvani potential is experimentally inaccessible. However, by the use of a reference electrode which has a stable potential, the so-called electrode potential E, which is equal to the sum of the Galvani potential at the two electrode-solution interfaces, can be experimentally evaluated.

The standard electrode potential E° is the fundamental thermodynamic parameter of a redox couple. It is the equilibrium value of E when both 0x and Red are in their standard states (i.e., their activities equal to one). However, the formal potential E^{f} is more frequently used, which is evaluated for equal concentration of 0x and Red instead of equal activity.

Since at the standard state $\Delta \overline{G}^{\circ} = 0$, then $\Delta \overline{G}^{\circ}$ for the reactions (2.1) at a given electrode potential E can be formulated as

$$\Delta \overline{G}^{\circ} = nF(\phi_{m} - \phi_{m}^{\circ})$$

$$= nF(E - E^{\circ}) \qquad (2.3)$$

where ϕ_m° corresponds to E°. Therefore, the overall driving force $\Delta \overline{G}^\circ$ of an electrochemical redox couple reaction can be evaluated from the measurement of (E - E°), even the individual values of ϕ_m° and ϕ_m are unknown (or experimentally inaccessible).

The general form of the net current of an electroreduction reaction at a given electrode potential can be written as ¹⁸

$$i = i^{\circ} \{ \exp[-\alpha n f_{\eta}] - \exp[(1-\alpha)n f_{\eta}] \}$$
 (2.4)

where f = RT/F (R is the gas constant, T is the absolute temperature, F is the Faraday constant), η = (E - E°) is the so-called overpotential, i° is the exchange current at equilibrium state and α is the cathodic transfer coefficient. The transfer coefficient provides a measure of the symmetry of the energy barrier for the electrode reaction.

For small values of η , i.e., $|\eta| << 1/nf$, Equation 2.4 becomes

$$i = i^{\circ} (nf\eta)$$
 (2.5)

and the resulting Equation 2.5 shows the linear relation between i and η . For large values of η , a Tafel relation can be obtained

$$i = i^{\circ} \exp(-\alpha n f_{\eta}) \tag{2.6}$$

·
,
ę -
31
£.
,
•
ង
an an

or

$$\eta = \frac{RT}{\alpha nF} \ln i^{\circ} - \frac{RT}{\alpha nF} \ln i$$
 (2.7)

The plot of η vs. ℓ ni is termed a Tafel plot; the slope is frequently used to evaluate the apparent transfer coefficient.

It is quite reasonable to assume first-order kinetics for simple electrode reactions such as the redox reaction 2.1. Then the measured rate constants are

$$k_{ob}^{c} = \frac{i_{c}}{nFC_{ox}}$$
 (2.8)

and

$$k_{ob}^{a} = \frac{i_{a}}{nFC_{red}}$$
 (2.9)

for the cathodic and anodic processes respectively. Therefore, the relationship between the observed rate constant and the applied electrode potential E (i.e., driving force) can be generated by substituting Equation 2.8 into Equation 2.4 for the cathodic reaction

$$k_{ob}^{C} = k_{ob}^{S} \exp[-\alpha n f(E - E^{\circ})]$$
 (2.10)

and Equation 2.9 into Equation 2.4 for the anodic reaction

$$k_{ob}^{a} = d_{ob}^{s} \exp[(1-\alpha)nf(E - E^{\circ})]$$
 (2.11)

where k_{ob}^{S} is the standard rate constant for reaction 2.1. Then the transfer coefficient α can be calculated from

$$\alpha = \frac{-2.3RT}{F} \left(\frac{\partial \log k_{ob}}{\partial E} \right) \tag{2.12}$$

There are many ways in which the observed rate constant will be influenced, such as the temperature, the composition of the supporting electrolyte solution, and the nature of the electrode material, and these influences will be discussed as follows.

2. The Structure of the Electrical Double Layer 19

Since electrode reactions are expected to occur only within the so-called "electrical double layer" region, it is important to consider the structure and the behavior of the double layer before any further discussion of the theoretical treatment of the elementary electron-transfer reaction. The first model describing the structure of the electrified electrode-solution interface was proposed by Helmholtz (1853) and Quincke (1861), which assumed the double layer as a parallel plate capacitor. Then Gouy (1910) and Chapman (1913) independently modified this model by calculating the distribution of the electrode potential as a function of the electrolyte concentration by assuming a Boltzmann distribution of the ions between the double layer region and the bulk of solution. However, in the Gouy-Chapman model, ions are treated as point charges. Stern (1924) took account of the electrode potential, and

pointed out that the ions could not reach the electrode surface beyond some "plane of closest approach". The approximate validity of the Gouy-Chapman-Stern (GCS) model 19 was experimentally demonstrated by Grahame. 20,21 This double layer model is currently used by electrochemists.

According to the GCS model, the double layer can be divided into two regions (i) the compact (inner or Helmholtz) layer between the electrode and the plane of closest approach, (ii) the diffuse (outer) layer extending from the plane of closest approach to the bulk of solution. Figure 2.1 shows a schematic double layer. The measured double layer capacitance can be expressed as

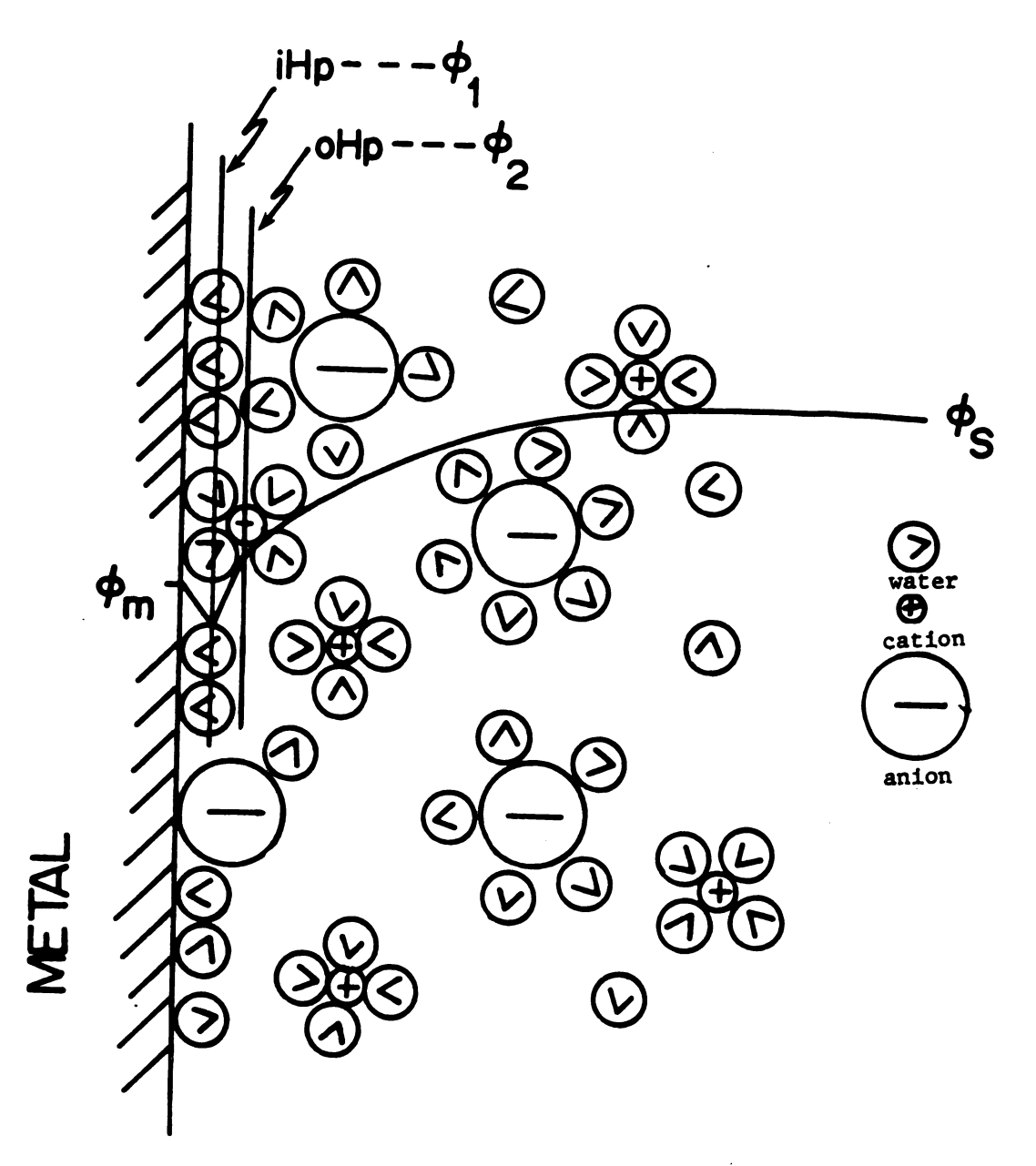
$$\frac{1}{C} = \frac{1}{C_{M-2}} + \frac{1}{C_{2-S}} \tag{2.13}$$

where the subscript M and S denote the metal and solution respectively, and C_{M-2} and C_{2-S} are the capacitance of the compact and diffuse layer respectively. According to the GCS model, ¹⁹ the electrode charge q^m is related to the potential at the outer Helmholtz plane ϕ_2 (for convenience the potential in the bulk of solution ϕ_s is always set at zero) by

$$q^{m} = \pm \left[\frac{RT\varepsilon}{2\pi} \Sigma C_{i}^{s} \left(e^{-Zf\phi_{2}} - 1\right)\right]^{1/2}$$
 (2.14)

where ϵ is the dielectric constant, Z is the ionic charge of ions i, and C_i^S is the bulk concentration of ions i. The differentiation of Equation 2.4 yields the diffuse layer capacitance

Figure 2.1 The electrode-solution interfical structure including the specifically adsorbed anions



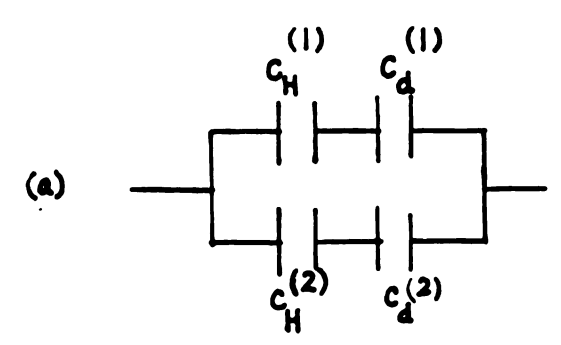
iHp-- inner Helmholtz plane (ϕ_1 is the corresponding potential) oHp-- outer Helmholtz plane (ϕ_2 is the corresponding potential) ϕ_m --- potential at the electrode surface ϕ_s -- potential at the bulk (set to zero)

Figure 2.1

$$C_{2-S} = |Z|fA \cosh \left(\frac{|Z|f\phi_2}{2}\right)$$
 (2.15)

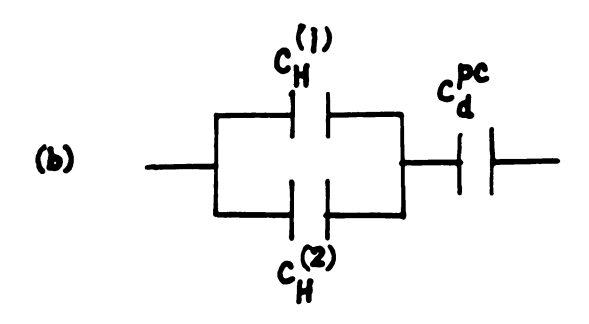
However, the calculation of the compact layer capacitance requires a much more complicated theoretical treatment. For a first approximation, it is reasonable to assume C_{M-2} to be independent of the electrolyte concentration. Good agreement between the experimental results and the GCS theory was obtained by Grahame 20,21 on the basis of this assumption.

However, this simple double-layer model may only work for homogeneous electrode surfaces, such as liquid electrodes and single crystals. The influence of the crystallographic structure of the polycrystalline electrode surface on the double-layer structure was first considered theoretically by Grigoryev. 22,23 Furthermore, the qualitative analysis of the models of electric double-layer structure at polycrystalline electrodes has been studied by Damaskin.²⁴ Figure 2.2 shows two possible equivalent circuits of the doublelayer of a polycrystalline electrode consisting of two single crystal faces. In Figure 2.2a, each single crystal face has its own Helmholtz and diffuse layers (Model I). In Figure 2.2b, each single crystal face possesses its own Helmholtz layer while the diffuse layer is common to the entire electrode surface (Model II). These models have been employed to study the effect of crystallographic inhomogeneity of a polycrystalline electrode surface on the resulting "average" point of zero charge (pzc). 24 They have also been examined in connection with the electroreduction of several anions. ²⁵ Figure 2.2 Equivalent electric circuit of polycrystalline electrode models: (a) Model I; (b) Model II



 $C_{H}^{(1)}$ and $C_{d}^{(1)}$ are the inner- and diffuse- layer capacitance of single-crystal face 1.

C_H and C_d are the inner- and diffuse- layer capacitance of single-crystal face 2



 $C_{H}^{(1)}$ and $C_{H}^{(2)}$ are the inner-layer capacitances of single-crystal face 1 and 2 respectively. C_{d}^{pc} is the common diffuse-layer capacitance.

Figure 2.2

The measurement of the electrocapillary curve is a straight-forward way to examine the thermodynamics of an ideal polarizable electrode surface. The phenomena of the electrocapillary curve, ¹⁹ surface tension as a function of electrode potential, can be described by utilizing the Gibbs adsorption isotherm ²⁶

$$-d_{\Upsilon} = q^{m} \cdot dE + \Sigma \Gamma_{i} \cdot d\mu_{i}$$
 (2.16)

where γ is the surface tension, Γ_i is the surface excess of the ionic species i, and μ_i is the chemical potential. Then the electrode charge q^m can be obtained from the corresponding Lippmann equation 27 by differentiating Equation 2.16

$$q^{m} = -\left(\frac{\partial \gamma}{\partial E}\right) \mu_{i} \tag{2.17}$$

at a constant temperature and pressure. At the electrocapillary maximum the electrode charge will equal zero as expected from Equation 2.17, and the corresponding electrode potential E is termed the pzc. ¹⁹ In general, the pzc coincides with the observed sharp minimum of the differential capacitance curve for a dilute solution consisting of nonspecifically adsorbing electrolytes. ¹⁹ The occurrence of the sharp minimum is a result of the parallel relation between the compact and diffuse layer capacitance. Since the diffuse layer capacitance decreases ¹⁹ with the square root of the electrolyte concentration and the compact layer capacitance is independent of the concentration, ¹⁹ a minimum in the capacitance curve can therefore be expected when the electrolyte concentration is decreased.

For the study of specific adsorption of anions at the electrode-solution interface, mixed electrolytes ²⁸ consisting of a salt of the adsorbing anions and the nonspecifically adsorbing base electrolyte at constant total ionic strength have often been employed. The so-called Hurwitz-Parsons ^{28,29} method is used to determine the concentration of the specifically adsorbed anions. In general, the Hurwitz-Parsons analysis is obtained from the Gibbs adsorption isotherm. By assuming the amount of the diffuse layer adsorption is proportional to the bulk concentration, the Gibbs adsorption Equation 2.16 can be reformulated as

$$-d\gamma = q^{m} \cdot dE + \Gamma_{X}^{i}RT \cdot d\Omega nx \qquad (2.18)$$

where Γ_X' is the component of Γ_X present in the inner layer i.e., the surface concentration of specifically adsorbed anions, and x is the molar fraction of the adsorbing anions. Two cross-differential equations can be obtained from Equation 2.18

$$\left(\frac{\partial E}{\partial \Gamma_{x}^{'}}\right)_{q^{m}} = RT \left(\frac{\partial Lnx}{\partial q^{m}}\right)_{\Gamma_{x}^{'}} \tag{2.19}$$

and

$$\left(\frac{\partial q^{m}}{\partial \Gamma_{x}^{'}}\right)_{E} = -RT \left(\frac{\partial \ln x}{\partial E}\right)_{\Gamma_{x}^{'}} \tag{2.20}$$

Equation 2.19 was utilized by Dutkiewicz 29 and Parsons 28 and Equation 2.20 was employed by Weaver and Anson 30 in their analysis of the specific adsorption of iodide from the mixed electrolytes

containing iodide and fluoride. Parsons, et al. 28 found that the adsorption was well described by an isotherm congruent with respect to the electrode charge density q^m . This implied that $(\partial \ln x/\partial q^m)_{\Gamma_X^i}$ was independent of the Γ_X^i , then the Equation 2.19 could be integrated at constant a^m to give Equation 2.21 and from which the value of Γ_X^i was calculated.

$$\Gamma_{X}' = \Delta Eq^{m}/RT \left(\frac{\partial \ln x}{\partial q^{m}}\right)_{\Gamma_{X}'}$$
 (2.21)

In a similar way, Γ_X^1 can be evaluated from Equation 2.22 which is derived from Equation 2.20.

$$\Gamma_{X}^{\prime} = -\Delta q^{m} E/RT \left(\frac{\partial Ln_{X}}{\partial E}\right)_{\Gamma_{X}^{\prime}}$$
 (2.22)

Details of the calculation of the surface concentration of the specifically adsorbed anions are discussed in Chapter IV.

Theoretical Treatment of Heterogeneous Electron-Transfer Kinetics

Most of the theories 1,7-9 of electron-transfer reactions were originally developed for homogeneous reactions. Heterogeneous reactions can be treated in a similar way 31 to homogeneous reactions; the former is an especially simple type of electron-transfer process in which only one reactant needs to be activated for the reaction to occur. Analogous to homogeneous reactions, electrode reactions can be divided into two broad classes, 1 outer-sphere and inner-sphere

pathways. Figure 2.3 illustrates the essential differences between inner- and outer-sphere reactions. Outer-sphere reactions can be defined as those where there is no direct interaction between the reacting ions and the electrode surface, i.e., the inner-shell solvent molecules adjacent to the electrode surface remain intact during the formation of the precursor state and transition state. If there is strong interaction between the reactants (to be more precise, the coordinated ligands) and the electrode surface, i.e., the reacting ions can penetrate through the inner-layer solvent molecules to form specifically adsorbed precursor and transition states, those reactions are labelled inner-sphere reactions.

Two methods 32 have been developed for distinguishing between inner- and outer-sphere electrode reaction mechanisms. These are (i) the response of the reaction rate to the addition of strongly adsorbed but chemically inactive anions and (ii) the difference in the potential dependence of the reaction rate, i.e., inferring mechanisms from the values of α . The corresponding change of ϕ_2 as a result of the change of the electrode charge by the addition of strongly adsorbed anions will result in the change of the observed reaction rate

$$(\Delta \log k_{ob}^{E}) = (\alpha_{I} - Z) \frac{F}{2.3RT} (\Delta \phi_{2})_{E}$$
 (2.23)

Since the adsorption of anions will produce negative values of $(\Delta \phi_2)_E$, for cationic reactants undergoing outer-sphere reactions their reaction rates will be enhanced by the addition of specifically

Figure 2.3 Proposed reaction sites for Cr(III) aquo and ammine complexes at the electrode-aqueous interface

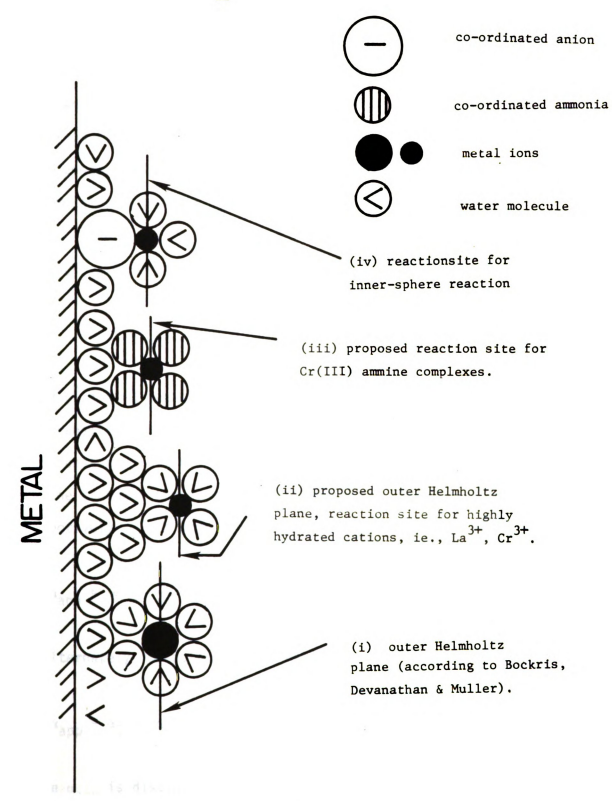


Figure 2.3

adsorbed anions. For inner-sphere reactions, however, the strongly repulsive interaction existing between the anionic bridging ligands of the reacting ions and the specifically adsorbed anions will diminish reaction rates as a result of repelling the reacting ions away from the electrode surface.

A general form of the rate expression for both classes of reaction mechanisms was derived 33

$$logk_{app}^{E} = logk + log\gamma^{b} - log\gamma^{\dagger} - \frac{1}{2.3RT} [\alpha_{I}(\Delta G_{AP}^{\circ} - \Delta G_{AR}^{\circ} + FE) + \Delta G_{AP}^{\circ}]$$

$$(2.24)$$

where γ^b and γ^{\dagger} are the activity coefficients of the bulk reactant and transition state respectively, and k is a potential-independent rate constant, E is the electrode potential, and ΔG_{AR}° and ΔG_{AP}° are the standard free energy of adsorption of the reactant and product respectively. Then from Equation 2.12, α_{app} can be expressed as

$$\alpha_{\text{app}} = \frac{\alpha_{\text{I}}}{F} \left[\frac{(\Delta G_{\text{AP}}^{\circ})}{\partial E} \right] + \frac{1 - \alpha_{\text{I}}}{F} \left[\frac{(\Delta G_{\text{AR}}^{\circ})}{\partial E} \right] + \alpha_{\text{I}}$$
 (2.25)

or alternately for outer-sphere reactions

$$\alpha_{app} = \alpha_{I} - (\alpha_{I} - Z) \left(\frac{\partial \phi_{2}}{\partial E}\right)_{\mu}$$
 (2.26)

where α_{app} is distinguished from the intrinsic α_I . The typical values of $(\partial \phi_2/\partial E)_{_{U}}$ in nonadsorbing electrolytes at ionic strengths

of 0.5-1 M are 0.02-0.05. 30,35 For a simple electrode reaction, $\alpha_{\rm I}$ can be taken as 0.5. Therefore, for reactants (Z \geq 1) undergoing outer-sphere reactions, the values of $\alpha_{\rm app}$ will be greater than 0.5 as predicted from Equation 2.26.

For inner-sphere reactions, to the spontaneous adsorption of reactants and products is too weak to measure, it is relatively difficult to evaluate both $\partial(\Delta G_{AP}^{\circ})/\partial E$ and $\partial(\Delta G_{AR}^{\circ})/\partial E$ in Equation 2.26. However, a number of isothiocyanate complexes of chromium(III)³⁶ have been found to be adsorbed in measurable quantities and the corresponding values of $\partial(\Delta G_{\Delta}^{\circ})/\partial E$ were found to be negative. This is opposite to what is expected for cationic reactants whose free energy of adsorption will become more negative as the negative charge on the electrode surface increases. The resulting negative values of $\partial(\Delta G^{\circ}_{A})/\partial E$ of isothiocyanate metal complexes implies that the anionic ligand will retain at least part of their anionic character when holding the complexes at the electrode surface. Thus, it is reasonable to assume the values of $\partial(\Delta G_{AP}^{\circ})/\partial E$ and $\Delta(\partial G_{AR}^{\circ})/\partial E$ to be negative for anion-bridged inner-sphere reactions. Thus if α_T = 0.5 from Equation 2.25 the values of $\alpha_{\mbox{\scriptsize app}}$ for inner-sphere reactions are expected to be less than 0.5. The mechanistic diagnoses based on these two methods have been found to be valid for distinguishing between a number of inner- and outer-sphere reactions at mercury electrodes. 32

Similar to homogeneous reactions, heterogeneous electron-transfer processes are anticipated to proceed via two steps:⁴ (i) the formation of a precursor state by bringing the reacting ions from

the bulk to a suitable site within the double layer region where the electron-transfer reaction can occur (ii) the thermal activation of the precursor state enabling the electron to transfer and subsequent deactivation to form the product successor state. Thus, Reaction 2.1 can be rewritten as

Ox(solution)
$$\pm$$
 Ox*

$$0x^* + ne \stackrel{?}{=} Red^*$$
 (2.27)

Red^{*}

Red

where $0x^*$ and Red^* indicate the precursor and successor states, respectively. Assuming that the elementary electron-transfer step is rate determining, we can write the observed (overall) rate constant k_{ob} as (pre-equilibrium model)⁴

$$k_{ob} = k_{et} \cdot K_{p} \tag{2.28}$$

where K_p is the equilibrium formation constant of precursor states and $k_{\mbox{et}}$ is the first order rate constant for the elementary electron-transfer reaction within the precursor state. For the outer-sphere reaction K_p can be expressed as

$$K_p = K_0 \cdot \exp(-W_p/RT) \tag{2.29}$$

where K_0 is the statistical value of K_p when $W_p = 0$, and W_p is the

work required to bring the reacting ions to the reaction site. The value of K_0 can be taken as the reactant radius r, indicating that all the reacting species within the distance r of the plane of closest approach will have a rough equal chance of undergoing electron transfer. For a first approximation, the work term W_p can be attributed to the Coulombic interaction, so that $W_p = ZF\phi_{rp}$, where Z is the net charge of the reacting ion, ϕ_{rp} is the average potential at the reaction plane. This work term is mainly responsible for the double layer effect upon the observed rate constants.

For the elementary electron-transfer step, $k_{\mbox{et}}$ can be expressed utilizing a "semi-classical" model⁴

$$k_{et} = \kappa_{el} \cdot \Gamma_{n} \cdot \nu_{p} \cdot \exp(-\Delta \overline{G}^{\dagger} / RT)$$
 (2.30)

where κ_{el} is electron transmission (tunneling) coefficient, Γ_n is nuclear tunnelling factor (in general, Γ_n roughly equals unity), ν_p is a nuclear frequency factor ($\sim 10^{13}~{\rm sec}^{-1}$), and $\Delta \overline{\rm G}^{\dagger}$ is the electrochemical free energy of reorganization for the elementary reaction. Therefore the overall rate constant of Reaction 2.1 derived from the pre-equilibrium model is

$$k_{ob} = K_0 \cdot \kappa_{el} \cdot \nu_p \exp(-W_p/RT) \exp(-\Delta \overline{G}^{\dagger}/RT)$$
 (2.31)

However, a different model, a so-called "reactive-collision" model, ³ is commonly used in the study of outer-sphere reactions. The expression of the overall rate constant derived from the reactive-

collision model is

$$k_{ob} = \kappa_{el} Z_e \exp(-W_p/RT) \exp(-\Delta \overline{G}^{\dagger}/RT)$$
 (2.32)

where Z_e is the electrochemical collision frequency ($\sim 10^{11} \text{ sec}^{-1}$). For simplification Equation 2.31 and 2.32 can be written as

$$k_{ob} = A \cdot \exp(-\Delta G^{\dagger}/RT)$$
 (2.33)

where A is the pre-exponential factor, which is 3×10^5 and 5×10^3 cm sec^{-1} for the pre-equilibrium and reactive-collision models, respectively. The comparison between these two models has been thoroughly discussed from theoretical as well as experimental points of view.

4. Double Layer Effect on Electrochemical Kinetics

For the first approximation, the work term W_p in the rate expression Equation 2.32 can be assumed to be mainly due to the double-layer effect. Figure 2.4 shows the free energy profile for a simple electrochemical reaction Ox + e = Red plotted against the nuclear reaction coordinate. In Figure 2.4, P and S denote the precursor and successor states, respectively, and O and R denote the oxidized and reduced species, respectively. According to Figure 2.4 $\Delta \overline{G}_{S-P}^o = \Delta \overline{G}_{C}^o + (W_S - W_P)$ and $\Delta \overline{G}_{C}^o = F(E - E^o)$ at a given electrode potential E, then $\Delta \overline{G}_{S-P}^o = F(E - E^o) + W_S - W_P)$. According to the relation

$$\frac{\partial (\Delta \overline{G}^{\dagger})}{(\overline{G}_{S-P}^{\circ})} = \alpha_{I}$$
 (2.34)

Figure 2.4 Free energy profile for simple electrochemical reaction

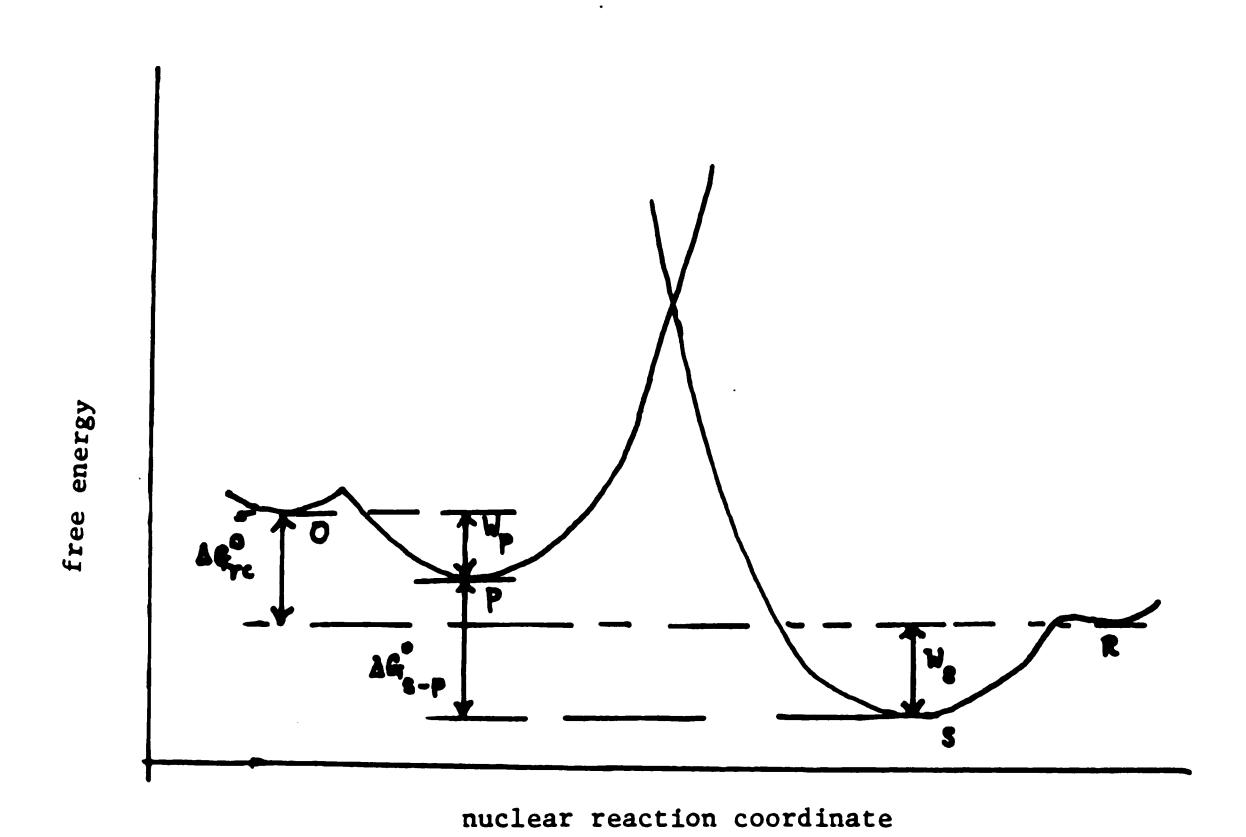


Figure 2.4

where $\Delta \overline{G}^{\dagger}$ is the reorganization free energy and α_{I} is the intrinsic transfer coefficient, it denotes to what extent the reorganization free energy will change upon altering the electrochemical driving force $\Delta \overline{G}^{\circ}_{S-P}$. Therefore $\Delta \overline{G}^{\dagger}$ can be correlated to $\Delta \overline{G}^{\dagger}_{int}$ by

$$\Delta \overline{G}^{\dagger} = \Delta \overline{G}_{int}^{\dagger} + \alpha_{I}(W_{S} - W_{p}) + \alpha_{I}(E - E^{\circ})$$
 (2.35)

where $\Delta \overline{G}_{int}^{\dagger}$ is the intrinsic barrier for electron-transfer reactions. $\Delta \overline{G}_{int}^{\dagger}$ will be the free energy of the overall reaction when there are no thermodynamic driving forces, i.e., $W_S = W_P = 0$ and $E = E^\circ$.

By substituting Equation 2.35 into Equation 2.32 and taking the natural logarithm of both sides, it yields Equation 2.36.

$$RTlnk_{ob}^{E} = RTlnk_{el}K_{0}v_{p} - \Delta \overline{G}_{int}^{\dagger}$$

$$- [W_{p} + \alpha_{I}(W_{S} - W_{p})] - [\alpha_{I}F(E - E^{\circ})] \qquad (2.36)$$

The last term of the right hand side of Equation 2.36 is the thermodynamic driving force and the second term is the intrinsic free energy barrier. It is useful to rewrite Equation 2.36 as

$$RTlnk_{corr}^{E} = RTlnk_{ob}^{E} + [W_{p} + \alpha_{I}(W_{S} - W_{p})]$$
 (2.37)

where k_{corr} is defined as the "double layer corrected" rate constant. As mentioned before, the work terms (W_{S} and W_{P}) can be treated as a result of the electrostatic interaction. Therefore, for the one

electron reduction reaction, $W_p = ZF_{\phi_{rp}}$ and $W_S = (Z-1)F_{\phi_{rp}}$ since the charge of the product is (Z-1). Then the Equation 2.37 will become

$$\ln k_{ob}^{E} = \ln k_{corr}^{E} - (Z - \alpha_{I}) f_{\phi_{rp}}$$
 (2.38)

where $(Z-\alpha_I)$ can be regarded as the effective charge on the reacting ion in the transition state. Then the term $(Z-\alpha_I)f\phi_{rp}$ can be taken as the work term required to bring the reactants from the bulk to the transition state. This equation is also known as a form of the Frumkin relation, 37 and is frequently used to correct the double layer effect for outer-sphere reactions.

5. Activation Parameters of Electrode Kinetics

The significance of electrochemical activation parameters has often been misunderstood. The energetics of the transition state of the electron-transfer reaction can be explored by the measurement of activation parameters. There are different definitions 15 of the electrochemical activation parameters which depend on which electrical state of the electrode reaction is controlled. The "ideal" and "real" activation parameters are the temperature dependence of reaction rate constants evaluated at constant Galvani potential $\phi_{\rm m}$ and constant overpotential (with respect to formal potential) respectively, and were first defined by Temkin. 15

From the simplified rate constant expression Equation 2.34 and together with the Gibbs free energy relation

$$\Delta G^{\dagger} = \Delta H^{\dagger} - T \Delta S^{\dagger} \tag{2.39}$$

where ΔH^{\ddagger} and ΔS^{\ddagger} are the activation enthalpy and entropy, respectively, the rate constant can be related to the corresponding activation parameters as

$$k_{ob}^{E} = A \cdot exp \left(\frac{-\Delta H^{\dagger}}{RT}\right) exp \left(\frac{\Delta S^{\dagger}}{R}\right)$$
 (2.40)

Therefore, the reaction enthalpy and entropy of activation can be evaluated from the study of the temperature dependence of rate constants (Arrhenius relation).

It has been critized about the experimental accessibility of the "ideal" activation parameters, because at least one component of the overall cell potential other than φ_m which is expected to be held constant will change when the temperature is varied. By the use of nonisothermal cells, however, may be a possible way to get around this cause for doubt. If the nonisothermal cell potential $E^{n\, i}$ is held constant, the temperature dependence of the metal-solution Galvani potential φ_m will be 39,40

$$\left(\frac{\partial \phi_{m}}{\partial T}\right)_{\text{FNi}} = -\left(\frac{d\phi_{\text{tij}}}{dT}\right) + \left(\frac{d\phi_{\text{tc}}}{dT}\right) \tag{2.41}$$

where $\phi_{\mbox{tij}}$ is the Galvani potential difference across the thermal liquid junction between the "hot" and "cold" electrolyte, and $\phi_{\mbox{tc}}$ is the "thermocouple" potential difference between the hot and cold

regions of the working electrode. The value of $(d\phi_{tc}/dT)$ has been shown to be very small (+ 15 μ V/deg). The value of $(d\phi_{tij}/dT)$ cannot be determined experimentally. However, it is probably also small (50 μ V/deg). Therefore, it is appropriate to assume that $(d\phi_m/dT)_{Eni} \simeq 0$. Therefore, holding E^{ni} constant as the temperature is changed could also maintain the Galvani potential constant at least within these limits. The uncertainty of ΔS^{\ddagger} , which results from the assumption $(d\phi_m/dT)_{Eni} = 0$, can be estimated to be about ± 0.5 cal deg^{-1} mole⁻¹. 17

From Equation 2.40 the "ideal" activation enthalpy can be expressed as

$$\Delta H_{ideal}^{\ddagger} = -R \left[\frac{\partial (\ln k_{ob} - \ln T^{1/2})}{\partial (\frac{1}{T})} \right]_{\phi_{m}}$$
 (2.42)

where the term $\ln T^{1/2}$ results from the temperature dependence of the collision frequency Z_e of the reactive-collision model. Therefore, the "ideal" activation enthalpy can be obtained from the slope of the plot of $(\ln k - \ln T^{1/2})$ vs. T^{-1} . Furthermore, the double-layer corrected activation enthalpy $\Delta H_{corr}^{\ddagger}$ can be gained by combining Equation 2.42 with Equation 2.38

$$\Delta H_{corr}^{\dagger} = \Delta H_{ideal}^{\dagger} + \frac{E}{F} \{ (\alpha_{corr} - Z) \left[\frac{\partial \phi_{rp}}{\partial (\frac{1}{T})} \right]_{\phi_{m}} \}$$
 (2.43)

From Equation 2.43, it is necessary to evaluate the temperature dependence of the potential at the reaction plant ϕ_{rp} from the measurement of the temperature dependence of the pzc in order to evaluate

the coefficient $\left[\partial \phi_{rp}/\partial (\frac{1}{T})\right]_{\phi_m}$.

The relationship between the "ideal" and "real" entropies of activation can be written as follows

$$\Delta S_{ideal}^{\dagger} = \Delta S_{real}^{\dagger} + \alpha \Delta S_{rc}^{\circ}$$
 (2.44)

where ΔS_{rc}° is the reaction entropy of a redox couple.³⁹ The value of ΔS_{rc}° is also obtained by the use of a nonisothermal cell from the measurement of the temperature dependence of the formal potential of a redox couple. Thus, ΔS_{rc}° can be evaluated from the following equation

$$F(\frac{dE_f^{ni}}{dT}) = F(\frac{d\phi_f^m}{dT} + \frac{d\phi_{tc}}{dT} + \frac{d\phi_{tij}}{dT}] \simeq F(\frac{d\phi_f^{ni}}{dT}) = \Delta S_{rc}^{\circ}$$
 (2.45)

where $(d\phi_{\mbox{tij}}/dT)$ and $(d\phi_{\mbox{tc}}/dT)$ are close to zero as discussed before. The "real" activation entropy $\Delta S_{\mbox{real}}^{\mbox{\dagger}}$ can be correlated to the temperature dependence of the intrinsic reorganization barrier 42 λ_e for the electron-transfer reaction as appears in Marcus theory 8 by the relation

$$\Delta S_{\text{real}}^{\downarrow} = -\frac{d\lambda_{e}}{4dT}$$
 (2.46)

where $\lambda_e/4$ is equal to the value of $\Delta G_{\text{corr}}^{\ddagger}$. By substituting the dielectric continuum expression^{8,9,26} for λ_e into Equation 2.46, the value of $\Delta S_{\text{real}}^{\ddagger}$ is estimated to be close to zero (0.25 e.u.). The

"real" activation entropy is the mean of the entropic driving force of the forward and backward reactions

$$\Delta S_{real}^{\dagger} = 0.5 \left(\Delta S_{corr}^{\dagger, f} + \Delta S_{corr}^{\dagger, b} \right)$$
 (2.47)

According to the Marcus theory, $\Delta S_{corr}^{\dagger} = -\Delta S_{corr}^{\dagger}$ by assuming that the free energy curve is symmetrical, i.e., the transition state for the electron-transfer reaction has a similar environment to that for the reactants and products, then the value of $\Delta S_{real}^{\dagger}$ is also equal to zero.

The study of the activation entropy ΔS^{\dagger} provides a means to evaluate electron tunneling as well as the frequency factor for the kinetics of the elementary electron-transfer processes. In addition, the validity of the application of the Marcus theory to the present study can also be tested.

In the derivation of the Frumkin Equation 2.38, the work terms have been assumed to be totally due to Coulombic interaction. However, other contributions to the work terms are still possible, such as the specific solvent interaction presented between the reacting ions and the electrode surface. Thus, it is worthwhile to formulate the activation parameters in a general form as follows.

Another equivalent form of the rate expression Equation $^{43-45}$ 2.23 is

$$RTlnk_{ob}^{E} = RTlnA - \Delta G_{int}^{\ddagger} - [\Delta G_{p}^{\circ} + \alpha_{I}(\Delta G_{S}^{\circ} - \Delta G_{p}^{\circ})] - [\alpha_{I}F(E - E^{f})]$$
(2.48)

where ΔG_{S}^{o} and ΔG_{S}^{o} represent the free energies required to form the precursor and successor states from the bulk reactant and product, respectively, and ΔG_{int}^{\dagger} is the so-called "intrinsic barrier". ΔG_{int}^{\dagger} is the activation energy for the elementary electron-transfer step when the work terms ΔG_{S}^{o} and ΔG_{P}^{o} , and the overall driving force $F(E-E^f)$ each equal zero. The "real" activation enthalpy $\Delta H_{real}^{\dagger}$ can then be expressed as

$$\Delta H^{\ddagger} = -R \left[\frac{d(\ln k_{ob}^{E})}{d(\frac{1}{T})} \right] = \Delta H_{int}^{\ddagger} + \left[\Delta H_{p}^{\circ} + \alpha_{I} (\Delta H_{S}^{\circ} - \Delta H_{p}^{\circ}) \right]$$
 (2.49)

where ΔH_{P}^{o} and ΔH_{S}^{o} are enthalpic components of the work terms of ΔG_{P}^{o} and ΔG_{S}^{o} , and $\Delta H_{int}^{\ddagger}$ is the "intrinsic" activation enthalpy for the elementary electron-transfer step. In a similar way, the "real" activation entropy $\Delta S_{real}^{\ddagger}$ can be related to the "intrinsic" activation entropy $\Delta S_{int}^{\ddagger}$ by

$$\Delta S^{\dagger} = \Delta S_{int}^{\dagger} + [\Delta S_{p}^{\circ} + \alpha_{I} (\Delta S_{S}^{\circ} - \Delta S_{p}^{\circ})]$$
 (2.50)

where ΔS_S^o and ΔS_P^o are entropic components of the work term ΔG_S^o and ΔG_P^o .

CHAPTER III

EXPERIMENTAL

1. General Apparatus

The three-electrode configuration was used in this study. the measurements of electrode kinetics a conventional two-compartment electrochemical cell 46 was usually employed, in which the reference compartment was separated from the working compartment with a fine grade glass frit (Corning Co.). The glass frit was to prevent the mixing of the working solution with the electrolyte solution diffusing from the reference electrode and also to provide sufficient electrical conductivity for the operation of the potentiostat. A three-compartment cell was used for bulk electrolysis, which utilized a mercury pool as the working electrode and had another glass frit to separate the counter electrode in order to prevent the mixing of products. For the temperature dependence measurements, a nonisothermal cell was used, in which the temperature of the working compartment was varied while keeping the temperature of the reference compartment constant. In order to vary the temperature of the working solution, a water insulator jacket was also fabricated around the working compartment to maintain the temperature by a flow of thermostat water. A large counter electrode, either platinized gauze or spiraled platinum wire, was utilized for the measurement of the differential double layer capacitance. The large capacitance of the counter electrode minimizes its influence upon the measured double layer capacitance of the working electrode.

The reference electrode employed in all of the measurements was

the saturated calomel electrode (SCE) (Sargent-Welch Corp.). The KCl filling solution of the SCE was changed to NaCl solution when measurements were performed in ${\rm Cl0}_4^-$. This was done to prevent the precipitation of ${\rm KCl0}_4$ in the fiber junction. The potentials of reference electrodes were occasionally checked with a fresh home made "master" KSCE (potassium SCE). Since the electrochemical measurement was very sensitive to the presence of impurities, especially for solid electrodes, a relatively thorough, as well as tedious, procedure was used in this laboratory to clean glassware. The glassware were first soaked in a 1:1 HNO $_3$ and H $_2$ SO $_4$ solution for one day, then rinsed and soaked in a highly purified water for two days.

2. Reagents.

The quality of water used to prepare all of the solutions was very critical to the electrochemical measurement. In this laboratory, a great deal of effort has been taken in the preparation of highly purified water. The water from a "Milli-Q" purification unit (Millipore Corp.) was suitable for mercury electrodes. However, much more highly purified water was needed for solid electrodes and the measurement of double layer capacitance. Conway and coworkers proposed a relatively complicated method to purify water (pyrodistillation). The purification procedure involves passing water vapor through a column packed with platinum gauze and heated to 750° to 800° C in a stream of oxygen. In this way the organic materials could be catalytically combusted and entirely removed. The other way was to use a quartz subboiling still (Dida-Science Inc.)

which offered an efficient way to remove cationic impurities. In the subboiling distillation, infrared heaters vaporized liquid from the surface without boiling, thus minimizing the problem of entrainment associated with ordinary distillation. The purity of prepared water could be evaluated from the reproducibility of electrode kinetics and the stability of the measured differential double layer capacitance.

Since oxygen is chemically active, the dissolved oxygen in the working solution was generally removed by purging solutions with a flow of purified inert gas (such as N_2 , Ar, or He). The purification of inert gas was accomplished either by bubbling through an aqueous solution containing vanadous ions and amalgamated zinc or a more efficient way by passing through a heated catalytic column packed with BASF R3-11 catalyst (Badische Aniline und Soda-Fabrik).

Analytical grade reagents were used without further purification for mercury electrode studies. However, for solid electrode experiments they were recrystallized from highly purified water. Sodium perchlorate, which was used to prepare most of the solutions, was recrystallized from a solution prepared from 60% perchloric acid and sodium carbonate. A $\text{Cr}(\text{OH}_2)_6^{3+}$ stock solution was prepared by dissolving Cr_2O_3 in HClO_4 with the addition of H_2O . The syntheses of Cr(III) complexes followed standard published procedures. The double salt aquopentaaminechromium(III) ammonium nitrate 49 was used as the starting material for the preparation of $\text{Cr}(\text{NH}_3)_5\text{OH}_2^{3+}$, 49 $\text{Cr}(\text{NH}_3)_5\text{N}_3^{2+}$, 51 $\text{Cr}(\text{OH}_2)_5\text{N}_3^{2+}$, 53 $\text{Cr}(\text{NH}_3)_5\text{Cl}^{2+}$, 49 $\text{Cr}(\text{NH}_3)_5\text{SCN}^{2+}$, 50 and $\text{Cr}(\text{OH}_2)_5\text{SCN}^{2+}$. 52 $\text{Cr}(\text{OH}_2)_5\text{F}^{2+}$, 49 $\text{Cr}(\text{OH}_2)_5\text{Cl}^{2+}$, and $\text{Cr}(\text{OH}_2)_5\text{OSO}_3^4$, were also prepared as described in the literature.

3. Electrochemical Techniques

Generally, the electrical response of an electrochemical cell is equivalent to the electrical circuit shown in Figure 3.1. $R_{\rm s}$ is the solution resistance, R_{ct} is the frequency-dependent impedance, and C is the double layer capacitance. Due to the adsorption of ions or the heterogeneity of the electrode surface, Figure 3.1 could be modified by adding either resistors or capacitors. Most of the electrochemical techniques used in this study were performed with controlled potential methods by using a potentiostat. Figure 3.2 shows a simple diagram of a single-amplifier potentiostat. The operation of the potentiostat is quite straightforward if two basic principles are kept in mind: (i) the amplifier input currents are assumed to be negligibly small, and (ii) if there is a closed feedback loop from the output to the invert input, the amplifier will maintain the inverting input at the same potential as the noninverting (+) input. Therefore, by means of the feedback loop through the counter electrode, the amplifier forces current through the working electrode until E_W = E_S where E_W is the potential of the working electrode and E_c is the potential of the signal generator (both are referred to the reference electrode).

a. <u>Cyclic Voltammetry</u>

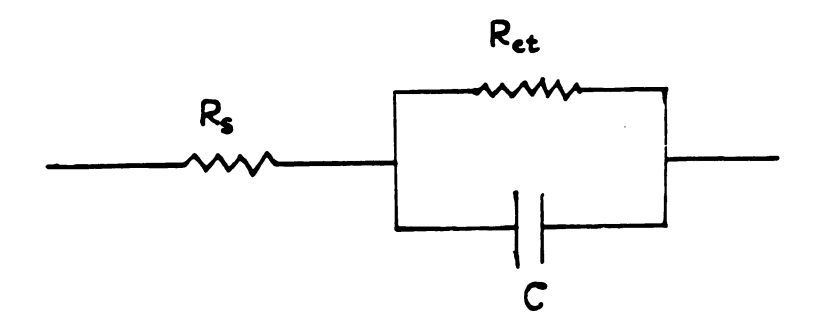
A convention PAR (Princeton Applied Research) 174 or 174A polarographic analyzer, which would produce a triangular wave potential at a rate of 20 to 500 mV per second, together with Hewlett-Packard HP7045A X-Y recorder were employed in the measurement of

(upper)

Figure 3.1 Schematic diagram of an electrochemical cell

(lower)

Figure 3.2 Single amlifier potentiostat

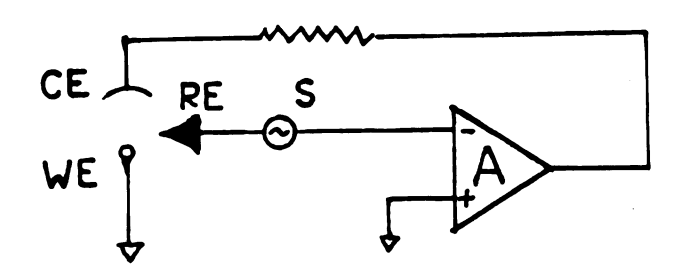


R_s: solution resistance

 R_{ct} : frequency-dependent impedance

C: double layer capacitance

Figure 3.1



A: operational amplifier

S: signal generator

WE: working electrode

RE: reference electrode

CE: counter electrode

Figure 3.2

cyclic voltammetry. A stationary electrode is required in this technique; either a hanging mercury drop electrode (HMDE) (Metrohm Model E441, Brinkman Instrum.), a hanging gallium drop electrode (HGDE), a metal foil electrode, or a rotating-disk electrode were used. The HGDE was prepared by replacing the mercury of a short capillary HMDE with gallium. All the experiments involving the HGDE were performed in a dry box which was heated to about 30°C by a thermostat in order to prevent freezing of the gallium. Cyclic voltammetry is a convenient technique with which to do an initial check of the purity of the solution and the potential region available to the working electrode employed. At the same time, electrode kinetics could also be obtained from cyclic voltamograms by utilizing the equations derived by Nicholson and Shain 55 (for quasi-reversible) or Galus 62 (for totally irreversible).

If the desirable potential sweep rate was above 500 mV/sec, a universal programmer PAR 175 coupled with PAR 173 served as a fast-potential ramp generator, and a Nicolet Explorer I digitized scope was used as a recorder. The PAR 175 could generate a potential sweep at rates up to 1000 V/sec. The advantage of employing the Nicolet explorer I is that it has an X-Y mode and also has a pen output option with an adjustable pen recording speed. Thus, an ordinary X-Y recorder could be coupled to the Nicolet Explorer I in order to obtain a quantitative record. The analysis of fast cyclic voltamograms was described elsewhere. ⁵⁶

b. DC and Pulse Polarography

The instruments employed in this technique were similar to those for the cyclic voltammetry. Usually, for the measurement of the polarography, the potential sweep rate was adjusted to between 2 to 10 mV/sec. A dropping mercury electrode (DME) was required to perform the polarography. The analysis of DC polarography was done by the conventional Koutecky method, ⁵⁷ and equations derived by Oldham and Parry were used to analyze pulse polarograms. ⁵⁸

c. Rotating-Disk Voltammetry

For electrodes other than mercury, the rotating-disk electrode is the most convenient device. The theories as well as the derivation of equations of the rotating-disk voltammetry ⁵⁹ have already been thoroughly developed and discussed. The basic ideal of analyzing the voltammogram is to calculate the reactant concentration just outside the double layer region which is

$$C_r = C_b \left(1 - \frac{1}{1_0}\right)$$
 (3.1)

where C_b is the bulk concentration and i_ℓ is the diffuse limiting current. Then the heterogeneous rate constant at an electrode potential E is given as $k_{ob}^E = i/FAC_r$ where A is the electrode area. The normal pulse technique was also employed at rotating-disk electrodes.

d. Capacitance Measurements

- (i) <u>AC Bridge</u> The use of the ac bridge is the most common way to measure the differential double-layer capacitance. A Wien bridge 61 was built in this department. The principle of the operation of the ac bridge is to match the adjustable pair of capacitor and resistor with the corresponding component of the electrochemical cell until a null point (when there is no phase difference) is detected by a scope. The advantage of the ac bridge is its simplicity, however, the disadvantage is the tedious procedure.
- (ii) "Phase-Detection" Technique A PAR 175 was combined with a PAR 173 which also coupled with a PAR 174/50 ac polarographic analyzer to scan the electrode potential as required, while a PAR 5204 lock-in amplifier was employed to measure the corresponding inphase (resistive component) current i_I and the quadrature (capacitor component) current i_Q . The differential double layer capacitance, then, can be calculated as

$$C = \frac{1}{\omega V} \left(\frac{i_{I}^{2} + i_{Q}^{2}}{i_{I}} \right)$$
 (3.2)

where ω and V is the applied ac frequency and peak to peak potential, respectively. The constant term $1/\omega V$ can be found from the calibration of the lock-in amplifier with a dummy cell.

4. Electrode Pretreatments

The purity of the lead rod used to fabricate the rotating-disk lead electrode was 99.999% (Atomergic Chemical Co.). The rotating-disk electrodes were either obtained from Pine Co. or made in this department. The problem of air bubbles inside the lead rod caused difficulties in the electrode fabrication. The lead rod was first trimmed down to the suitable dimension (0.2 cm dia.) and glued on a stainless steel (5 cm) support with a special silver epoxy, silverbond type 50 (Transene Company Inc.), then was pressed into a hot Teflon or Kel-F sheath. Thus the cooled sheath would assure the tight seal between the sheath and the lead.

Several pretreatments were tested in order to evaluate the dependence of the measured capacitance upon the chemical and physical state of the electrode surface. The Russian school described a relative complicated method (A). ⁶³ In method (A), the electrode was electrochemically polished in a solution of sodium acetate in acetic acid. As the cathode in the polishing bath, they used six rods made of spectrally pure graphite arranged symmetrically around the electrode to be polished at a distance of 5 cm. After polishing, the electrode was carefully washed with double distilled water and then placed in the measuring cell where, for two hours, it was cathodically polarized in an atmosphere of hydrogen at a potential of -1.34 vs.

Bewick⁶⁴ used method (B) to study the inner-layer water structure at lead electrodes using reflectance spectroscopy. In method (B) the electrode was initially mechanically polished and a freshly

prepared solution mixed from acetic acid, hydrogen peroxide, and methanol of the 2:3:5 ratio, was poured over the polished electrode 10 times. After rinsing the electrode with water, it was quickly transferred while wet to the degassing 0.5 M sodium perchlorate solution; then cathodically polarized at -1.5 V vs. SCE for thirty minutes.

There is also an electrochemical method 65 (C). The electrode was mechanically polished on roughened glass, electrochemically etched in perchloric acid (20%) and finally chemically etched in the perchloric acid for thirty minutes.

Methods (B) and (C) as described above were employed in this work. We also used a relative simple mechanical polishing method (D), to pretreat the polycrystalline lead electrode. In the first part of the pretreatment, method (D) was similar to methods (B) and (C) in that the electrode was mechanically polished with 1μ alumina polishing powder (Buehler Ltd.) on a polishing wheel (Buehler 44-1502-160) using water as a lubricant. After a bright surface was obtained, the electrode was quickly transferred while wet to a degassing water solution to rinse it. Then the electrode was transferred immediately to a 0.5 M sodium perchlorate solution and the electrode potential was repeatedly scanned between -0.7 V and -1.6 V vs. SCE in order to stabilize this mechanically polished electrode surface.

CHAPTER IV

DOUBLE LAYER STRUCTURE AT THE LEAD-AQUEOUS INTERFACE

1. Introduction

The study of the double layer structure and the accompanying phenomena of single-crystal and polycrystalline solid electrodes is currently a very active research area in electrochemistry. ⁶⁶ From the measurement of the differential double-layer capacitance, a correction for the ionic double-layer effect due to the Coulombic interaction between the reacting ions and the electrode surface on the electrode reactions can be obtained.

In this study, the specific adsorption of anions at the polycrystalline lead-aqueous interface was examined as a means to investigate the intrinsic properties of the electrode-solution interface. The extent of the specific adsorption of anions was evaluated from the measurement of the differential double layer capacitance in solutions of mixed electrolytes having a general composition of (0.2 - x) M NaF+xNaX, where X is the adsorbed anions examined. The so-called Hurwitz-Parsons analysis 28 , 29 was employed to calculate the surface concentration $\Gamma_{\rm X}^{\prime}$ of the specifically adsorbed anions. The free energy of specific adsorption, $\Delta G_{\rm a}^{\circ}$, was then obtained by utilizing the Frumkin isotherm 67 which includes an interaction parameter g. Comparison of the values of $\Delta G_{\rm a}^{\circ}$ at lead and mercury electrodes was made in order to evaluate the dependence of the energies involved in specific adsorption of anions upon the nature of the electrode material.

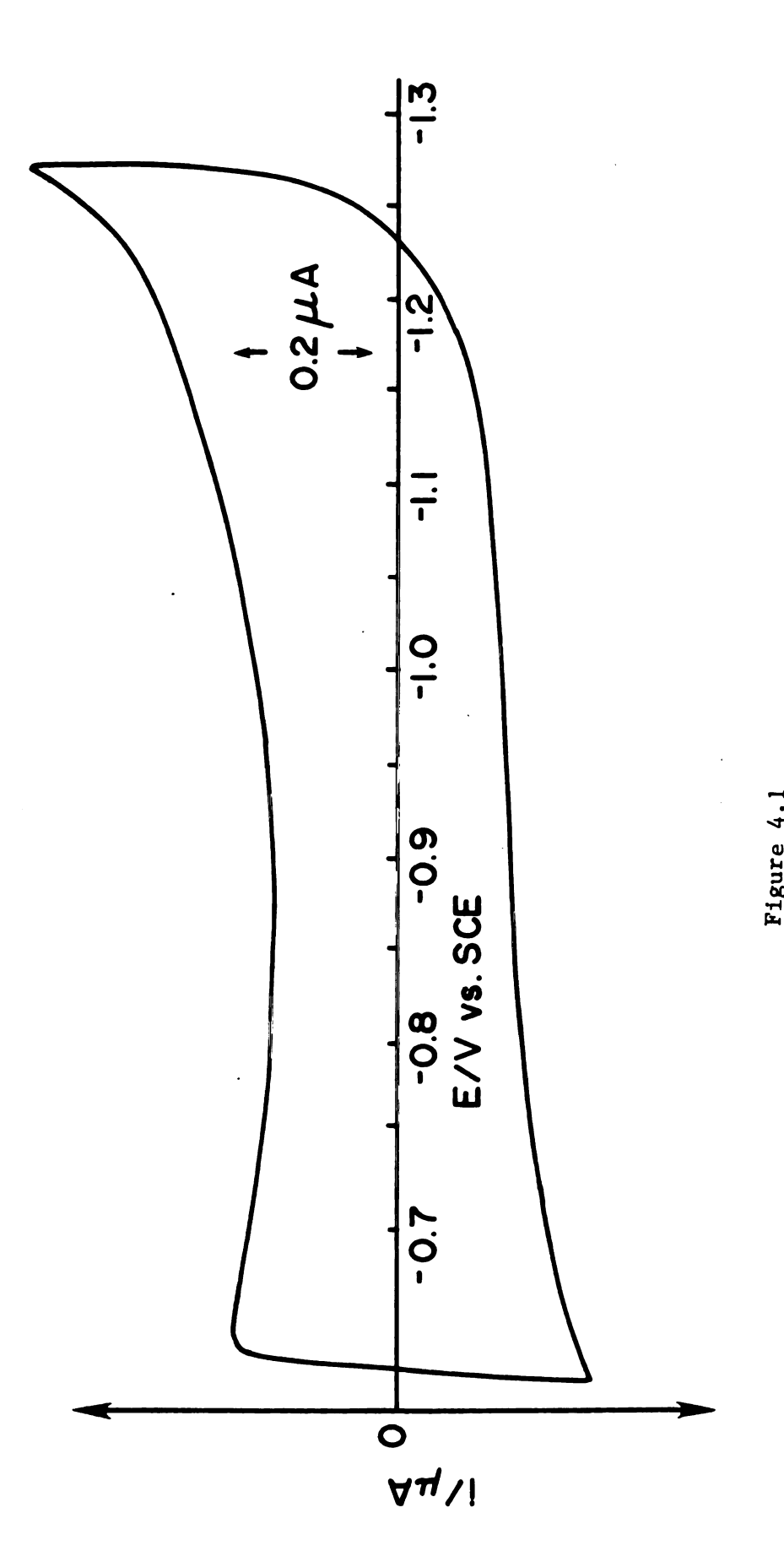
Several electrode pretreatments for the polycrystalline lead are

available in the literature. $^{63-65}$ Thus, it is interesting to study the pretreatment dependence of the specific adsorption of anions at a lead surface. The difference in the values of ΔG_a^o for various electrode pretreatments can be attributed to the difference in surface activities. Upon comparing the measured capacitance curves at the lead electrode in a 10 mM solution of sodium fluoride to that of sodium perchlorate, it seems that perchlorate ions are significantly adsorbed at the lead surface. Therefore, it is worthwhile to perform the measurement of specific adsorption of anions in perchlorate electrolytes with which to investigate the influence of the adsorption of supporting electrolytes $^{68-70}$ on the amount of the specifically adsorbed anions studied.

2. Characterization of the Electrode Surface

The study of the double-layer structure at the electrode-solution interface is necessarily based on the possession of an ideally polarizable electrode surface. Figure 4.1 is a typical cyclic voltammogram for a solution of 0.5 M sodium perchlorate at the polycrystalline lead surface prepared by method (D). The lead pretreatment methods (A), 63 (B), 64 (C), 65 and (D) have been described in Chapter III. As shown in Figure 4.1, the double-layer charging and discharging current-potential curves are smooth and symmetrical without any special features. This indicates that an ideally polarizable lead surface can be obtained by pretreatment method (D). Furthermore, the values of the integral capacitance 71 obtained from Figure 4.1 are comparable ($\pm 15\%$) with the values of the measured differential

Figure 4.1 Typical cyclic voltammogram for polycrystal-line lead electrode (prepared by method D) at 0.1 V \sec^{-1} in 0.5 M NaClO_4 .



capacitance that will be presented below.

3. Results

a. <u>Capacitance Measurements in Non-specifically Adsorbing</u> <u>Electrolytes</u>

The differential capacitance of the lead-solution interface was measured with an ac bridge or "phase-detection" technique as described in Chapter II. Figure 4.2 shows the differential capacitancepotential curves for solutions of sodium fluoride at polycrystalline lead electrodes. This figure also includes literature data, curve (a) which was extracted from Reference 63, in order to illustrate the dependence of the differential capacitance upon the electrode pretreatment. The capacitance curves (a), and (b) which were obtained by the use of method (A), 63 and (D), respectively, at 200 Hz, are compatible with each other. As described in Chapter II, the potential of zero charge (pzc) can be generally taken as the electrode potential at the minimum of the capacitance-potential curve for the dilute solution of non-specifically adsorbing electrolyte, for example, 10 mM sodium fluoride solution. However, this definition may not be true for the polycrystalline electrode and will be discussed later. By the use of method (B), Bewick⁶⁴ obtained the same value of the pzc in fluoride electrolyte at the polycrystalline lead as reported by Leikis with method $(A)^{63}$ (curve (a) of Figure 4.2). The curve (c) of Figure 4.2, which was obtained by the use of method (D) in this study, shows that the resulting pzc is also -0.8 V vs. SCE. Thus, all different pretreatment methods (A), (B), and (D)

Figure 4.2 Differential capacitance ys. electrode potential for polycrystalline lead in the following conditions: (a)--method (A) in 10 mM KF at 210 Hz extracted from Ref. 64; (b)--method (D) in 10 mM NaF at 200 Hz; (V) method (D) in 10 mM NaF at 50 Hz; (A) method (D) in 10 mM NaF at 10 Hz; (A) method (D) in 0.2 M NaF at 200 Hz; (O) method (D) in 0.2 M NaF at 1000 Hz

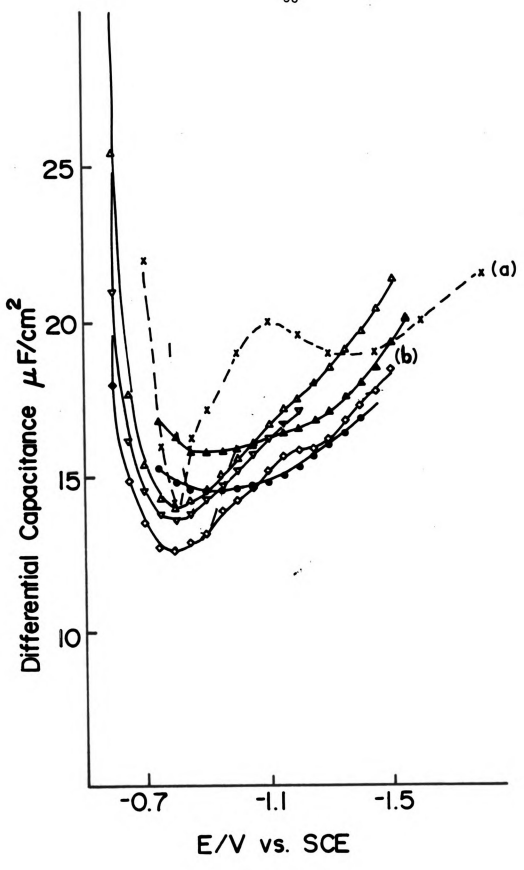


Figure 4.2

yielded roughly the same pzc (see below).

The Russian school reported 63 that with method (A) the frequency dispersion of the measured capacitance at lead was relatively small (5 - 10% with variation of the frequency from 210 to 1000 Hz). According to Figure 4.2, for method (D) there is no significant frequency dependence for the 0.2 M sodium fluoride solution (5 - 15% with variation of the frequency from 200 to 1000 Hz) and for the 10 mM sodium fluoride solution (10 - 15% with variation of the frequency from 10 to 200 Hz).

Figure 4.3 shows the differential capacitance-potential curves for solutions of sodium perchlorate with various concentrations at lead electrodes prepared by method (D). Upon comparing curve (a) for Figure 4.3 with the curve (c) for Figure 4.2, it is seen that the electrode potential (-0.9 V vs. SCE) at the minimum of the capacitance curve of the 10 mM sodium perchlorate is more negative than that of the 10 mM sodium fluoride solution. This negative shift of the minimum of the capacitance curve may be attributed to the adsorption of perchlorate ions. ⁷²

b. Time Dependence of the Measured Capacitance

By the use of method (D), the measured capacitance values were found to vary $(\pm 10\%)$ between consecutive pretreatments, which is probably due to fluctuations in the electrode area. Figure 4.4 shows an interesting result of the study of the time dependence of the differential capacitance at the lead electrode prepared by method (D) of 0.1 M sodium perchlorate solution at 1000 Hz. In Figure 4.4,

Figure 4.3 Differential capacitance at 1000 Hz vs. electrode potential for polycrystalline lead prepared method (D) in the various concentrations of NaClO₄: (x) 10 mM, (O) 50 mM, (△) 0.5 M, (◇) 1.0 M, (▽) 5.0 M

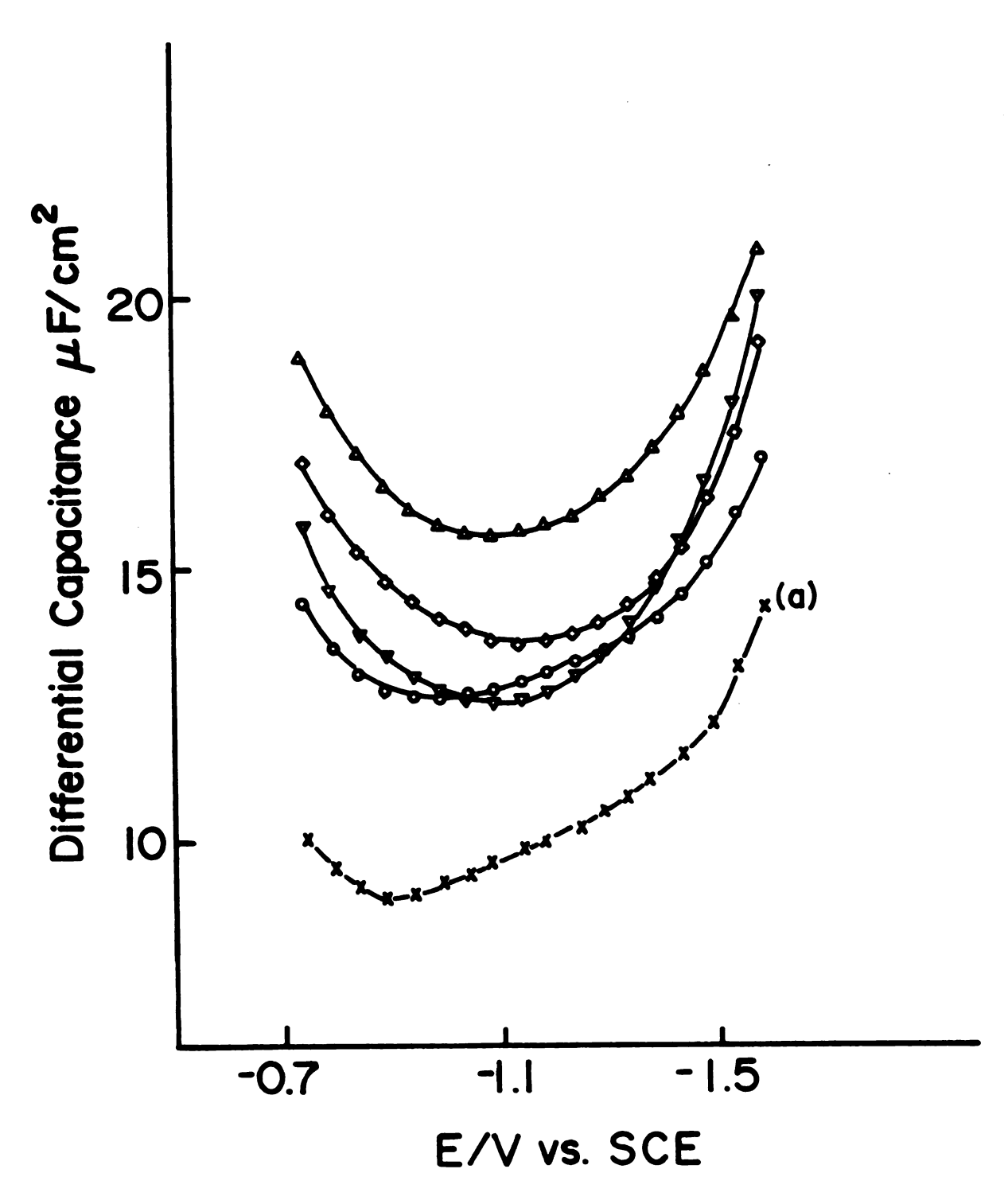


Figure 4.3

Figure 4.4 Time dependence of the differential capacitance at 1000 Hz for polycrystalline lead in 0.1 M $$\rm NaC10_4$$

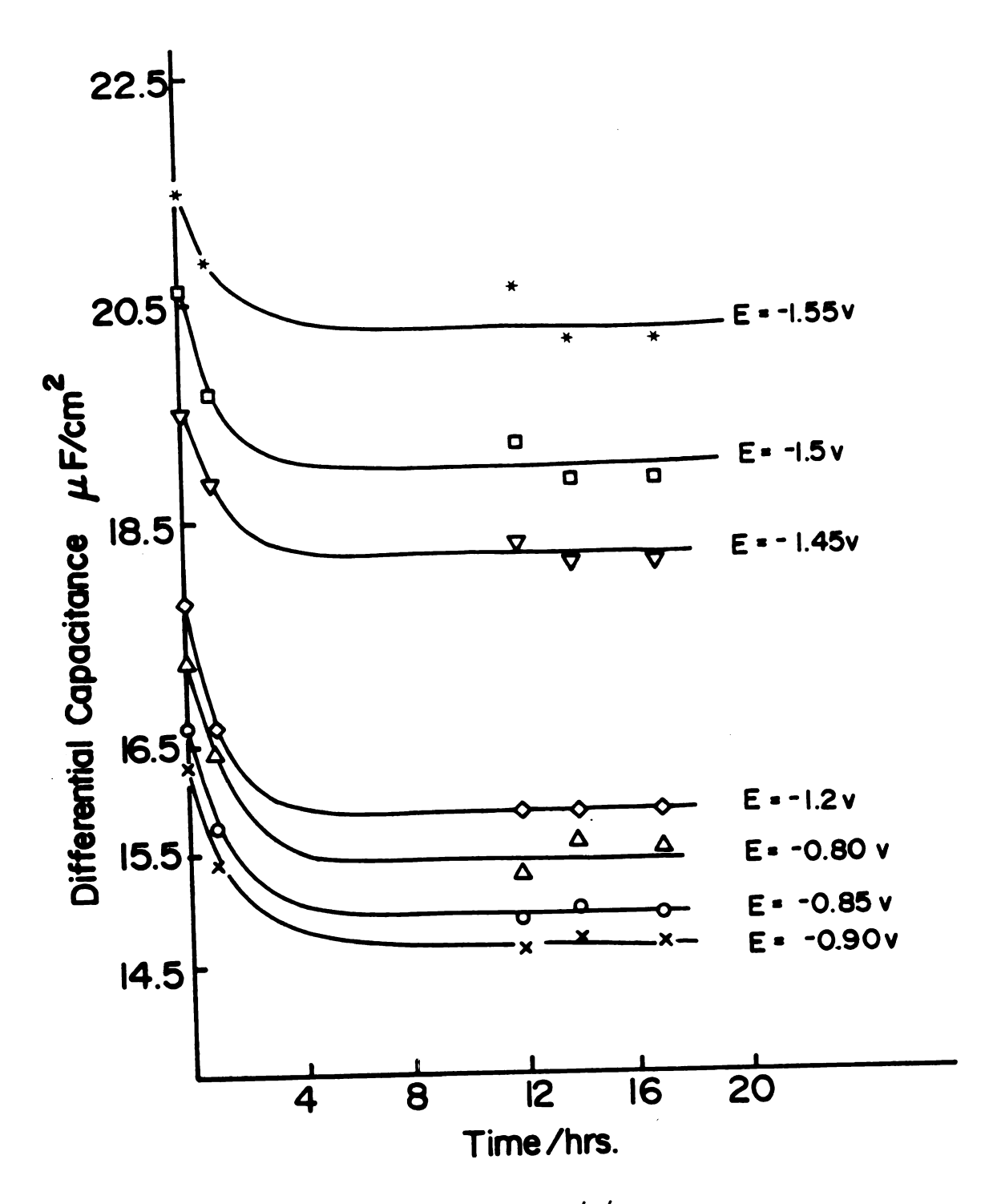


Figure 4.4

the capacitance is plotted against time for various electrode potentials, and the first reading was taken immediately after the mechanical polish. As seen in these plots, the capacitance values diminished substantially within the first hour, then they gradually reached some stable values.

c. <u>Specific Adsorption of Anions from Capacitance Measure-</u> <u>ments</u>

Mixed electrolyte solutions with constant ionic strengths having the composition of xM NaX + (0.2 - x) M NaF where X is I^- , Br^- , Cl^- , SCN^- , or N_3^- were used to study the specific adsorption of anions at lead surfaces from measurements of the differential double layer capacitance. Due to the time dependence of the measured capacitance, all the reported capacitance-potential curves were obtained by normalizing the corresponding measured capacitance curves to a constant value at -1.6 V vs. SCE. The capacitance values were found to be roughly independent of the NaX concentration at this and more negative potentials.

(i) <u>Iodide Adsorption in Fluoride-Based Electrolyte</u> - Figure 4.5 shows the capacitance-potential curves obtained by the use of method (D) at 200 Hz in solutions of xM NaI + (0.2 - x)M NaF where the concentration of NaI varies from 1 mM to 100 mM. As described in Chapter II, the surface concentration $\Gamma'_{\rm X}$ due to the specifically adsorbed anions can be calculated by the so-called Hurwitz-Parsons analysis 28,29 at constant electrode charge utilizing the equation

Figure 4.5 Differential capacitance at 200 Hz vs. electrode potential for polycrystalline lead prepared by method (D) in mixed NaF/NaI electrolytes at an ionic strength of 0.2. Key to iodide concentrations: (x) 0; (○) 2 mM; (△) 4 mM; (◇) 10 mM; (▽) 25 mM

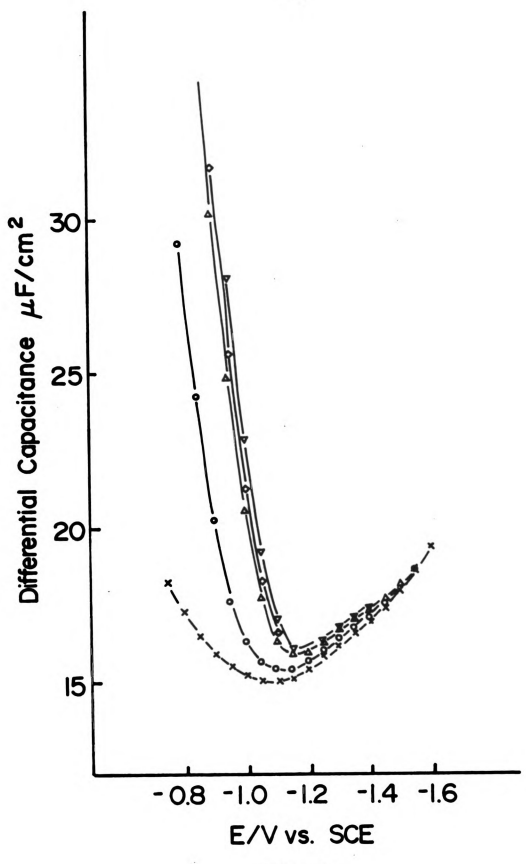


Figure 4.5

$$\Gamma_{X}' = \Delta E_{qm} / RT \left(\frac{\partial \ell n_{X}}{\partial q^{m}} \right)_{\Gamma_{X}'}$$
 (2.21)

Alternatively, one can utilize a modification due to Weaver and Anson³⁰ at constant electrode potential involving the equation (derived from Equation 2.20)

$$\Gamma_{x}' = -\Delta q_{E}^{m}/RT \left(\frac{\partial \ln x}{\partial E}\right)_{\Gamma_{x}'}$$
 (2.22)

where $(\Delta E)_{q^m}$ is the difference of the electrode potential between the base electrolyte and a given iodide-containing solution at a given electrode charge q^m , and $(\Delta q^m)_E$ is the difference of the electrode charge between the base electrolyte and a given iodide-containing solution at a given constant electrode potential E. These two quantities $(\partial \ln x/\partial q^m)_{\Gamma_X^i}$ and $(\partial \ln x/\partial E)_{\Gamma_X^i}$ were obtained from the displacement of the corresponding charge-potential curves, which were integrated from the corresponding capacitance-potential curves for various solution compositions.

The quantity RT/F $(\partial \ln x/\partial E)_{\Gamma}$, is the so-called "electrosorption valency" (EV). In an earlier report from this laboratory, the values of the electrosorption valency for specifically adsorbed anions at polycrystalline silver electrodes were found to decrease with decreasing negative electrode potential; for example, for the adsorption of chloride ions, at -0.9 V, EV = 0.25; at 0.3 V, EV = 0.15. In this study, the polycrystalline lead electrode exhibits relatively constant values of the electrosorption valency for iodide

ions over the entire electrode potential region examined. Thus, the values of EV vary only from 0.53 to 0.56 with variation of the electrode potential from -0.7 to -1.0 V. Furthermore, the EV values of lead electrodes are significantly larger than those of mercury electrodes (~ 0.42).

When the values of EV vary significantly with the electrode potential, an alternative way to calculate the surface concentration $\Gamma_{\rm x}'$ is to utilize the equation 75,76

$$\Gamma_{x}' = \frac{1}{2.3RT} \int_{E_{1}}^{E_{2}} \left(\frac{\partial q^{m}}{\partial \log x}\right)_{E} \cdot dE$$
 (4.1)

where all the symbols have the same meanings as those in Equation 2.21. In this method, q^m - E curves were obtained by integrating the corresponding C - E curves. The required coefficient $(\partial q^m/\partial \log x)_E$ was obtained by differentiating the set of q^m - £nx curves at constant E. Thus, by integrating the resulting coefficient $(\partial q^m/\partial \log x)_E$ over the electrode potential interval, it yielded the desired surface concentration Γ_X^i . On the other hand, Γ_X^i can be also obtained by differentiating the γ (relative surface tension) - £nx curves that result from the double integration of C - E curves at constant E. In this method, 77 there is no need to assume that the electrosorption valency is constant. There is, however, a limitation for the practical use of this method in that enough capacitance-potential curves of a number of concentrations of NaX are required to calculate accurately the differential term $(\partial q^m/\partial \log x)_E$.

In this work, both methods were employed to calculate the surface

concentration of iodide ions, and yielded comparable results $(\pm 10\%)$. Figure 4.6 shows the resulting plot of the surface concentration of the specifically adsorbed iodide ions against the electrode charge.

The measurement of the specific adsorption of iodide, ions at lead prepared by method (A) has been studied by the Russian school; their data are shown in Figure 4.7. From a comparison of Figure 4.7⁷⁸ with Figure 4.5, it seems that with method (A) the Russian school obtained a relatively higher degree of specific adsorption of iodide ions at lead electrodes. The Hurwitz-Parsons method was also used to analyze the capacitance curves of Figure 4.7. The resulting surface concentration of the specifically adsorbed iodide for the mixed KF/KI electrolytes containing 10 mM KI is shown in Figure 4.8 curve (a).

Measurements of the specific adsorption of iodide ions in the fluoride medium at the lead-aqueous interface prepared by method (D) were also performed at 1000 Hz in order to check the frequency dependence of the specific adsorption of iodide ions. The result is shown in Figure 4.9 and the corresponding plot of Γ_X^i vs. q^M for a solution containing 10 mM NaI is also shown in Figure 4.8 curve (d). The frequency dispersion of the specific adsorption of iodide ions at lead electrodes prepared by method (D) is small (10% between 200 Hz and 1000 Hz) by comparing curves (d) and (c) which was obtained in the same condition except at 200 Hz of Figure 4.8.

Since method (B) was also used to pretreat lead electrodes to study electrode kinetics, it is of interest to examine the adsorbabilities of various anions at lead electrodes pretreated in such a manner. The measured capacitance curves are shown in Figure

Figure 4.6 The concentrajon of specifically adsorbed iodide plotted against electrode charge for polycrystalline lead prepared by method (D) in mixed NaF/NaI electrolytes at an ionic strength of 0.2 (at 200 Hz). Key to iodide concentration: (○) 1 mM; (△) 10 mM; (△) 25 mM; (▼) 63 mM

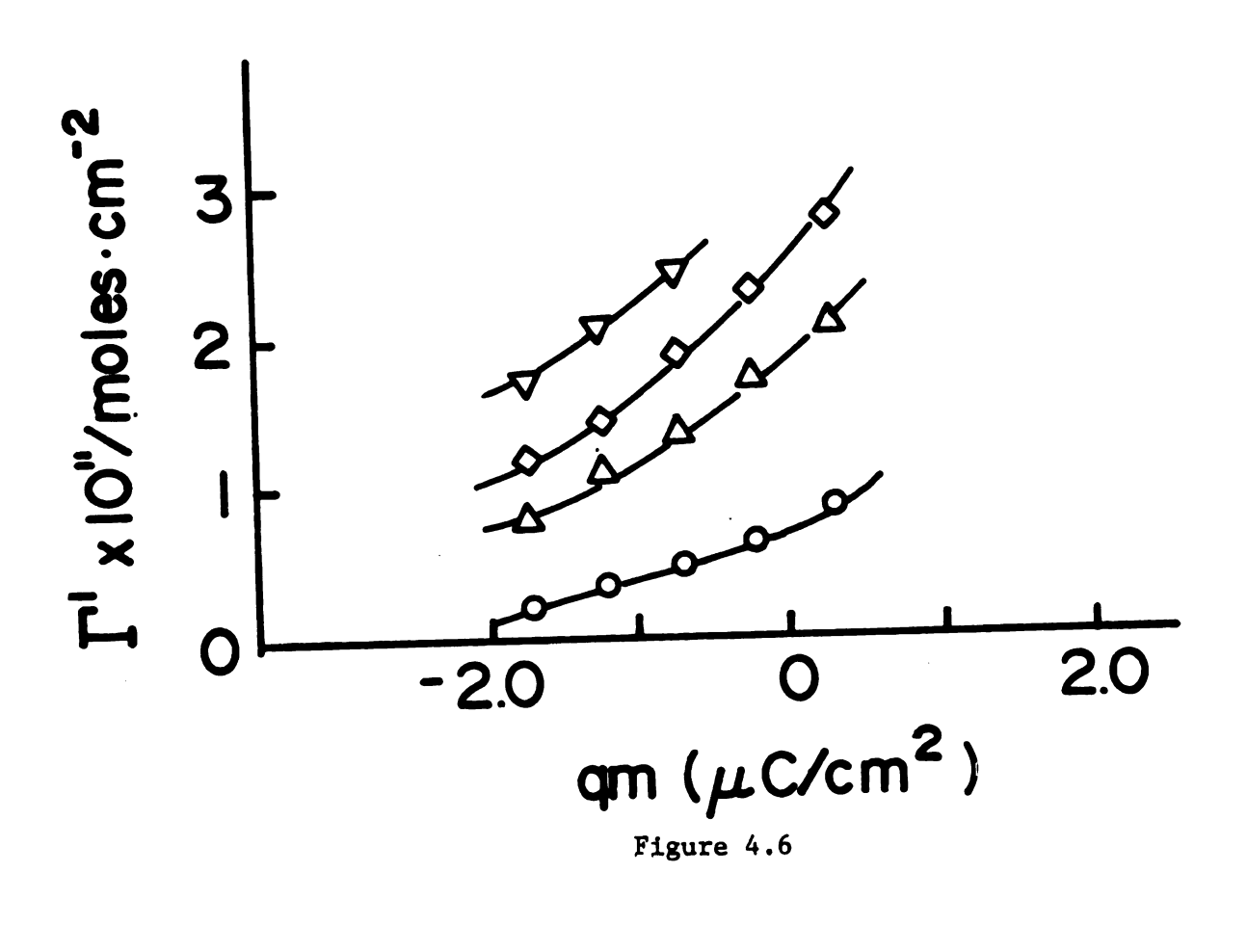


Figure 4.7 Differential capacitance at 210 Hz vs.
electrode potential for polycrystalline lead
prepared by method (A) in mixed KF/KI electrolytes at an ionic strength of 0.2. Key
to iodide concentrations: (x) 0; (Φ) 1 mM;
(Δ) 4 mM; (∇) 10 mM; (□) 25 mM; (Φ) 70 mM.
This figure was extracted from Reference
78

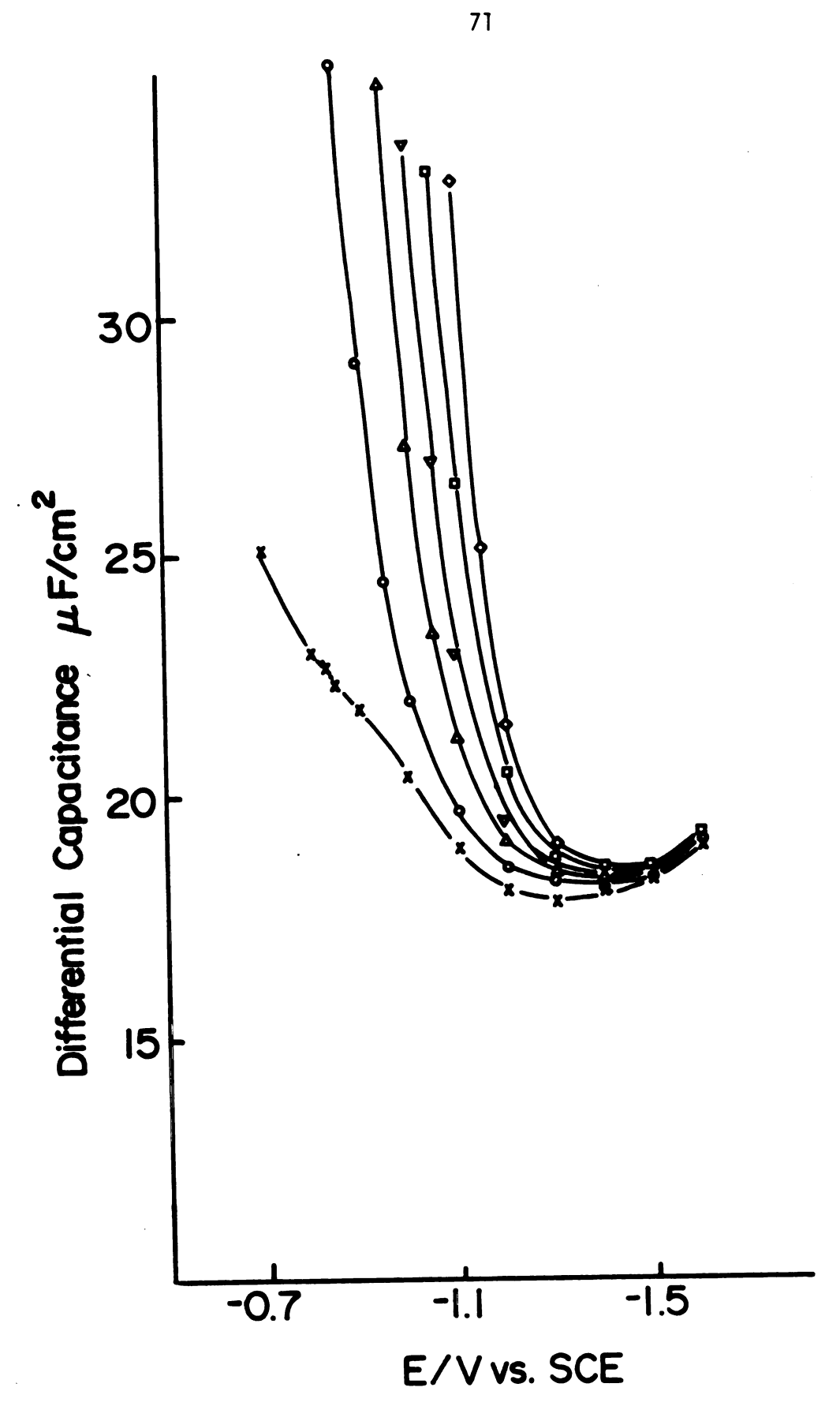


Figure 4.7

Figure 4.8 The concentration of specifically adsorbed anions (bulk anion concentration 10 mM) plotted against electrode charge for polycrystalline lead in fluoride electrolytes unless otherwise noted in the following conditions: (a)--method (A) for iodide at 210 Hz obtained by analyzing the corresponding capacitance curves in Ref. 78; (b)--method (B) for iodide at 1000 Hz; (c)--method (D) for iodide at 200 Hz; (d)--method (D) for iodide at 1000 Hz; (e)--method (D) for iodie (in perchlorate electrolytes) at 1000 Hz; (x) method (D) for chloride at 1000 Hz; (O) method (D) for azide at 1000 Hz; (7) method (D) for bromide at 1000 Hz; (Δ) method (D) for thiocyanate at 1000 Hz

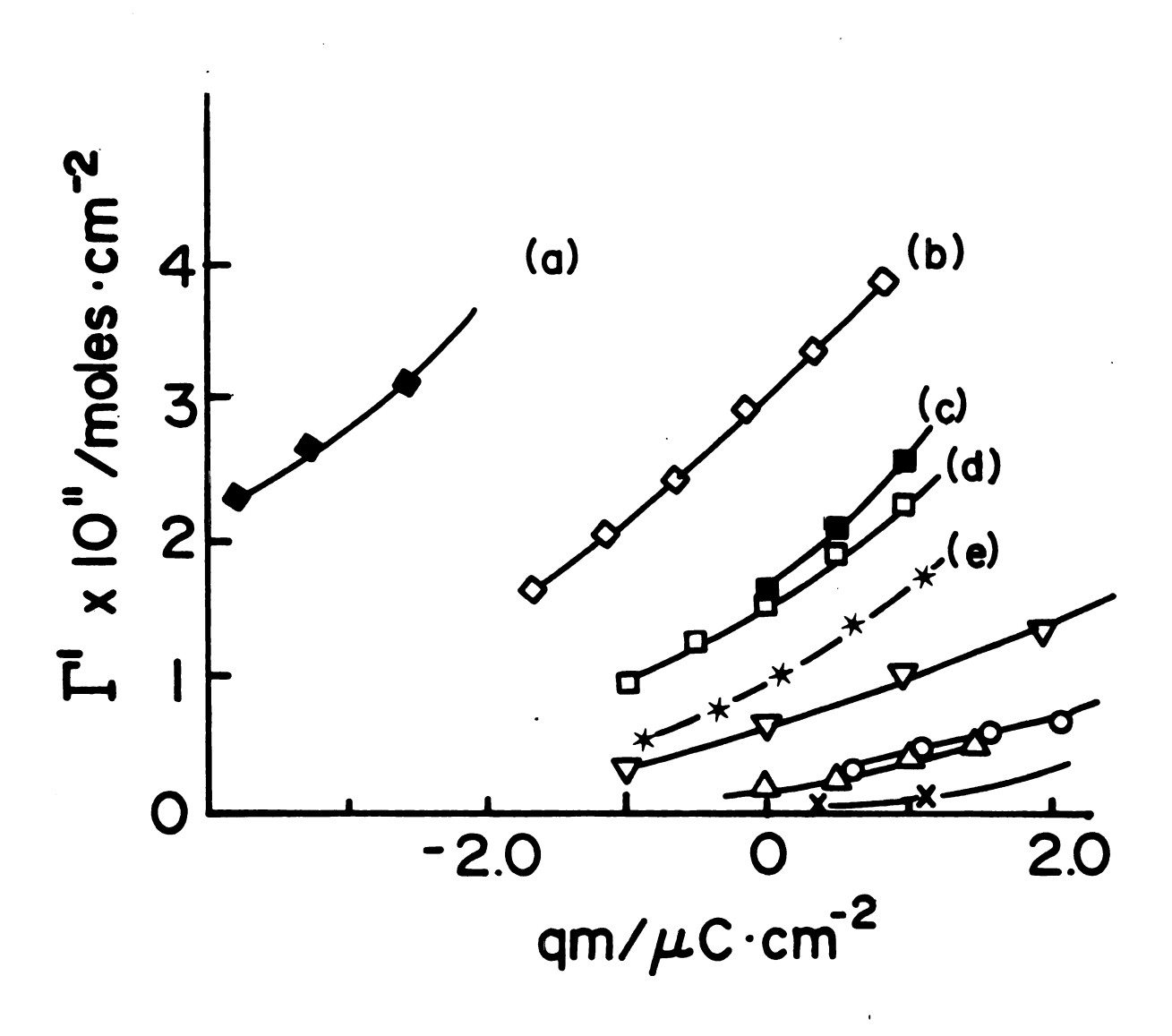


Figure 4.8

Figure 4.9 Differential capacitance at 1000 Hz vs.
electrode potential for polycrystalline lead
prepared by method (D) in mixed NaF/NaI
electrolytes at an ionic strength of 0.2.
Key to iodide concentrations: (x) 0;
(○) 1 mM; (△) 10 mM; (◇) 25 mM; (♥) 65 mM

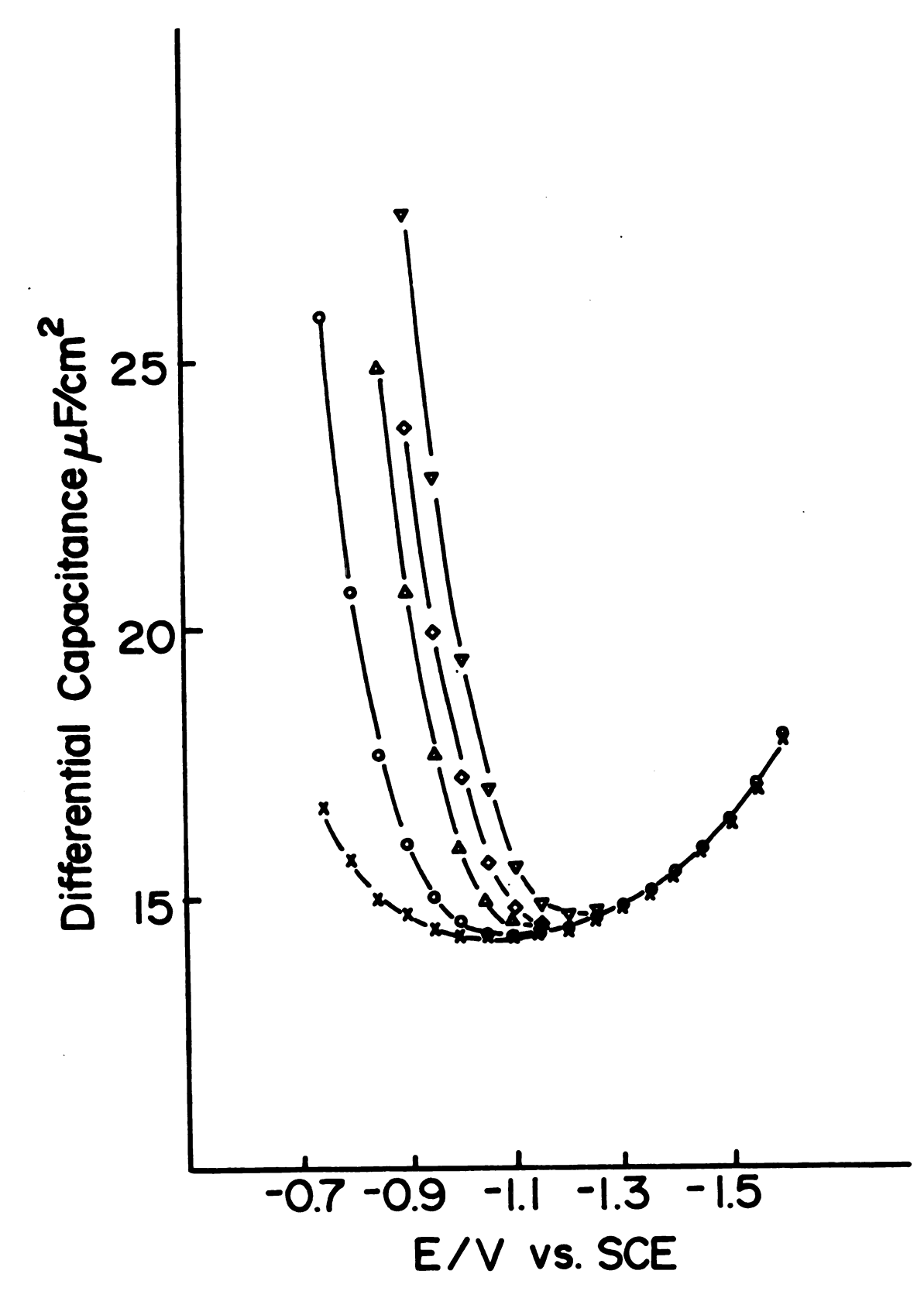


Figure 4.9

4.10 and the corresponding plot of Γ_X' vs. q^M for a solution containing 10 mM NaI is also shown in Figure 4.8 curve (b).

(ii) Iodide Adsorption in Perchlorate-Based Electrolytes - As mentioned above, the perchlorate ion has been shown 72 to adsorb weakly at polycrystalline lead. Thus, it is useful to study in more detail how the weakly adsorbing supporting electrolyte, i.e., perchlorate ion, will influence the specific adsorption of iodide ions at lead surfaces. The effect of the adsorption of supporting electrolytes on the measurement of the specific adsorption of added anions has already been examined by some authors. In this work, the measurement of the specific adsorption of iodide ions was also performed in sodium perchlorate solutions and the results are shown in Figure 4.11. The corresponding $\Gamma_{\mathbf{X}}^{\mathsf{L}}$ vs. \mathbf{q}^{M} plot for the solution containing 10 mM NaI is shown in Figure 4.8 curve (e).

In summary, curves (a), (b), and (c) of Figure 4.8 show the dependence of the surface concentration of the specifically adsorbed iodide ions Γ_X^i at polycrystalline lead on the electrode pretreatments. However, curve (a) was obtained by analyzing the corresponding capacitance curves in Reference 78. Furthermore, curves (d) and (e) show the dependence of Γ_X^i at lead prepared by method (D) at 1000 Hz on electrolytes.

(iii) Evaluation of the Free Energy of Specific Adsorption - The surface concentration $\Gamma_{\rm S}$ for a monolayer coverage of specifically adsorbed iodide ions is estimated to be 102 μ C/cm² from the ionic radius of iodide ion (2.19 Å). According to the $\Gamma_{\rm X}^{\prime}$ vs. q^m plots

Figure 4.10 Differential capacitance at 1000 Hz vs.
electrode potential for polycrystalline lead
prepared by method (B) in mixed NaF/NaI
electrolytes at an ionic strength of 0.2.
Key to iodide concentrations: (x) 0; (○)
1 mM; (△) 10 mM; (◇) 25 mM; (▽) 65 mM

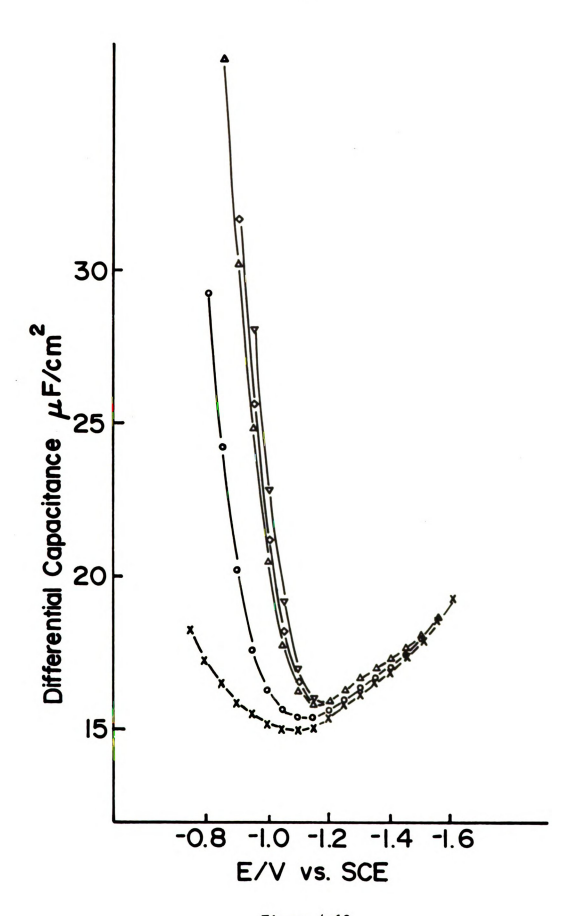


Figure 4.10

Figure 4.11 Differential capacitance at 1000 Hz vs.
electrode potential for polycrystalline lead
prepared by method (D) in mixed NaClO₄/NaI
electrolytes at an ionic strength of 0.5.
Key to iodide concentrations: (x) 0; (○)
1 mM; (△) 10 mM; (◇) 25 mM; (▽) 65 mM

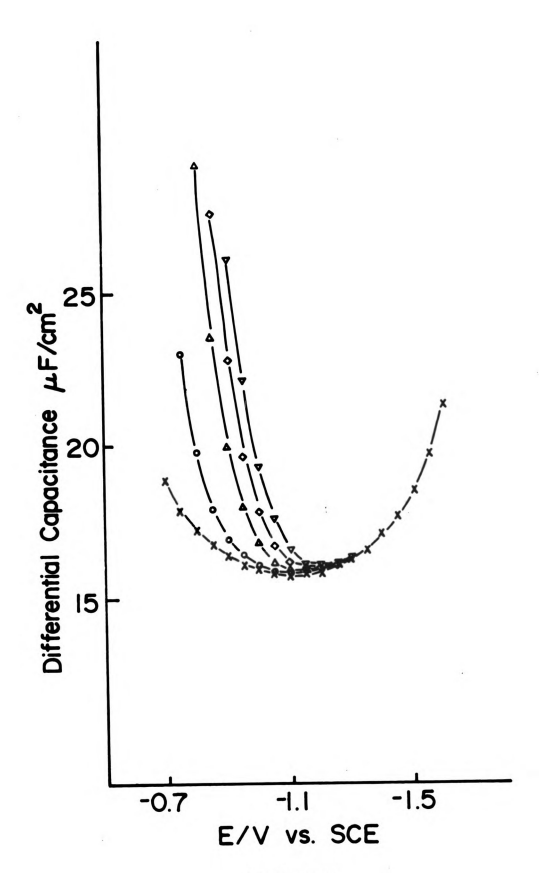


Figure 4.11

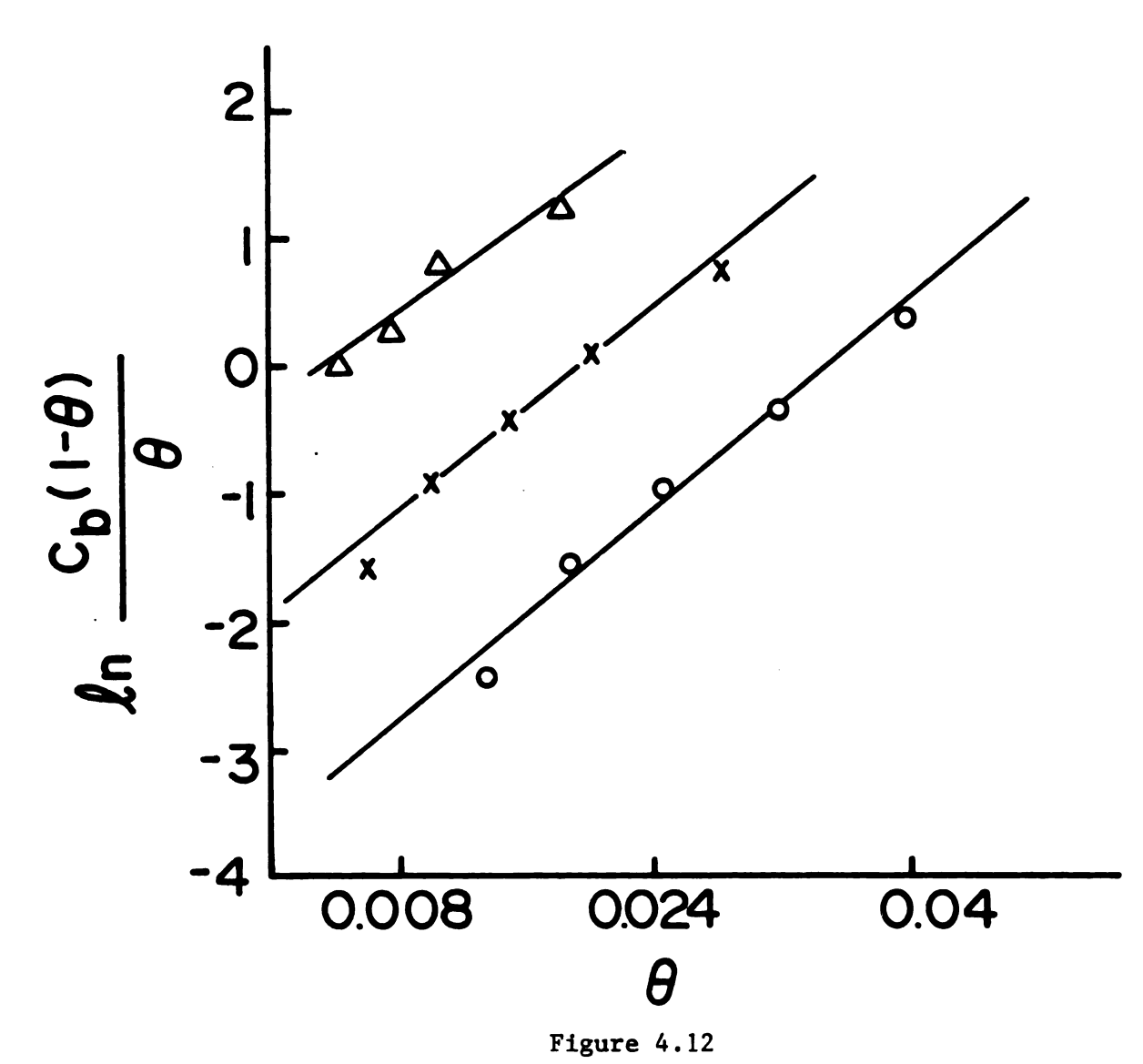
•
:
ę
·
en e
er.
ids
il production of the state of t

of Figure 4.6, the average coverage ($\theta = \Gamma_{\rm X}^{\rm I}/\Gamma_{\rm S}$) of the specifically adsorbed iodide ions at lead surfaces is relatively low (\leq 7%) compared with that of other surfaces such as silver and mercury. ⁷⁵ However, Henry's law does not apply to the present systems, which is probably due to repulsive interactions between the specifically adsorbed ions. Thus, the analysis of the adsorption isotherm at the lead surface was performed using a Frumkin isotherm. ⁷⁴ The Frumkin isotherm can be expressed as

$$\frac{C_b}{C_o} \exp\left(\frac{-\Delta G_a^o}{RT}\right) = \frac{\Gamma_s}{\Gamma_o} \left(\frac{\theta}{1-\theta}\right) \exp\left(g \cdot \theta\right) \tag{4.2}$$

where Γ_S is the surface concentration corresponding to a monolayer coverage, C_0 and Γ_0 are the standard state concentrations for the adsorbing species in the bulk and at the electrode surface, respectively, θ is the fractional coverage (= Γ_X^i/Γ_S), g is a surface interaction parameter, and ΔG_a^o is the standard free energy of adsorption. Plots of $(\ln C_b - \ln (\theta/1-\theta))$ against θ were drawn in order to determine the interaction parameter g from the slope and the standard free energy of adsorption ΔG_a^o from the intercept. The resulting plots of $\ln \left[C_b (1-\theta)/\theta \right]$ vs. θ are shown in Figure 4.12. From the slope and the intercept of the plots of Figure 4.12, the surface interaction parameter and standard free energy of adsorption at the pzc are 180 and 90 KJ mole⁻¹ respectively. The large positive values of g indicate that a repulsive interaction exists between the specifically adsorbed iodide ions, and they are an electrode charge dependent parameter. The larger the negative electrode charge, the larger

Figure 4.12 $\ln(\frac{C_b(1-\Theta)}{\Theta})$ vs. Θ for specific adsorption of iodide for polycrystalline lead prepared by method (D) at 200 Hz in mixed Na/NaI electrolytes at an ionic strength of 0.2. Key to various electrode charges: (O) 1.0; (x) 0.0; (Δ) -1.0 μ C/cm²



value of q.

(iv) Specific Adsorption of Thiocyanate, Bromide, Azide, and

Chloride - The effect of the nature of the anion including chloride,

bromide, and iodide on the differential capacitance at the poly
crystalline lead prepared by method (A) has been studied by Leikis.

However, of these anions, only iodide was employed to study the specific adsorption by utilizing the mixed electrolyte method.

The measurements and the analyses of the specific adsorption of thiocyanate, bromide, azide, and chloride at the polycrystalline lead prepared by method (D) at 1000 Hz were performed in a same manner as described above. Figure 4.8 summarizes the plots of the surface concentration as a function of the electrode charge for each of the anions examined. The summary of the standard free energy of adsorption of these anions is given in Table 4.1 which also contains corresponding data for mercury extracted from literature results. 81-83

4. Discussion

From the study of the time dependence of the measured capacitance, the diminution of capacitance values with time is uniform over the whole polarizable potential region as shown in Figure 4.4. It seems likely that this diminution cannot be exclusively explained by the possible existence of trace impurities of organic materials in the test solution. It, however, could possibly be associated with the reconstruction of the electrode surface. In general, the adsorption of organic molecules will depress the measured capacitance to a great

Table 4.1. Standard Free Energy of Adsorption $\Delta G_{\mbox{\scriptsize a}}^{\mbox{\scriptsize o}}$ for Several Anions at Lead, Mercury, and Silver Electrodes.

Electrolyte	Anion	(Pb) Method	Frequency (Hz)	-∆G°(q ^m mol	=0)KJ/ e ^e	g f
0.2M KF	ı-	Α	210	94	92*	50
0.2M NaF	I ⁻	D	200	90	86*	90
0.2M NaF	I ⁻	D	1000	90	86*	180
0.2M NaF	I ⁻	В	11	93	92*	117
0.2M NaF	NCS-	D	10	86	80*	200
0.2M NaF	Br ⁻	11	11	79	76*	120
0.2M NaF	N ₃ -	**	11	80	76*	140
0.2M NaF	ci-	II	11	∿74		
0.5M NaC10 ₄	ı-	II	11	83	77*	180
0.5M NaC104	NCS-	II .	10	81	75*	200
0.5M NaC104	Br ⁻	**	H	80	74*	350
1.0M KF	C1 ⁻	Hg	u	82		(b)
1.0M KF	Br ⁻	**	**	90		
0.95M NaF	N ₃	11	18	86		
0.95M NaF	NCS-	II	11			
0.95M NaF	I ⁻	11	п			
0.5M NaF	C1 ⁻	Ag	11	83	(c)	
0.5M NaF	Br ⁻	11	**	96		
0.5M NaF	N ₃ -	II	•	93		
0.1M NaC10 ₄	NCS-	n ·	п	115 ^(d)		

Evaluated at $\Theta = 0.01$.

^bThe g values at mercury are about 15 to 20.

^CThe g values at silver are about 10 to 15. d Evaluated at q^{m} = 15 μ C/cm².

^eFree energy of specific adsorption evaluated from the Frumkin isotherm.

fInteraction parameter.

extent in the region of the pzc. This is due to the decrease of the dielectric constant within the compact layer as a result of the enhancement of the dipole-dipole interaction between water and organic molecules in the pzc region.

The pzc is a fundamental characteristic of an electrode, and some studies have been done to try to correlate 84,85 the value of the pzc of various electrode materials to the work function, electronegativity, hydrophility, and heat of formation of surface oxide. The polycrystalline lead electrode 85 was shown to follow this correlation. As mentioned before, the pzc of the polycrystalline lead surface is the same for all three different pretreatment methods (A), (B), and (D). However, the distribution of individual single-crystal faces of the polycrystalline electrode can be significantly dependent on the way how the electrode surface is prepared. Since each singlecrystal face of a polycrystalline surface has its own pzc, then the pzc of the polycrystalline electrode might be a weighted average of the pzc's of individual single-crystal faces depending on their distribution.²⁴ Therefore, the difference in the effective pzc of polycrystalline electrodes of different combinations of individual single-crystal faces can be expected due to the difference in the electrode pretreatments. It has been shown that the pzc of the polycrystalline electrode is determined by the single-crystal face with the most negative value of pzc; 74 for example, $(1,1,1)^{86}$ at lead and (1,1,0)²⁴ at silver. Therefore, it is possible that different pretreatments can yield the same value of the pzc for the polycrystalline electrode, even though they may result in different

combinations of individual single-crystal faces.

According to the curve (a) of Figure 4.2, with method (A) the Russian school reported⁶³ a much sharper minimum in the capacitance curve at the pzc than that of curve (c) which was obtained by the use of method (D). It is likely that method (A) may preferentially etch the (1,1,1) single-crystal face of the polycrystalline lead electrode. In other words, this may imply that with method (A) the polycrystalline lead electrode possesses a greater degree of homogeneity. Furthermore, from the study of cyclohexane adsorption on the individual faces of lead single-crystal electrodes, 87 it shows that the property of the polycrystalline lead electrode pretreated by method (A) is similar to that of (1,1,1) lead single-crystal electrode. On contrast, the appearance of the broad minimum in the curve (c) at the pzc may indicate that with method (D) the polycrystalline lead electrode exhibits greater inhomogeneity. Another possible explanation for the broad minimum observed is related to the cause of the unexpected low value of the inner-layer capacitance.

Figure 4.3 shows that for concentrated (\geq 1 M) sodium perchlorate solutions the capacitance values decreased as the concentration increased. This was also noted for lead in Reference 88. This result may be associated with the pecularities of perchlorate adsorption, $^{89-92}$ which is only slightly hydrated. They can squeeze onto the surface in a fashion similar to organic molecules. However, a further increase in the capacitance values at fairly negative electrode potential is also observed, which can be explained by a reduction in the size of the hydration shell of cations 8 in strongly concentrated

solutions. 89-92

As seen in Figure 4.8, with method (A), curve (a), 78 the polycrystalline lead electrode shows a higher tendency to adsorb anions than that with methods (B) and (D), curves (b) and (c) respectively. This suggests that the (1,1,1) single-crystal face has higher activity for the adsorption of anions than other single-crystal faces. The high degree of inhomogeneity may be responsible for the relatively small adsorbabilities of anions at the polycrystalline lead electrode prepared by method (D). Furthermore, the difference in the capacitance values of curves (a), (b), and (c) of Figure 4.2 can also be attributed to the difference in the degree of homogeneities of the polycrystalline electrode. In general, the difference in the amount of the specifically adsorbed iodide ions at lead surfaces caused by the difference of the electrode pretreatments can be attributed to the difference in the availability of active sites on the lead surface for the specific adsorption of anions.

The values of g of the Frumkin isotherm are shown in Table 4.1. The g values of all the anions examined at lead electrodes are significantly larger than those for the corresponding anions at mercury electrodes. These high g values at lead electrodes may be attributed to the limitation of the active sites for the specific adsorption of anions.

The effect of the adsorption of perchlorate ions on the specific adsorption of interesting anions at lead electrodes is more significant in the case of weakly adsorbing anions. When the coadsorption of supporting electrolytes is considered, the complete

Gibbs adsorption equation 28 (cf. Equation 2.18) for mixed electrolytes having a composition xM NaX + (0.5 - x)M NaClO $_4$ will be

$$-d_{Y} = q^{m} \cdot dE + [\Gamma'_{X} - \{x/(0.5 - x)\}\Gamma'_{C10_{4}}]RTdlnx$$
 (4.3)

where Γ_X^+ and $\Gamma_{C10_4}^-$ are the components of Γ_X and $\Gamma_{C10_4}^-$ present in the inner layer, i.e., the surface concentration of specifically adsorbed anions. The derivation of Equation 4.3 assumes that the components of Γ_X and $\Gamma_{C10_4}^-$ in the diffuse layer, Γ_X^d and $\Gamma_{C10_4}^d$, respectively, are present in the same ratio as the anion mole fractions, i.e., Γ_X^d / $\Gamma_{C10_4}^d = x/(0.5-x)$. Figure 4.13 gives the differential capacitance curves for solutions of 0.5 M NaF and 0.5 M NaClO₄ at 1 K Hz. By assuming the value of EV to be 0.25 for the adsorption of perchlorate ions, the surface concentration of the adsorbed perchlorate ions at the pzc can be roughly calculated to equal 0.7 x 10^{-11} mole/cm² from the Hurwitz-Parsons analysis. This surface concentration corresponds to about 0.5% surface coverage. Therefore, the influence of the adsorption of perchlorate ions on the evaluation of the surface concentration of specifically adsorbed anions is negligible.

The surface coverage of the adsorbed perchlorate ions (0.5 M) at the polycrystalline lead at the pzc is about 0.5% as described above. Due to the limited active sites at lead electrodes prepared by method (D), even this small amount of coverage of perchlorate ions could diminish the adsorption of other anions. This effect is more pronounced in the measurement of the specific adsorption of bromide, azide, and chloride. For example, the surface coverage of

Figure 4.13 Differential capacitance at 1000 Hz vs. electrode potential for polycrystalline lead prepared by method (D) in (O) 0.5 M NaF and (x) 0.5 M NaClO $_4$

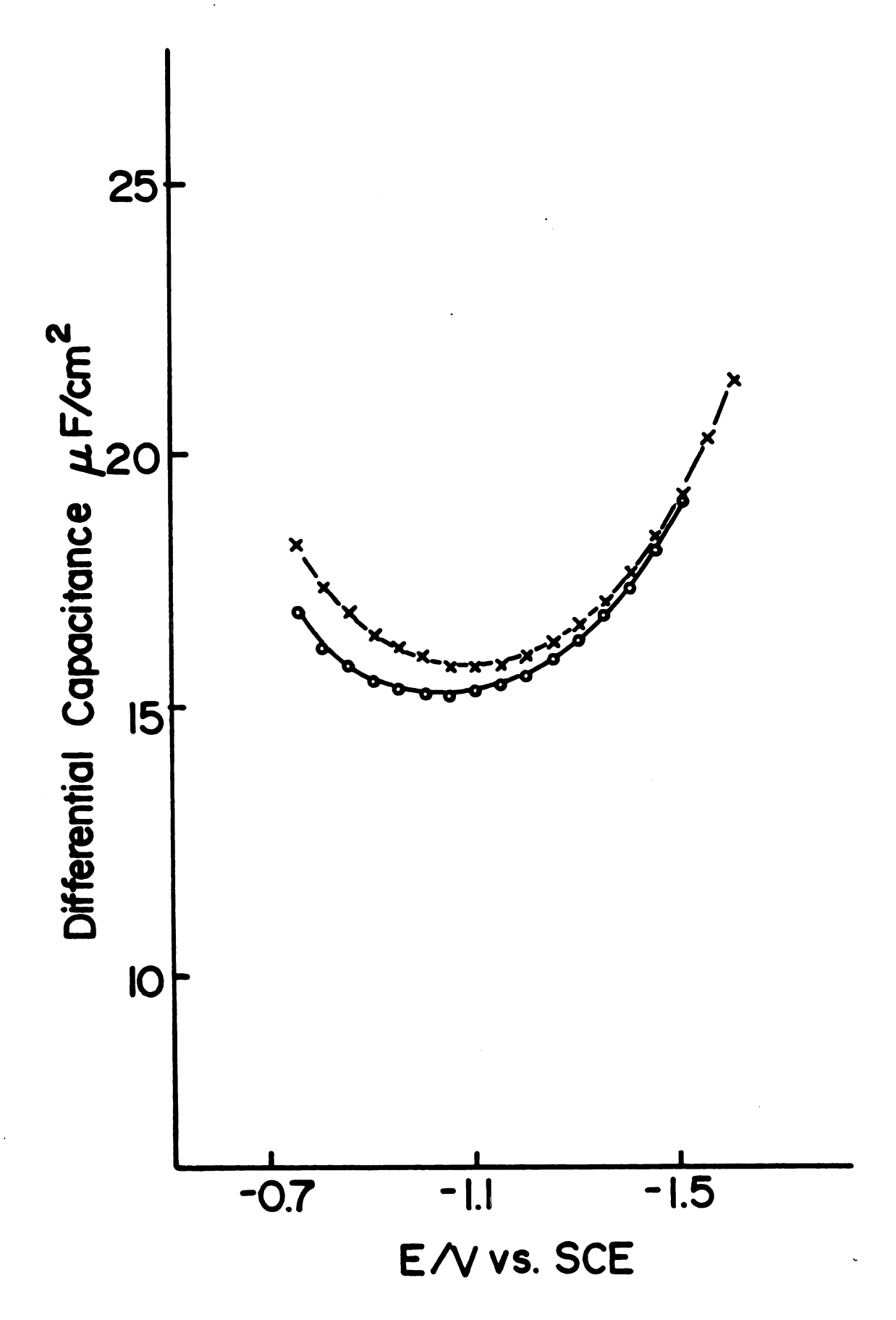


Figure 4.13

the specifically adsorbed bromide ions in 0.1 M NaBr + 0.4 M NaClO $_4$ solution is 0.56% at the pzc, which is quite compatible with the surface coverage of perchlorate ions for solution of 0.5 M NaClO $_4$ (\sim 0.5%). The g value for the specific adsorption of bromide ions changes from 120 to 350 as shown in Table 4.1 when the electrolyte is altered from fluoride to perchlorate. Thus, the effect of the competitive adsorption greatly influences the specific adsorption of anions at lead surfaces prepared by method (D), which is mainly due to the limited available active sites for the adsorption of anions. Furthermore, the g value is dependent on the electrode pretreatment as shown in Table 4.1. This can be attributed to the difference in the degree of homogeneity of the polycrystalline electrode.

Because of the large variation of the values of g as shown in Table 4.1, the free energy of adsorption is also evaluated at θ = 0.01. According to the values of the standard free energy of adsorption G_a° shown in Table 4.1, the order of the adsorbabilities of various anions examined at lead electrodes is $I^- > SCN^- > Br^- \ge N_3^- > C1^-$ which is similar to that of mercury 81-83 and silver 74 electrodes. Furthermore, the variations in the adsorbabilities of the anions examined at lead surfaces are larger in fluoride than in perchlorate electrolytes as judged from the difference in the values of ΔG_a° . $\Delta (\Delta G_a^\circ)^{I-Br}$ (= $(\Delta G_a^\circ)^{I}$ - $(\Delta G_a^\circ)^{Br}$) is about 3 KJ/mole in the perchlorate solutions, while it is about 6 KJ/mole in the fluoride solutions. This difference can be attributed to the effect of the adsorption of perchlorate ions.

According to Table 4.1, the extent of adsorption of all the anions examined at lead electrodes are lower than those of the corresponding

anions at mercury electrodes at a given electrode charge. The energies involved in the specific adsorption of ions at metal-solution interfaces can be attributed to the interactions between ion-ion, ion-metal, ion-solvent, and solvent-metal, as have been discussed in the literature. 93 As pointed out by Trasatti, 93 people tend to neglect the work connected with water desorption as an ion becomes adsorbed. 94-96 Thus, from the study of the effect of the nature of the electrode material upon the energies involved in the specific adsorption of ions, Trasatti^{85,97} emphasized the role of the solventmetal interaction. He⁸⁵ correlated the difference in the adsorbability of a certain anion at various metals to the difference in the surface potential of water $g_{M}^{H_2O}$ (dipole), which arises from the oriented water dipole, of various electrodes. The influence of the chemisorption of water upon the specific adsorption of ions was first brought out by Frumkin 98 in the analysis of the double layer structure of gallium electrodes. The water molecules tend to orient preferentially their oxygen ends toward the electrode surface, so that the orientation of inner-layer water molecules is independent of the nature of the electrode material at very negative electrode surfaces. 98 By the use of the above concepts, Trasatti⁸⁵ has calculated the surface potential of water $g_{M}^{H_2O}$ at the polycrystalline lead to be -104 mV, 34 mV more negative than that of mercury electrodes (-70 mV). In other words, lead exhibits a higher affinity for water than mercury. Therefore, a straightforward explanation for the low adsorbabilities of anions at lead surfaces compared with those at mercury surfaces can be drawn on the basis of the difference in the values of $g_{M}^{H_{2}O}$. In addition, from the measurement of the differential

capacitance at lead-nonaqueous interfaces prepared by method (D), we found out that a trace of water will significantly influence the measured capacitance values. This, again, implies that lead surfaces have a strong affinity for water molecules.

In this work, the value of the inner-layer capacitance at the pzc of lead electrodes prepared by method (D) was estimated to be $20 \text{ }_{\text{L}}\text{C/cm}^2$. This is relatively small compared to the literature value 40 $\mu\text{F/cm}^{285}$ (by the use of method (A)). The small inner-layer capacitance might be due to the high degree of inhomogeneity of polycrystalline lead electrodes prepared by method (D) or the existence of more than one water layer in the inner-layer region. The increase of the thickness of the inner-layer will result in the decrease of the innerlayer capacitance (= C_{M-2} = $\epsilon/4\pi d$). Therefore, the dielectric constant of water molecules adjacent to the electrode surface can be significantly dependent on the electrode pretreatment. Thus, the resulting thicker inner-layer of lead prepared by method (D) will prevent the incoming anions from specifically adsorbing at the electrode surface. However, with method (B) the adsorbabilities of anions at lead surfaces are much higher than those with method (D), even though these two methods yield the same value of C_{M-2} . This difference can be explained by the difference in the availability of active sites for the adsorption of anions between these two methods as described above.

As pointed out before, the values of EV for the specific adsorption of anions at lead surfaces are relatively larger than those at mercury surfaces. Usually, the value of EV is employed as a means of evaluating the partial charge transfer 100 in specific adsorption of ions at the electrode surfaces. However, it can also be taken

as a geometric factor 100 EV(g) which describes the position of the center of the adsorbed ions in the double layer in terms of potential and is defined as

$$EV(g) = \frac{\phi_{ad} - \phi_{S}}{\phi_{m} - \phi_{S}} \tag{4.4}$$

where ϕ_{ad} , ϕ_m , and ϕ_s are the potentials in the center of the adsorbed ion (i.e., iHp), the metal surface, and the bulk solution, respectively. The value of $(\phi_m - \phi_s)$ is the same for both lead and mercury electrodes at a given electrode charge. Therefore, according to Equation 4.4 the larger the values of EV, the larger the values of $|\phi_{ad} - \phi_s|$. To a first approximation, the position of the center of the adsorbed anions at lead surfaces is assumed to be the same as that at mercury surfaces. Then, the larger values of $|\phi_{ad} - \phi_s|$ are indicative of the smaller gradient of the potential profile in the double layer. Furthermore, the smaller gradient of the potential profile is indicative of the thicker inner-layer at the lead-aqueous interfaces compared with that at mercury surfaces. This is consistent with the estimated inner-layer capacitance at these two surfaces, $C_{M-2}^{Hg} > C_{M-2}^{Pb}$ as discussed above.

CHAPTER V

ELECTRODE KINETICS AT LEAD AND GALLIUM SURFACES

A. Rate Constants for Mechanistically Simple Transition-Metal Complexes

1. Introduction

Even though the double-layer structure of polycrystalline lead electrodes has been relatively well studied by other authors, 72,78,86,88 electrode kinetics at these surfaces have scarcely been investigated except for studies of the reduction of some anions. A number of electrode kinetics studies under well-defined conditions have been reported at mercury, 35 silver, 14 platinum, 14 and gold 14 electrodes. However, of these surfaces, only mercury has a double-layer structure which is understood in detail. In this study, measurements of the differential double-layer capacitance are combined with corresponding kinetics measurements for simple transition-metal reactants at lead electrodes prepared by method (D) in order to ascertain if the reactivity difference between lead and other surfaces, notably mercury, are explicable in terms of the conventional double-layer model described in Chapter II.

In this work, chromium(III) aquo and ammine complexes were chosen as reactants because of (i) the simplicity of electrode reactions involving these complexes which involve no bond breaking and formation during the electron-transfer process, (ii) the negative potential at which these reactants are reduced via an one-electron step is compatible with the negative polarizable potential region

characteristic of lead electrodes, (iii) the substitution inertness of chromium(III) complexes which eliminates the problem of ligand equilibrium yielding unknown reacting species, and (iv) the availability of relatively straightforward syntheses of these reactants.

The double-layer structure of the electrode-solution interface has been shown to play a very important role in the interpretation of electrochemical kinetics 35 as discussed in Chapter II. The most common way to correct the double-layer effect is to utilize the Frumkin equation. Some unexpected results for the electroreduction of several mechanistically simple transition-metal complexes were obtained at polycrystalline lead electrodes in this work. The difference of the rate constants observed between polycrystalline lead and mercury electrodes could not be simply explained by the conventional GCS double-layer model. It has been shown that at the potential of zero charge (pzc) the structure of water molecules adjacent to the gallium surface is drastically different from that at mercury. 85 Therefore, in this work kinetics measurements were also done at a hanging liquid gallium drop electrode (HGDE). In this study, the dependence of electrode kinetics upon the nature of the electrode material was examined, and reasons for the observed significant difference in rate constants remaining after the Frumkin correction are discussed.

2. Results

a. The Pretreatment Dependence

As shown in the last chapter, the amount of specifically adsorbed anions is greatly dependent upon the electrode pretreatment. Rate parameters were obtained on lead surfaces that were prepared by three different methods (B), 64 (C), 65 and (D), as described in Chapter III in order to examine to what extent the kinetics are sensitive to the history of the surface. Several chromium(III) complexes were chosen to examine this influence and typical results are shown in Table 5.1. From Table 5.1, it is evident that method (C) and (D) yield similar results for all the complexes examined, which is in accordance with the corresponding similarity of the differential double-layer capacitance obtained using these methods as described in Chapter II. On the other hand, method (B) yielded higher reaction rates for the complexes considered compared with methods (C) and (D). These three difference pretreatment methods yielded similar values of α_{app} for all the complexes examined. However, the reaction rate constants obtained using method (B) were found to decrease with time. Eventually, the reaction rate constants approached the values obtained on surfaces prepared using methods (C) and (D) within about twenty minutes. One possible reason for the decrease of reaction rates is that the lead surface is activated by the chemical polishing method (B) and is deactivated gradually.

For $Cr(0H_2)_5NCS^{2+}$ the difference in the rate constants obtained on surfaces pretreated using method (B) with respect to methods (C)

Table 5.1. The Pretreatment Dependence of the Measured Rate Constants at Lead Electrode for a Number of Transition-Metal Complexes.

	Meth	od B ^a ,f	Met	hod Ca	Met	hod Da
Reactant	lpha app	k _{app} cm/sec	α app	hod C ^a k _{app} cm/sec	lpha app	k _{app} cm/sec
Cr(OH ₂) ₆ ^{3+c}	0.62	7.9x10 ⁻⁴	0.6	3.5x10 ⁻⁵	0.6	2.0x10 ⁻⁵
Cr(OH ₂) ₅ 0SO ₃ ^{+d}	0.44	5.0x10 ⁻³	0.48	1.1x10 ⁻³		
Cr(NH ₃) ₅ C1 ^{2+C}	0.43	3.5x10 ⁻³	0.35	2.0x10 ⁻³	0.35	2.0x10 ⁻³
Cr(OH ₂) ₅ NCS ^{2+c}	0.44	1.7x10 ⁻¹	0.44	4.4x10 ⁻³		

^aLead pretreatment methods B, C, and D are described in the Experimental Chapter.

 $^{^{\}rm b}$ Apparent rate constant measured in 0.5 M NaClO $_4$ (pH = 2).

 $^{^{\}rm C}{\rm k}_{\rm app}$ evaluated at -1000 mV vs. SCE.

dk_{app} evaluated at -1200 mV vs. SCE.

^eDefined by $\alpha_{app} = -(2.3RT/F)(\Delta \log k_{app}/\Delta E)_{u}$.

 $^{^{}f}$ Since rate constants measured at lead electrodes prepared by method B were very unstable and decreased with time, the k_{app} listed were measured immediately after pretreatment.

and (D) is much larger than those for other complexes. Furthermore, the rate constants for the electroreduction of $Cr(OH_2)_5NCS^{2+}$ at surfaces prepared by method (B) after stabilization with time was still larger than that at surfaces pretreated using methods (C) and (D). Since the potential region at which $Cr(OH_2)_5NCS^{2+}$ is reduced is very close to the pzc of lead, the double-layer effect should be relatively small. Therefore, the large difference in the rate constants for $Cr(OH_2)_5NCS^{2+}$ may be due to the difference in the degree of adsorption of NCS at lead surfaces among different pretreatments. From measurements of specific adsorption of anions, method (B) has been shown to yield surfaces having a greater tendency to adsorb anions than that of method (D) as described in Chapter IV. Strictly speaking, the measured rate constant is a hybrid of those for competing inner-and outer-sphere reactions, and therefore dependent upon which reaction pathway will dominate. Due to the higher affinity for the adsorption of thiocyanate ions at lead surfaces prepared by method (B), it seems that the reduction of $Cr(OH_2)_5NCS^{2+}$ at lead electrodes pretreated using method (B) is more likely to follow inner-sphere pathways than that at lead surfaces prepared by other methods.

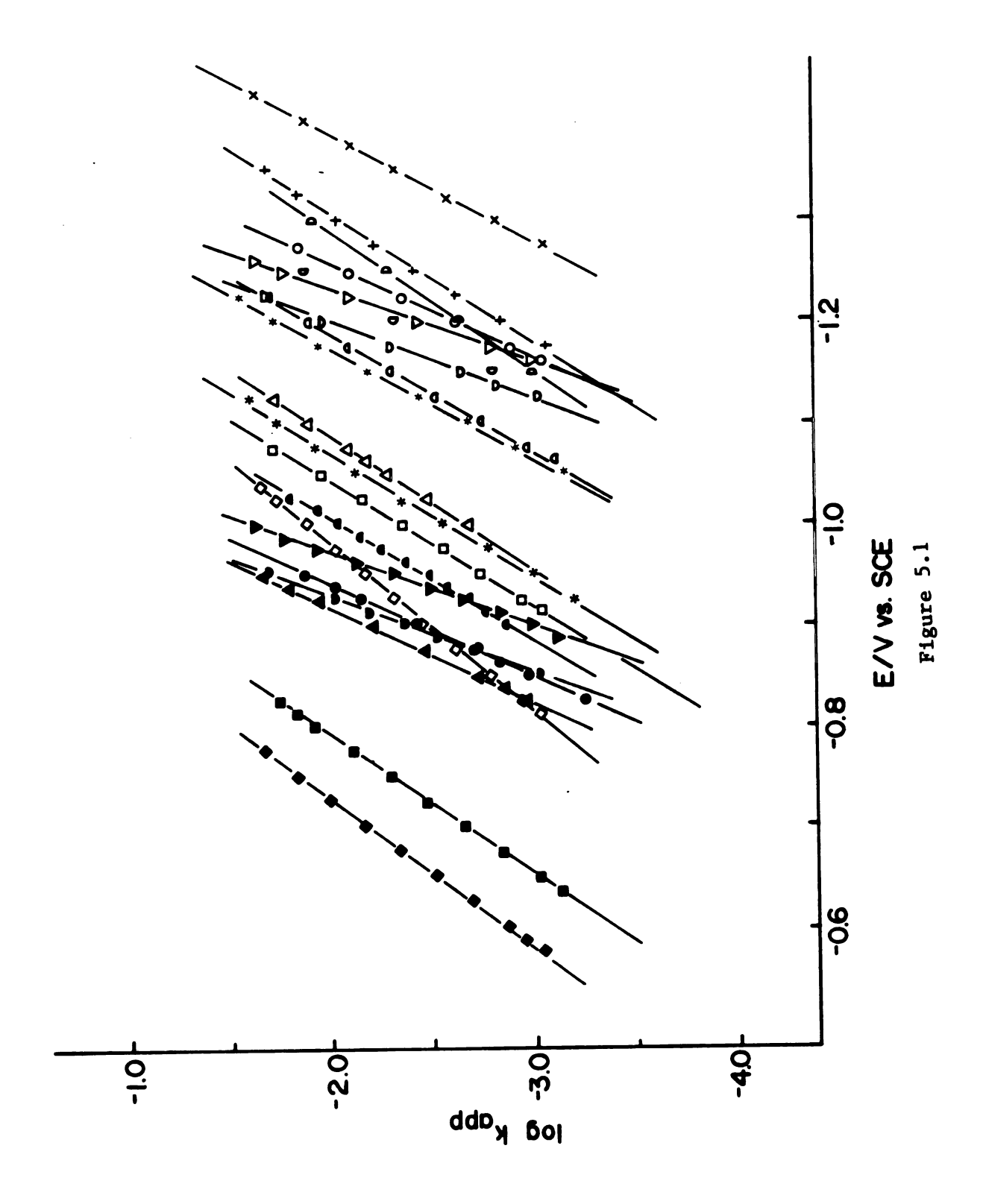
As metnioned in Chapter IV, the degree of homogeneity of poly-crystalline electrodes may significantly depend on the electrode pretreatment, which may be responsible for the pretreatment dependence of electrode kinetics. Table 5.1 shows that the electrode reaction rate constants for a number of transition metal complexes measured at lead surfaces are dependent on the electrode pretreatments. In this work, method (D) was used to prepare lead surfaces to study

electrode kinetics because the procedure is straightforward and yielded reproducible electrode surfaces.

b. The Apparent Rate Constants for the One-Electron Electroreduction of Cr(III) Aquo and Ammine Complexes at the LeadAqueous Interface

Measurements of the electroreductions of several Cr(III) complexes were performed at lead-aqueous interfaces using normal as well as pulse rotating-disk voltammetric techniques that are described in the Experimental Chapter. The analysis of the voltammograms was performed by using a conventional method utilizing the Levich equation. Figure 5.1 summarizes the resulting Tafel plots of log k_{app} , where k_{app} is the measured rate constant at a certain electrode potential, against the electrode potential E for some $Cr(OH_2)_5 X^{2+(+)}$ and $Cr(NH_3)_5 X^{3+(2+)}$ complexes where the ligand X is F⁻, Cl⁻, NCS⁻, $SO_{4}^{=}$, or OH_{2} , at both polycrystalline lead and mercury electrodes. The entire figure might look fairly complicated. However, it shows a very clear-cut trend. From the position of these Tafel plots, lead electrodes (open symbols) uniformly exhibit less electroactivity than mercury electrodes (closed symbols), i.e., at a given electrode potential the electroreduction rates of all the complexes examined are diminished when the electrode is changed from mercury to a polycrystalline lead electrode. These differences may be due to the large difference in the pzc between these two electrodes ($\Delta E_{pzc} \simeq 400$ mV). However, in spite of this significant difference in the observed rate constants, and in contrast to other solid electrodes such as

Figure 5.1 Log k_{app} , where k_{app} is the measured rate constant, vs. electrode poltential at mercury (closed symbols) and polycrystalline lead prepared by method (D) (open symbols) in 0.5 M NaClO₄ except for $Cr(NH_3)_5NCS$ in 40 mM La(ClO_4)₃ for a number of transition-metal complexes as follows: (o) $Cr(OH_2)_6^{3+}$; (∇) $Cr(NH_3)_6^{3+}$; (Δ) $Cr(NH_3)_5Cl^{2+}$; (\Box) $Cr(OH_2)_5NCS^{2+}$; (∇) $Cr(OH_2)_5Cl^{2+}$; (Δ) $Cr(NH_3)_5NCS^{2+}$; (∇) $Cr(NH_3)_5OH_2^{3+}$; (∇) $Cr(OH_2)_5N_3^{2+}$; (∇) $Cr(NH_3)_5OH_2^{3+}$; (∇) $Cr(OH_2)_5N_3^{2+}$; (∇) $Cr(NH_3)_5OH_2^{3+}$; (∇) $Cr(OH_2)_5OSO_3^{4+}$



silver, ¹⁴ platinum, ¹⁴, and gold, ¹⁴ the Tafel slopes obtained at lead electrodes are remarkably close to those of the corresponding Tafel slopes at mercury.

As mentioned in Chapter II, the difference in the rate constants for the electroreduction of several Cr(III) complexes between lead and mercury electrodes as shown in Figure 5.1 can arise from a number of factors, such as electrostatic double-layer effect, variation in the pre-exponential factors including electron tunneling and the frequency factor, and the influence of the solvent structure between the reacting species and the electrode surface.

c. Double-Layer Corrected Rate Constants

The conventional GCS model has long been applied successfully to the study of electrode kinetics. The electrostatic double-layer effect involves the Coulombic interaction between the reacting ion with an effective charge (Z - α_I) in the transition state and its surrounding double layer. Therefore, the work term due to the ionic double-layer effect can be formulated as (RT/F)[(Z - α_I) ϕ_{rp}]. The Frumkin relation, Equation 2.38, was utilized to calculate the corrected rate constants as described in Chapter II.

Table 5.2 lists the measured and double-layer corrected rate constants, k_{app} and k_{corr} , respectively, for a number of Cr(III) complexes and also Eu(III), V(III), and U(IV). For the calculation of the corrected rate constants, the potential at the average reaction plane ϕ_{rp} can be replaced by ϕ_2 that is calculated from the GCS model if the reacting ions are assumed to be at the outer Helmholtz

Table 5.2. Summary of Rate Constants for the Electroreduction of Several Transition-Metal Complexes at Lead and Mercury Electrodes.

Reactant	Electrode ^e	α app	k-1000mV ^a app	k ^{-1000mV^d corr}
Cr(OH ₂) ₆ ³⁺	Hg	0.63	4.4x10 ⁻²	2.8x10 ⁻³
	Pb	0.61	3.1x10 ⁻⁵	1.0x10 ⁻⁵
Cr(OH ₂) ₅ F ²⁺	Hg	0.55	2.5x10 ⁻⁴	4.8x10 ⁻⁵
	Pb	0.55	2.9x10 ⁻⁶	1.5x10 ⁻⁶
$Cr(OH_2)_5OSO_3^+$	Hg	0.49	2.8x10 ⁻³	1.6x10 ⁻³
	Pb	0.46	5.7x10 ⁻⁵	4.6x10 ⁻⁵
Cr(NH ₃) ₆ ³⁺	Hg	0.80	2.3x10 ⁻²	8.7×10 ⁻⁵
	Pb	0.76	5.7x10 ⁻⁶	3.8×10 ⁻⁷
$Cr(NH_3)_5OH_2^{3+}$	Hg	0.76	5.7x10 ⁻²	3.5×10 ⁻³
	Pb	0.73	1.8x10 ⁻⁵	6.4×10 ⁻⁶
$Cr(OH_2)_5N_3^{2+}$	Hg	0.42	1.4x10 ⁻²	2.7x10 ⁻³
	Pb	0.39	8.3x10 ⁻⁵	1.1x10 ⁻⁵
$Cr(NH_3)_5N_3^{2+}$	Hg	0.56	4.2x10 ⁻³	1.5x10 ⁻⁴
	Pb	0.48	6.9x10 ⁻³	8.7x10 ⁻⁶
Cr(OH ₂) ₅ C1 ²⁺	Hg	0.40	7.1x10 ⁻¹	1.4x10 ⁻¹
	Pb	0.35	1.3x10 ⁻²	6.9x10 ⁻³
Cr(NH ₃) ₅ C1 ²⁺	Hg	0.49	6.6x10 ⁻²	2.3x10 ⁻³
	Pb	0.35	2.0x10 ⁻³	2.5x10 ⁻⁴
cr(0H ₂) ₅ NCS ²⁺	Hg	0.43	3.3x10 ⁻¹	6.3x10 ⁻²
	Pb	0.44	4.4x10 ⁻³	1.6x10 ⁻³
Cr(NH ₃) ₅ NCS ^{2+C}	Hg	0.51	8.7x10 ⁻³	4.2x10 ⁻⁴
	Pb	0.50	2.3x10 ⁻⁴	8.0x10 ⁻⁵
Eu(OH ₂) ₆ ³⁺	Hg	0.62	2.5	1.5x10 ⁻¹
	Pb	0.41	6.1x10 ⁻³	2.2x10 ⁻³
V(OH ₂) ₆ ³⁺	Hg Pb	0.45	2.0x10 ⁻¹	7.1x10 ⁻²
υ0 <mark>2+</mark>	Hg Pb	0.60	8.7x10 ⁻⁵	1.8x10 ⁻⁵

^aApparent rate constant determined at an electrode potential of -1000mV vs. SCE at 23.5 \pm 0.5°C in 0.5 M NaClO₄ (pH \simeq 2).

^bApparent transfer coefficient derived from slope of Tafel plot.

^CDetermined in 40 mM $La(C10_4)_3$ (pH \simeq 2).

dRate constant corrected for ionic double layer effect.

^eLead electrodes were prepared by method D.

^{*}Rate constant is in cm/sec.

plane (oHp). The potential ϕ_2 can be calculated by knowing the electrode charge q^m as described in Chapter II. This can be obtained by integrating the experimental differential capacitance curves together with a knowledge of the pzc. The interaction between the coordinated ligands and surrounding solvent molecules can be significantly different for various complexes examined, which then can result in having different reaction planes. 46 The dependence of the value of $\varphi_{\mbox{\scriptsize rD}}$ used to calculate the corrected rate constants upon the structure of the metal complexes has been thoroughly discussed in the case of mercury. 46 In the aqueous solutions, for the reduction of Cr(III) aguo complexes due to strong hydrogen bonding between the coordinated aquo ligands and the surrounding water molecules, it is possible that there is another water layer separating the aquo complexes from the electrode surface as shown in Figure 2.3. The importance of hydrogen bonding between the coordinated aquo ligand and the surrounding water molecules has been demonstrated in the study of the isotopic effect 103 on the electroreduction rate constants of Cr(III) complexes.

From the study of electrode kinetics of several Cr(III) complexes at mercury electrodes, 46 it is seen that the reaction site for the electroreduction of Cr(III) aquo complexes in the sodium-based electrolytes could be outside the oHp which was judged from the disagreement between the experimental values of $(\partial_{\phi_2}/\partial_{\phi_1}^m)_{\mu}^{46}$ and the values predicted from the GCS model. The value of $(\partial_{\phi_2}/\partial_{\phi_1}^m)_{\mu}^m$ was determined from $(\partial_{\phi_2}/\partial_{\phi_1}^m)_{\mu}^m = (1/C)(\partial_{\phi_2}/\partial_{\phi_1}^m)_{\phi_2}^m$, where C is the average differential electrode capacitance in the appropriate electrolyte. This may be

associated with the dissimilar hydrated radii of sodium and chromium ions. Therefore, it is reasonable to take $\phi_2/2$ as ϕ_{rp} in the calculation of k_{corr} . The agreement of the coefficient of $(\partial\phi_2/\partial q^m)_{\mu}$ between the experimental data and that calculated from the GCS model has been taken as evidence that the reaction site for the electroreduction of Cr(III) aquo complexes could be at the oHp, i.e., ϕ_2 can be taken as ϕ_{rp} . Furthermore, the hydrated radii of lanthanum and chromium ions are very similar.

On the other hand, for the reduction of Cr(III) ammine complexes, it will be appropriate to use ϕ_2 as ϕ_{rp} in the calculation of k_{corr} because hydrogen bonding between the ammine ligands and the surrounding water molecules is relatively weak compared with that of aquo complexes. Thus, the radii of the ammine complex is also smaller than that of the aquo complex, i.e., ammine complexes will be expected to approach closer to the electrode surface.

The comparison of the electroactivity of lead and mercury electrodes for various complexes under consideration necessarily involves a certain degree of extrapolation of the corresponding Tafel plots due to the wide range of electrode potentials at which these complexes are reduced at the two electrode surfaces. However, as stated above, the Tafel slopes for most of the complexes examined at lead are quite comparable to those of the corresponding complexes at mercury electrodes, so that the extrapolation of the Tafel plots can be expected not to cause large errors. The values of $\alpha_{\rm app}$, (the transfer coefficient = - (RT/F)($\partial \ln k_{\rm app}/\partial E$) as defined earlier in Chapter II), are also included in Table 5.2. According to Table 5.2, the $k_{\rm corr}$ of lead electrodes are smaller than those of mercury electrodes. This

difference in the k_{corr} between lead and mercury can be attributed to a "specific substrate" effect. Furthermore, a general term, "M" allowing for the "specific substrate" effect, can be added to the Frumkin relation, Equation 2.38 can then be rewritten as

$$\ln k_{corr}^{E} = \ln k_{app}^{E} - \frac{F}{RT} (\alpha_{I} - Z)_{\phi_{rp}} + M$$
 (5.1)

where M can be attributed to the influence of the nature of the electrode material on the interaction between the metal complexes and their surrounding solvents, frequency factor, or even electron tunneling. The factors determining the term M can be partly illustrated by the evaluation of the activation parameters, which will be discussed later.

Since the applicability of the conventional GCS model for the study of the double-layer structure at polycrystalline electrodes has been discussed. 24,105 As noted in Chapter II Damaskin has proposed two distinct models to describe the polycrystalline-solution interfacial structure. In Damaskin's models, 24 the diffuse and compact layers of each individual single-crystal face of a polycrystalline electrode are considered. Thus, the dependence of the double-layer corrected rate constants upon the ionic strength of the supporting electrolyte has to be checked in order to test the validity of the GCS double-layer model used in the calculation of \mathbf{k}_{corr} that are listed in Table 5.2. Table 5.3 lists the rate constants of a number of Cr(III) complexes measured at polycrystalline lead and mercury electrodes in 0.5 M NaClO $_4$ as well as 40 mM La(ClO $_4$) $_3$ solutions. Table 5.3 also shows the corresponding values of α_{app} . Due

Rate Constants for Electroreduction of Some Cr(III) Complexes Measured at Lead and Mercury Electrodes in 0.5 M NaCl 0_4 and 40 mM La(Cl 0_4) $_3$. Table 5.3.

Reactant	Electrode	Electrolyte	app	k-1000mV ^a app	k-1000mV ^{b,d} corr	k-1000mv ^{b,c} corr
Cr(0H ₂) ₆	Нg	0.5M NaClO ₄ 40mM La(ClO ₄) ₃	0.64	4.4×10 ⁻² 1.4×10 ⁻²	2.8x10 ⁻³ 2.0x10 ⁻³	1.8x10 ⁻⁴ 2.9x10 ⁻⁴
	Pb	0.5M NaClO ₄ 40mM La(ClO ₄) ₃	0.61	3.1×10 ⁻⁵ 2.6×10 ⁻⁵	1.0x10 ⁻⁵ 1.1x10 ⁻⁵	3.7×10 ⁻⁵ 4.5×10 ⁻⁶
Cr(NH ₃) ₆	Н	$0.5M \text{ NaClO}_4$ $40mM \text{ La(ClO}_4)_3$	0.80	2.3x10 ⁻² 1.2x10 ⁻²	1.4×10 ⁻³ 1.7×10 ⁻³	8.7×10 ⁻⁵ 2.5×10 ⁻⁴
	Q	0.5M NaC10 ₄ 40mM La(C10 ₄) ₃	0.76	5.7×10 ⁻⁶ 5.9×10 ⁻⁵	1.9x10 ⁻⁶ 2.2x10 ⁻⁶	6.8×10 ⁻⁷ 1.0×10 ⁻⁶
cr(0H ₂) ₅ F ²⁺	Н	0.5M NaC10 ₄ 40mM La(C10 ₄) ₃	0.55	2.5×10 ⁻⁵ 5.9×10 ⁻⁵	4.8x10 ⁻⁵ 1.8x10 ⁻⁵	8.8×10 ⁻⁶ 5.7×10 ⁻⁶
	P	$0.5M \text{ NaClO}_4$ $40mM \text{ La(ClO}_4)_3$	0.55	2.9x10 ⁻⁶ 5.2x10 ⁻⁶	1.5×10 ⁻⁶ 3.1×10 ⁻⁶	8.1×10 ⁻⁷ 1.8×10 ⁻⁶
сr(0H ₂) ₅ 0S0 [‡]	Н	0.5M NaC10 ₄ 40mM La(C10 ₄) ₃	0.47	2.8x10 ⁻³ 1.5x10 ⁻³	1.6x10 ⁻³ 1.0x10 ⁻³	9.2×10 ⁻⁴ 6.9×10 ⁻⁴
	Pb	0.5M NaClO ₄ 40mM La(ClO ₄) ₃	0.46	5.7×10 ⁻⁵ 4.8×10 ⁻⁵	4.6x10 ⁻⁵ 3.9x10 ⁻⁵	3.7×10 ⁻⁵ 3.4×10 ⁻⁵

Table 5.3. Continued.

^ak_{app} is apparent rate constant evaluated at -1000mV vs. SCE.

 $b_{corr}^{b_{corr}}$ is rate constant corrected for ionic double layer effect. Determined from log $k_{corr} = \log_{app} \frac{1}{2.3 \, \text{RT}} \phi_{rp}$, where ϕ_{rp} is the potential at the average reaction plane. c_{corr} determined by taking ϕ_2 as ϕ_{rp} , where ϕ_2 is calculated from the GCS theory. $\phi_{corr}^{b_{corr}}$ determined by taking $\phi_2/2$ as ϕ_{rp} .

*Rate constant is in cm/sec.

to the discreteness-of-charge effect, 105 the micropotential at the reaction site ϕ_r may differ from the average (macro-) potential on the reaction plane ϕ_{rp} . The effect of the supporting electrolyte cation on the reaction site for the electroreduction of $\text{Cr}(\text{OH}_2)_6^{3+}$ and $\text{Cr}(\text{NH}_3)_6^{3+}$ has been well investigated at mercury electrodes. 106 In Table 5.3, both $\phi_2/2$ and ϕ_2 were used to calculate k_{corr} . These provide appropriately lower and upper limits, respectively, for the use of the GCS model in the calculation of k_{corr} .

According to Table 5.3, the k_{corr} of all the complexes measured in 0.5 M NaClO $_4$ are similar to those measured in 40 mM La(ClO $_4$) $_3$, and this is true for both lead and mercury electrodes. The similarity of k_{corr} in different ionic strength solutions supports the appropriate validity of the application of the conventional GCS model in the calculation of ϕ_{rp} and hence the corrected rate constants.

d. Rate Constants of Some Cr(III) Complexes Measured at a Hanging Liquid Gallium Drop Electrode (HGDE)

Damaskin and Frumkin 103 introduced the concept of chemisorbed water molecules with oxygen atom towards the metal as being responsible for the residual orientation of dipoles at the pzc. This concept has been successfully applied to explain the abnormally high inner-layer capacitance at pzc obtained at gallium-aqueous interfaces 85 compared with that at mercury-aqueous interfaces, for example, in 1 M Na $_2$ SO $_4$ solution 1 C $_{M-2}^{Hg}$ = 30 $_{\rm HF}$ /cm 2 and 1 C $_{M-2}^{Ga}$ = 135 $_{\rm HF}$ /cm 2 . Furthermore, Trasatti used the same notion to calculate the surface potential of water due to oriented water dipoles $g_{\rm M}^{\rm H2O}$ (dipole) as

discussed in Chapter IV. He found that at the pzc g_{Hg}^{H20} = -0.07 V in 0.1 M NaF and $g_{G_a}^{H20}$ = -0.32 V in 0.1 M NaClO₄.

Since the water structure at the gallium-aqueous interface is remarkably different from those at lead- and mercury-aqueous interfaces as described above. The study of electrode kinetics at the gallium-aqueous interface may provide insight into the observed "specific substrate" effect on outer-sphere electrode reactions between lead and mercury electrodes as mentioned before. A HGDE that is described in the Experimental Chapter was used to study electrode kinetics at gallium surfaces. Table 5.4 shows rate constants, kann and k_{corr} , for some Cr(III) complexes measured at mercury, lead, and gallium electrodes. The rate constants of gallium electrodes were evaluated from cyclic voltammograms. The analysis of cyclic voltammograms has already been described in Chapter III. As is expected, there are still significant differences in the rate constant after double-layer correction between gallium and the other two surfaces. This, again, is an indication of the presence of the "specific substrate" effect for the electrode reactions examined.

Since at the gallium electrode the potential at which $Cr(NH_3)_6^{3+}$ is reduced is near the anodic limit of the electrode (-0.9 V vs. SCE), the rate constants of $Cr(NH_3)_6^{3+}$ measured at the gallium surface as listed in Table 5.4 may be questionable.

Rate Constants for the Electroreduction of a Number of Cr(III) Complexes Measured at Mercury, Gallium, and Lead Electrodes. Table 5.4.

Reactant	(a)	k-1000mV ^C App	k_l000mv ^{d,e}	k_looomv ^{d,f} corr	k-1000mV ^{g,e} corr	k_1000mv9.f
Cr(0H ₂) ₅	Hg Gab Pb	4.4×10 ⁻² 6.3×10 ⁻⁶ 3.1×10 ⁻⁵	2.8×10 ⁻³ 1.2×10 ⁻⁶ 1.0×10 ⁻⁵	1.8×10 ⁻⁴ 2.2×10 ⁻⁷ 3.9×10 ⁻⁶	1.9×10 ⁻⁶	1.2×10 ⁻⁷
Cr(NH ₃) ₆	Hg Gab Pb	2.3x10 ⁻² ~ 4x10 ⁻⁴ 5.7x10 ⁻⁶	1.4×10 ⁻³ ~ 8×10 ⁻⁵ 1.9×10 ⁻⁶	8.7×10 ⁻⁵ ~ 2×10 ⁻⁵ 6.8×10 ⁻⁷	∿ 2×10 ⁻⁴	^ 3×10 ⁻⁵
Cr(NH ₃) ₅ 0H ₂	Hg Gab Pb	5.7x10 ⁻² 6.9x10 ⁻⁵ 1.8x10 ⁻⁵	3.5×10 ⁻³ 1.2×10 ⁻⁵ 6.4×10 ⁻⁶	2.1×10 ⁻⁴ 2.5×10 ⁻⁶ 2.2×10 ⁻⁶	1.6x10 ⁻⁵	1.5×10 ⁻⁶
сr(ОН ₂) ₅ 0S0 ⁺	Hg Gab Pb	2.8×10 ⁻³ 2.3×10 ⁻⁵ 5.7×10 ⁻⁵	1.6×10 ⁻³ 1.6×10 ⁻⁵ 4.6×10 ⁻⁵	9.2×10 ⁻⁴ 1.2×10 ⁻⁵ 3.7×10 ⁻⁵	1.3×10 ⁻⁵	7.5×10 ⁻⁶

^aElectrode.

^DData were obtained by the use of HGDE that was described in the Experimental Chapter. Rate constants were evaluated from cyclic voltammograms.

^CApparent rate constant at room temperature evaluated at -1000mV vs. SCE in 0.5 M NaClO₄. dRate constant corrected for double layer effect. Determined from logk corr=logk app $\frac{F(\alpha-Z)}{2.3}$ NHere ϕ_{rp} is the potential at the average reaction plane. e $\phi_{rp}=\phi_2/2$, where ϕ_2 is calculated from the GCS theory. f $\phi_{rp}=\phi_2$.

 $^{\psi}rp$ $^ ^{\psi}2^{\cdot}$. Gorrected rate constant at the peak potential of the corrected rate constant at the peak potential of the corresponding cyclic voltammogram at scan rate 100mV/sec, by assuming α_{corr} = 0.5.

*Rate constant is in cm/sec.

3. <u>Discussion</u>

a. Surface Contaminants

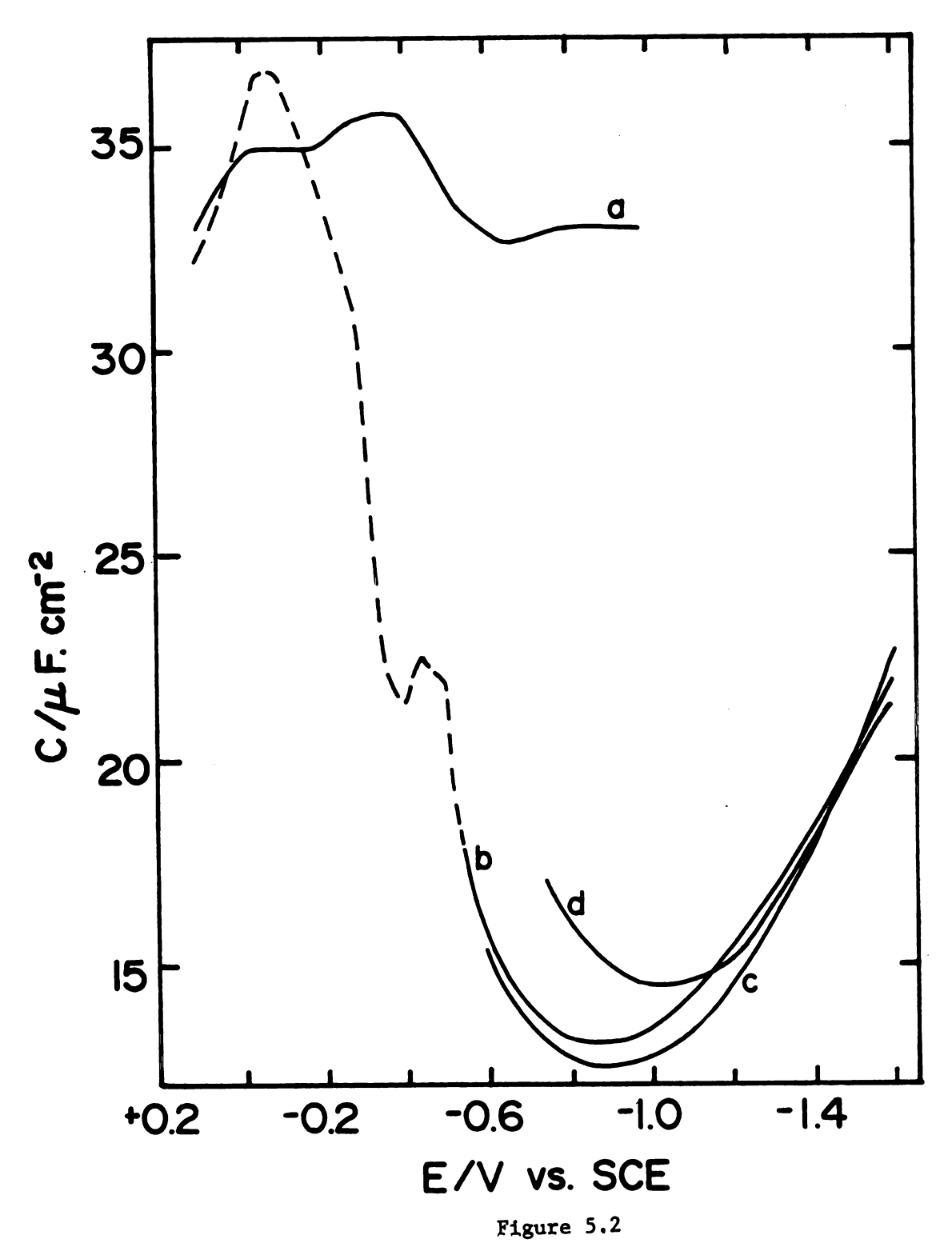
Most of the solid electrodes, such as silver, platinum, and gold, exhibit substantial electrocatalyses of electrode reactions compared with mercury electrodes. However, Table 5.2 shows that rate constants, measured as well as double-layer corrected, at polycrystalline lead electrodes are noticeably smaller than those at mercury electrodes. In this work, most of the experiments employed the mechanical pretreatment method (D) to prepare the lead electrode before each measurement.

One possible explanation for this "decatalysis" of electrode reactions at polycrystalline lead surfaces is that the lead surface is grossly contaminated by impurities from polishing agents, an oxide film, or defects in the lead sample used to fabricate the working electrode. Therefore, it is desirable to do some experiments in order to characterize the polycrystalline lead surface after the pretreatment. The activity of electrode reactions is very sensitive to the electrode-solution interfacial structure which is highly dependent on the way in which the electrode is prepared.

Any likelihood that the electrode surfaces used in this work are grossly contaminated can be largely precluded from the following experimental results.

(i) Lead upd (underpotential deposition) on a polycrystalline silver surface: Figure 5.2 presents the differential capacitance

Figure 5.2 Differential electrode capacitance C against electrode potential E for (a) polycrystalline silver. (b) silver containing a monolayer of upd lead. (c) as in (b) but with additional ca. two monolayers of bulk lead deposit. (d) polycrystalline lead. Lead layer prepared as indicated in Ref. 108. Electrolyte was 0.5 M NaClO₄, pH 3.5; for (b) and (c) additionally contained 0.6 µM Pb⁺²



curves of 0.5 M NaClO₄ solution at polycrystalline silver, polycrystalline lead, and lead upd surfaces at 1 KHz. The lead upd has been reported 108 to yield the same value of the pzc (in 10 mM NaF) as that of polycrystalline lead electrodes (-0.8 V vs. SCE). According to Figure 5.2, it is surprising to see that the behaviors of lead upd on silver, curves (b) and (c), in the measurement of the differential double-layer capacitance are drastically different from those of polycrystalline silver, curve (a), but are similar to those of polycrystalline lead curve (d). Since the deposition of the lead onto the silver surface was done in a deaerated solution, the possible formation of the oxide film should be avoided.

(ii) The addition of lead ions in the measurement of electrode kinetics at lead surfaces: 110 By the addition of lead ions, lead metal can be continuously deposited onto the working lead electrode surface. Since the rate of lead deposition (with $[Pb^{2+}] \geq 100~\mu\text{M})$ may be faster than the rate of diffusion-controlled surface contamination, the lead surface can be replenished continuously during the measurement of electrode kinetics. Even though these two processes are in parallel, the surface coverage of the lead electrode is dominated by the process of the continuous lead deposition (>99%); because the concentration of the impurities should be very small (<1 μM). Therefore, in this study, the observed electrode kinetics at the lead surface must be associated with the major coverage of the electrode surface, lead. As is expected, there was no significant change in the measured rate constants for $\text{Cr}(O\text{H}_2)_5\text{NCS}^{2+}$ with the addition of lead ions.

- (iii) Electrode kinetics at the gallium-solution interface.

 As will be described later, electrode kinetics at the gallium-aqueous interface is similar to that at the lead surface.
- (iv) Cyclic Voltammetry: 107 Cyclic voltammetry has been shown to be a very convenient technique to monitor the electrode surface condition. Figure 4.1 is a typical cyclic voltammogram for 0.5 M NaClO₄ solution at the polycrystalline lead pretreated using method (D), and different pretreatments yielded similar voltammograms. The resulting smooth voltammogram suggests that the electrode surface is ideally polarizable.

b. Reaction Mechanisms

In Chapter II, two methods 32 for the distinction of inner- from outer-sphere reactions are described; these involve measurements of (i) the response of the reaction rate to the addition of strongly adsorbed but chemically inactive anions and (ii) the potential dependence of the reaction rate (i.e., $\alpha_{\rm app}$).

The effect of the specific adsorption of chemically inert anions such as Cl⁻, Br⁻, or I⁻ on the electrode reaction rates is recognized as a straightforward way to distinguish inner- from outer-sphere reaction pathways. ³² The reaction mechanisms of all the complexes used in this work at mercury electrodes have already been discussed in detail. Most of the polarizable potential range of lead in aqueous solutions at which the reactants are reduced is on the negative side of the pzc. From the measurement of the specific adsorption of anions as discussed in Chapter IV, it is evident that the adsorbability

of anions is relatively small. Therefore, in the case of lead electrodes, this method may not be applicable. Anyway, the addition of iodide ions resulted in the increase and decrease of reaction rates of Eu(III) and $\text{Cr}(0\text{H}_2)_5\text{Cl}^{2+}$ respectively, and which is comparable to what was observed at mercury and outer- and inner-sphere pathways 32 are assigned to the electroreduction of Eu(III) and $\text{Cr}(0\text{H}_2)_5\text{Cl}^{2+}$ respectively. For other systems, due to the relatively negative potentials at which they are reduced, there are no significant changes in the observed reaction rates with the addition of iodide ions.

As outlined in Chapter II, the reaction mechanisms can be assigned according to the value of the corresponding transfer coefficient α_{app} , i.e., α_{app} < 0.5 assigned for inner-sphere pathways and α_{app} > 0.5 for outer-sphere pathways. In the case of mercury, for the reduction of several Cr(III) complexes used in this work, it has been 32 that the assignment of the reaction mechanisms of these reactants based on the values of $\boldsymbol{\alpha}_{\text{DD}}$ is consistent with that based the effect of the addition of strongly adsorbed but chemically inert anions. The Tafel slopes at lead in Figure 5.1 are close to those of the corresponding Tafel plots at mercury. Then, it is likely that the assignment of the reaction mechanisms of the reactants examined at lead surfaces can be done in a similar way. Thus, from Table 5.2, those complexes with $\alpha_{app} > 0.5$, such as $Cr(OH_2)_6^{3+}$, $Cr(NH_3)_6^{3+}$, and $Cr(NH_3)_5OH_2^{3+}$ follow outer-sphere pathways, and those with α_{app} < 0.5, such as $Cr(OH_2)_5C1^{2+}$, $Cr(NH_3)_5C1^{2+}$, $Cr(OH_2)_5NCS^{2+}$, and $Cr(NH_3)_5NCS^{2+}$ follow inner-sphere pathways.

c. <u>The Dependence of Outer-Sphere Electrode Kinetics on the Nature</u> of the Electrode Material

To a first approximation, it is expected that for outer-sphere electrode reactions, in which there is no direct interaction between the metal surface and reacting ions in the transition state, the nature of the electrode material should have no specific influence on the measured rate constants after Frumkin correction. 14,102 According to Table 5.2, the apparent rate constants, k_{app} , of all the complexes examined at lead surfaces are two to three orders of magnitude smaller than those at mercury. As noted above, these differences may be due to the large difference of the pzc between lead and mercury electrodes which will result in different values of φ_2 at a given electrode potential, i.e., these differences in k_{app} are due to the double-layer effect. However, k_{corr} , double-layer corrected rate constants, in Table 5.2 at lead are still significantly smaller than those at mercury. This implies that the existence of a "specific substrate" effect on outer-sphere reactions.

There is another way to illustrate the presence of the "specific substrate" effect as follows. Considering Equation 2.38

$$lnk_{app}^{E} = lnk_{corr}^{E} - (Z - \alpha_{I}) \frac{F}{RT} \phi_{rp}$$
 (2.38)

The difference in the observed rate constants between mercury and lead electrodes for the electroreduction of a given reactant can be expressed as

$$\Delta \log_{app}^{Hg-Pb} = \frac{-F(Z - \alpha_I)}{2.3RT} \Delta \phi_{rp}^{Hg-Pb}$$
 (5.2)

Equation 5.2 is derived under the condition that there is no "specific substrate" effect, i.e., $\Delta logk_{corr}^{Hg-Pb} = logk_{corr}^{Hg} - logk_{corr}^{Pb} = 0$. Since the values of $\Delta \rho_{rp}^{Hg-Pb}$ can be assumed to be the same for any reactant, the ratio of $\Delta logk_{app}^{Hg-Pb}$ for reactants with various charges shall be equal to the ratio of $(Z - \alpha_I)$ where Z is the charge of the reactant. Note that this method does not require a knowledge of the diffuse-layer potential at either surface. Therefore, upon comparing the rate constants of $Cr(OH_2)_6^{3+}$, $Cr(OH_2)_5^{5+2}$, and $Cr(OH_2)_5^{5+2}$, decay where $Cr(OH_2)_5^{5+2}$ is the expected ratio of $(\Delta logk_{app}^{Hg-Pb})^{Cr(OH_2)_6^{5+2}}$: $(\Delta logk_{app}^{Hg-Pb})^{Cr(OH_2)_5^{5+2}}$ is $(\Delta logk_{app}^{Hg-Pb})^{Cr(OH_2)_5^{5+2}}$ in the three reactants considered is 1.87 : 1.14 : 1., which is far from the expected ratio 5 : 3 : 1. This result strongly supports the presence of a "specific substrate" effect described as an extra term M to Equation 2.38, as in Equation 5.1.

The variation in $k_{\tt COTT}$ between these two surfaces examined are somewhat dependent upon the nature of the coordinated ligands of the metal complexes examined. This indicates the presence of a specific interaction between the coordinated ligands and the surrounding solvents within the transition state, and which depends on the nature of the electrode material.

As has been reported 46 at mercury electrodes, electrode kinetics of the reduction of $Cr(NH_3)_5OH_2^{3+}$, which is formed by simply replacing

one of the ammine ligands of $Cr(NH_3)_6^{3+}$ with an aquo ligand, are different from that of $Cr(NH_3)_6^{3+}$, but are similar to those of $Cr(OH_2)_6^{3+}$. Furthermore, the difference in k_{corr} between $Cr(NH_3)_6^{3+}$ and $Cr(NH_3)_5OH_2^{3+}$ is probably due to an inner-shell effect which depends on the bond length and bond strength between the center metal and its coordinate ligands. This observation was also found in this work. According to Table 5.2, k_{corr} of $Cr(NH_3)_5OH_2^{3+}$ at lead is close to that of $Cr(OH_2)_6^{3+}$, but much larger than that of $Cr(NH_3)_6^{3+}$. Because of the strong hydrogen bonding interactions between the aquo ligand and the surrounding water solvents, $Cr(NH_3)_5OH_2^{3+}$ the aquo ligand may orient toward the electrode surface, i.e., the electrode would mostly experience the aquo ligand during the electron-transfer process in spite of the presence of the five ammine ligands.

The study of electrode kinetics at the gallium-aqueous interfaces not only provides strong evidence against the possible formation of an oxide film at the lead surfaces used in this work but also emphasizes the importance of the role of the solvent molecules in the evaluation of the electron-transfer processes. According to Table 5.4, for $\text{Cr}(\text{OH}_2)_6^{3+}$ the order of the corrected rate constants for the three metal examined is $k_{\text{corr}}^{\text{Ga}} < k_{\text{corr}}^{\text{Pb}} < k_{\text{corr}}^{\text{Hg}}$ which is in accordance with the order of the values of $g_{\text{M}}^{\text{H2}0}$ of these electrodes. Gallium seems to influence greatly the extent of the interaction between the coordinated aquo ligand of metal complexes and the water molecules situated between the metal complexes and the electrode surface. The slow reaction rate of $\text{Cr}(\text{OH}_2)_6^{3+}$ observed at gallium can be partly explained by the change in the reaction site due to the presence of

a strong solvent-surface interaction. For $Cr(NH_3)_50H_2^{3+}$ and $Cr(0H_2)_5-SO_4^+$, the order of rate constants is also $k_{corr}^G \cong k_{corr}^{Pb} < k_{corr}^{Hg}$. This trend also shows the dependence of electrode kinetics of the aquo complexes upon the water structure at the electrode surface. As stated above, due to the possible presence of the ligand orientation effect for the electroreduction of $Cr(NH_3)_50H_2^{3+}$, it is expected to see $k_{corr}^G < k_{corr}^{Pb}$ for $Cr(NH_3)_50H_2^{3+}$. This is, however, contrary to what is observed $k_{corr}^G \cong k_{corr}^{Pb}$. These data seem to imply that the "specific substrate" effect is smaller for ammine as compared to otherwise similar aquo complexes. Thus, for the reduction of $Cr(NH_3)_6^{3+}$, k_{corr}^G is similar to k_{corr}^{Hg} .

B. Evaluation of Electrochemical Activation Parameters

1. Results

Measurements of the temperature dependence of rate constants for a number of Cr(III) complexes and Eu(III) were performed at polycrystalline lead electrodes utilizing a nonisothermal cell. In this work, a specially designed disk electrode that is described in Reference 56 was used. The procedure used to analyze the data obtained from the temperature dependence of the rate constants has been clearly illustrated in Chapter II. Table 5.5 shows the rate constants, k_{app} and k_{corr} , and the corresponding activation parameters of a number of Cr(III) complexes and Eu(III) at both mercury 47 and lead electrodes. The corrected rate constants k_{corr} were obtained by utilizing the Frumkin equation. According to Equation 2.43, it is necessary to

Activation Parameters for the Electroreduction of Various Trivalent Metal Complexes at the Mercury- and Lead-Aqueous Interfaces. Table 5.5.

Reactant	(a)	арр	(a) α_{app}^{c} kapp	k-1000mV ^d corr	ΔG _{corr}	AH [*] f	ΔS _o g rc	$\Delta S_{rc}^{\circ} \Delta S_{ideal}^{*} \Delta S_{corr}^{*}$	ΔS [*] i	Aj	ΔS*K
Eu(ОН ₂)3+	Hg Pb	0.62	2.5 6.1x10 ⁻³		6.1	11.5	47	25 -1.9	18 -3.9	3.0×10 ³ 9 5.0×10 ⁻³	-5.5 -27
$cr(0H_2)_2^{3+}$	ъ В	0.63	4.4×10^{-2} 3.1×10^{-5}	2.8×10^{-3} 1.0×10 ⁻⁵	8.5 11.8	14.7	49	27 1.0	21 -1.2	7.5x10 ² 2 1.2x10 ⁻²	-3.5 -30
Cr(NH ₃) ₆	5 6	0.80	1.2×10^{-2} 5.9×10^{-6}	2.5×10 ⁻⁴ 1.0×10 ⁻⁶	9.9	13.9	35	22 1.8	13	5.6×10 ² 8.8×10 ⁻³	-4.5 -26
$cr(NH_3)_{5}OH_2^{3+}$	Б 6	0.76	5.7×10 ⁻² 1.8×10 ⁻⁵	3.5×10^{-3} 6.4×10^{-6}	8.4	13.7	40	25 -14	17 -16	2.0 6.0×10 ⁻⁵	-2.0 -36
сr(0H ₂)5с1 ²⁺	P. G.	0.40	7.6×10^{-1} 1.3×10^{-2}	1.4×10^{-1} 6.9×10^{-3}		11.4		20 -1.9			
Cr(0H ₂) ₅ NCS ²⁺	Нд Ръ	0.43	3.3×10^{-1} 4.4×10^{-3}			12.9		21			

 a Measured in 40 mM La(ClO $_{4}$) $_{3}$.

^DApparent rate constant at 25°C. Determined at an electrode potential of -1000mV vs. SCE.

CApparent transfer coefficient derived from slope of Tafel plot, equal to -(RT/F)(3&nk_{app}/3E) .

^dRate constant corrected for ionic double layer effect.

f"Ideal" enthalpy of activation corrected for double layer effect (Kcal/mole), its determination was erree energy of activation corrected for double layer effect (Kcal/mole), determined from -ΔG* = $RT(lnk_{corr} - lnZ_e)$, where $Z_e = 5000 \text{ cm/sec}$.

described in Chapter II.

Table 5.5. Continued.

9"Thermodynamic" reaction entropy (cal/deg mole) for appropriate M(III)/M(II) couple. Data taken from Reference 39.

 $^{h}.Ideal"$ entropy of activation (cal/deg mole), derived from $^{\Delta H}_{ideal}$ using Equation 2.32 by assuming $_{i}^{\kappa}e_{l}$ = 1 and $^{2}e_{l}$ = 5.0x10³ cm/sec.

<code>iEntropy</code> of activation (cal/deg mole) after correction for double layer effect, determined at 25°C from T $\Delta S_{corr}^* = \Delta H_{corr}^* - \Delta G_{corr}^*$.

<code>iFrequency factor determined from k_corr = A exp ($\Delta S_{corr}^*/R$) exp($\Delta S_{corr}^*/R$) by assuming $\Delta S_{corr}^* = \Delta S_{rc}^*$.

<code>k"Real" entropy (cal/deg mole) of activation determined from $\Delta S_{real}^* = \Delta S_{corr}^*$.

*</code></code>

Rate constant is in cm/sec.

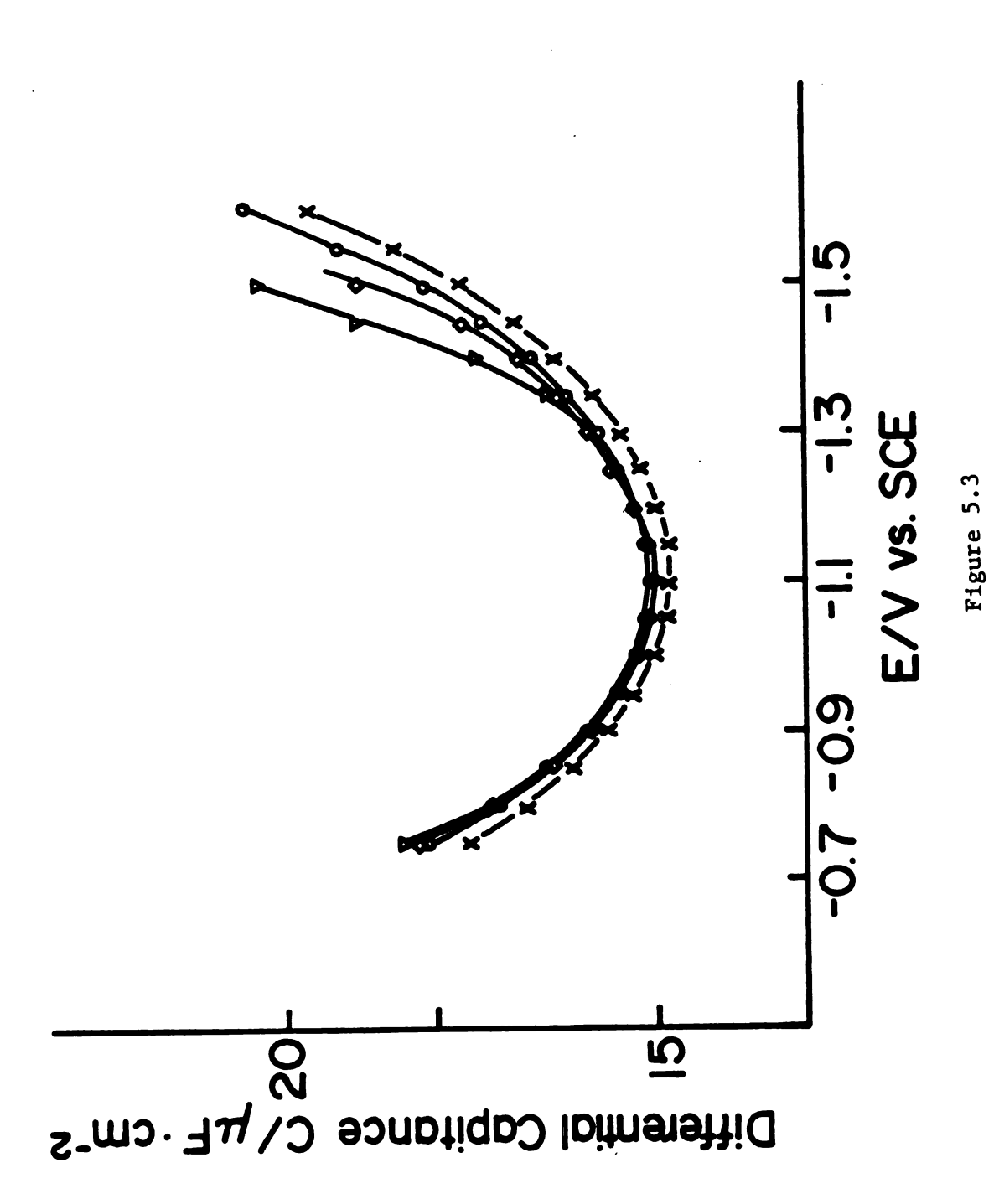
evaluate the temperature dependence of the potential at the reaction plane from the measurement of the temperature dependence of the differential double-layer capacitance in order to calculate the correct activation enthalpy $\Delta H_{\text{corr}}^{\ddagger}$. The temperature dependence of the differential capacitance curves over the temperature range 5°C to 40°C measured at lead surfaces are shown in Figure 5.3. It is evident that varying the temperature has only a minor effect on the measured capacitance at lead. Therefore, the value of $[\partial\phi_{rp}/\partial(1/T)]\phi_m$ of Equation 2.43 can be assumed to be zero. Then the value of $\Delta H_{\text{corr}}^{\ddagger}$ at lead can be a very close approximation to the value of $\Delta H_{\text{ideal}}^{\ddagger}$. For all the metal complexes under consideration the corrected activation enthalpies $\Delta H_{\text{corr}}^{\ddagger}$ at lead are three to five Kcal/mole smaller than those at mercury electrodes. This implies that lead electrodes yield more favorable enthalpic barriers for these reactants than mercury.

The activation entropies were obtained from the relation $T_\Delta S^{\dagger} = \Delta H^{\dagger} - \Delta G^{\dagger}$ where $\Delta G^{\dagger} = RT(\ell nk - \ell nA)$. The values of $\Delta S_{corr}^{\dagger}$ will be sensitive to the method used to compute k_{corr} and to the reaction model chosen to calculate the pre-exponential factor A. Although the uncertainty of the values of $\Delta S_{ideal}^{\dagger}$ and $\Delta S_{corr}^{\dagger}$ shown in Table 5.5 may be significant as described in Chapter II, only the comparison of values at mercury and lead surfaces will be emphasized in the Discussion. The relationship between the "real" and "ideal" entropies of activation can be written as follows

$$\Delta S_{ideal}^{\ddagger} = \Delta S_{real}^{\ddagger} + \alpha \Delta S_{rc}^{\circ}$$
 (2.44)

where ΔS_{rc}° is the reaction entropy of a redox couple. The value of

Figure 5.3 Differential capacitance at 1000 Hz vs.
electrode potential for polycrystalline lead
prepared by method (D) in 0.5 M NaClO₄ at
various temperatures: (x) 5.5 C; (o) 16.5°C;
(♦) 25.5°C; (∇) 36.2°C



 $\Delta S_{\text{real}}^{\dagger}$ can be set equal to zero as described in Chapter II. For all the metal complexes examined, the corrected activation entropies $\Delta S_{\text{corr}}^{\dagger}$ at lead are much more negative than those obtained at mercury electrodes, i.e., $(\Delta S_{\text{corr}}^{\dagger})^{\text{Hg}} - (\Delta S_{\text{corr}}^{\dagger})^{\text{Pb}} \approx 20$ e.u. Also the values of $\Delta S_{\text{real}}^{\dagger}$ in Table 5.5, which are obtained by substituting experimental values of $\Delta S_{\text{ideal}}^{\dagger}$ into Equation 2.44, are quite different from the value of zero that is predicted from the Marcus^{8,9} and other "weak overlap" outer-sphere theories.

Since the activation entropy and the pre-exponential term A are unable to be independently determined, the values of $\Delta S_{corr}^{\dagger}$ in Table 5.5 were obtained by assuming the value of A. Therefore, it is of interest to evaluate the pre-exponential term by assuming the values of $\Delta S_{ideal}^{\dagger}$. The evaluation of the pre-exponential factor A provides insight into the collision frequency, electron tunneling, and the applicability of the Marcus theory. The values of $\Delta S_{ideal}^{\dagger}$ was set to $\Delta \Delta S_{rc}^{\circ}$ as predicted from the Marcus theory to obtain the values of A that are shown in Table 5.5. The resulting values of A for both mercury and lead electrodes are listed in Table 5.5. The values of A at lead for all the reactants examined are significantly smaller than those at mercury electrodes. Furthermore, the values of A at lead are up to eight orders of magnitude smaller than the theoretical values, 5×10^3 and 3×10^5 cm/sec given by the reactive-collision and pre-equilibrium models 4 , respectively.

2. Discussion

Outer-sphere reactions, for which there is supposed to be no direct interaction between the metal complex and the electrode surface, the presence of the "specific substrate" effect as illustrated before is somewhat surprising.

According to Table 5.5, compared with mercury surfaces lead surfaces exhibit favorable enthalpic and unfavorable entropic barriers for these electrode reactions examined. The relatively small activation enthalpies $\Delta H_{corr}^{\ddagger}$ at lead are generally compensated by correspondingly small or even negative values of the activation entropy $\Delta S_{corr}^{\dagger}$ resulting in large values of $\Delta G_{corr}^{\dagger}$, i.e., smaller values of $k_{\mbox{corr}}$ at lead. It is surprising and unexpected to see that the values of $\Delta S_{corr}^{\dagger}$ at lead are relatively small or even negative. The reactants with +3 charge certainly have a higher tendency to order surrounding water structure than that of the corresponding products that have +2 charge. Therefore, the resulting $\Delta S_{corr}^{\dagger}$ (= ΔS_{p}^{\dagger} - ΔS_{r}^{\dagger}) is expected to be positive and close to ΔS_{rr}^{o} . In other words, the experimental values of $\Delta S_{\text{corr}}^{\ddagger}$ violate the Marcus theory 8 which predicts $\Delta S_{corr}^{\dagger} = \Delta S_{real}^{\dagger} + \alpha \Delta S_{rc}^{\circ}$ where $\Delta S_{real}^{\dagger} \simeq 0$. Table 5.5 also includes the corresponding values of $\Delta S_{real}^{\dagger}$ that were calculated from $\Delta S_{real}^{\ddagger} = \Delta S_{corr}^{\ddagger} - \alpha \Delta S_{rc}^{\circ}$. The values of $\Delta S_{real}^{\ddagger}$ at lead surface are extremely negative.

The relation $\Delta S_{real}^{\dagger} \simeq 0$ (or $\Delta S_{corr}^{\dagger,f} = -\Delta S_{corr}^{\dagger,b}$) is only true when the transition state for heterogeneous outer-sphere electron-transfer reactions has the same environment as the reactant and product states. However, the transition state for electrode reactions is inevitably

within the double-layer region where the solvent structure can be expected to be significantly different from that in the bulk state.

The adiabatic assumption is frequently used in the study of outer-sphere electron-transfer reactions, and the values of $\Delta S_{\text{corr}}^{\ddagger}$ shown in Table 5.5 were obtained under this assumption, i.e., the transmission coefficient for electron tunneling, κ_{el} , was assumed to be unity. Equation 2.31 derived in Chapter II shows the relation between the rate constants and $\Delta \overline{G}^{\ddagger}$

$$k_{app} = \kappa_{e1} K_o v_p \exp(\frac{-W_p}{RT}) \exp(\frac{-\overline{G}^{\dagger}}{RT})$$
 (2.31)

However, the possibility that electron-transfer processes could be nonadiabatic has been already noticed by several authors. 109 The relatively small (negative) values of $\Delta S_{corr}^{\ddagger}$ found at lead shown in Table 5.5 also suggest the possibility of nonadiabatic processes. Therefore, the evaluation of the pre-exponential factor A by assuming $\Delta S_{corr}^{\ddagger}$ found at lead shown in Table 5.5 also suggest the possibility of nonadiabatic processes. Therefore, the evaluation of the pre-exponential factor A by assuming $\Delta S_{corr}^{\ddagger}$ = $\alpha\Delta S_{rc}^{\circ}$ provides us with a means to examine the observed "specific substrate" effect as well as the experimentally small or even negative values of activation entropy at lead surfaces. Since there is no way to determine experimentally the activation entropy and frequency factor as mentioned above, in Table 5.5 both $\Delta S_{corr}^{\ddagger}$ and A were obtained under certain inevitable assumptions. Although there is a difference in the reactive-collision and pre-equilibrium models, for the present purpose it will

not make any difference to the values of A listed in Table 5.5 whether the former or latter model was used. Because the deviation of the values of A between calculated and theoretical values is so large $(10^{-5} \text{ to } 10^{-9} \text{ fold smaller})$, the possibility of nonadiabatic processes at lead surfaces seems likely to be valid irrespective of the model that is employed.

For a given reactant, the plane of closest approach to the electrode surface might be significantly different between polycrystalline lead and mercury electrodes. From the study of the double-layer structure at lead-aqueous interfaces, it shows that polycrystalline lead exhibits a higher affinity for water than mercury electrodes, which as noted above can be judged from the values of $g_{M}^{H_2U}$. The existence of strong interaction between the lead surface and water within the double-layer region results in constraining the reacting ions to be away from the electrode surface. The electron density associated with the orbitals at metal surfaces decreases exponentially with distance away from the surface. Therefore, the degree of orbital overlap between the reacting ions and electrons of lead electrode surfaces will be diminished resulting in the small value of $\kappa_{\mbox{\scriptsize el}}.$ In addition, the value of $K_{\mbox{\scriptsize p}},$ the equilibrium formation constant of the precursor state in the pre-equilibrium model may decrease when the plane of closest approach is moved further away from the lead surfaces as a result of diminution of the concentration of reacting species in the precursor state.

Although the explanation given above to illustrate the observed small frequency factor at lead surfaces is quite plausible, the

values of $\Delta H_{\text{corr}}^{\ddagger}$ reported in Table 5.5 are surprising on the basis of this model. Since the corrected activation enthalpy is an intrinsic barrier which shall be independent of the value of κ_{el} . Therefore, the difference in the electroactivity between lead and mercury electrodes cannot be simply attributed to the effect of electron tunneling.

The enthalpic barrier, $\Delta H_{corr}^{\ddagger}$, is the result of outer- and innershell reorganization energy for electron-transfer reactions. The inner-shell reorganization 4 energy, which depends on the bond length and bond strength between the center metal cation and its coordinated ligands, of the reactions under consideration at both electrode surfaces, mercury and lead, can be assumed with confidence to be the same. The outer-shell reorganization energy, 31b,d however, can be expected to be strongly dependent on the variation of the interaction between the electrode surface and solvent molecules surrounding the reacting ions in the transition state. In other words, the variation of $\Delta H_{corr}^{\dagger}$ between lead and mercury is attributed to the existence of a specific solvent effect. From this study, it is evident that the solvent plays a very important role in electron-transfer processes. Even for outer-sphere reactions, the electrode still shows certain degree of influence on the solvent structure between the metal surface and the reacting ions within the transition state. The strong solvent interaction within the double-layer region may be responsible for the small enthalpic barrier of activation for electrode reactions at lead electrodes. This, however, is compensated for by the resulting low (unfavorable) entropic barrier $T_{\Delta}S_{corr}^{\dagger}$. Therefore, the negative

entropic barrier obtained at lead surfaces, which more than compensates the favorably low enthalpic barrier, is responsible for the observed lower electroactivities of electrode reactions at lead compared with those at mercury.

In addition, the strong solvent interaction with the electrode surface existing at lead-aqueous interfaces 85 may influence the work term used in the calculation of the double-layer corrected rate constants. The work term employed to calculate $\Delta G_{\text{corr}}^{\dagger}$ and $\Delta H_{\text{corr}}^{\dagger}$ is usually assumed to be purely Coulombic in origin. This assumption may be roughly true for the relatively hydrophobic mercury electrodes, however, it may not be valid for other electrodes with strong solvent interaction between the reacting ions and the electrode surface. When the reacting ions approach the reaction plane, they may experience strong interaction with the solvent molecules in the double-layer region. Equation 2.49 presents a general expression for the relation between the "real" and "intrinsic" activation enthalpy

$$\Delta H^{\dagger} = \Delta H_{int}^{\dagger} + \left[\Delta H_{p}^{\circ} + \alpha_{I} (\Delta H_{S}^{\circ} - \Delta H_{p}^{\circ})\right]$$
 (2.49)

Therefore, if there are additional work terms other than electrostatic work terms which can be included in the terms of ΔH_{p}^{o} or ΔH_{S}^{o} , then it may significantly influence the evaluation of $\Delta H_{corr}^{\ddagger}$. This notion can also be applied to the evaluation of the activation entropic barriers.

In conclusion, the observed "specific substrate" effect is

attributed to the effect of electron tunneling and also to the effect of specific solvent interaction with the electrode surface. Furthermore, the influence of the specific solvent structure within the double layer region in the transition state for the electron-transfer step seems likely to dominate the observed "specific substrate" effect.

PART II

CHAPTER VI

ELECTROCATALYSIS OF OXYGEN REDUCTION

1. Introduction

Oxygen reduction 112 has been well studied and has been successfully employed as the cathodic reaction in some practical application of fuel cell technology. However, only the relatively expensive material platinum is known to be an efficient catalyst for the desirable four-electron reduction of oxygen molecules to water. Thus, the development 113-118 of an electrode material at which oxygen reduction can be significantly catalyzed is the focus of much current research. The pyrolytic graphite (PG) electrode has been extensively used in this study because it is cheap, has a wide polarizable potential range, and also has a strong affinity for a number of macrocyclic metal complexes which are anticipated to be able to catalyze oxygen reduction.

Recently, graphite electrodes chemically modified with macrocyclic metal complexes 113-116 has been shown in several cases to dramatically enhance the rate of oxygen reduction. At most modified graphite surfaces, oxygen molecules can only be reduced to hydrogen peroxide via two-electron reduction. Some iron(III) porphyrins 148 can catalyze the four-electron reduction, however, the corresponding reaction potential of oxygen reduction are fairly negative (-0.05 V vs. SCE). The two-electron reduction is the first step for the stepwise reduction of oxygen molecules to water: Scheme I (in 1 M acidic solution)

$$0_2 + 2H^+ + 2e^- + H_2O_2$$
 $E^\circ = 0.44 \text{ V vs. SCE}$ (6.1)

$$H_2O_2 + 2H^+ + 2e^- + 2H_2O$$
 $E^\circ = 1.54 \text{ V vs. SCE}$ (6.2)

However, it is the direct four-electron reduction of oxygen molecules to water that has the greatest practical application in fuel cell technology: Scheme II

$$0_2 + 4H^{+} + 4e^{-} + 2H_20$$
 $E^{\circ} = 0.99 \text{ V vs. SCE}$ (6.3)

Since the equilibrium concentration of hydrogen peroxide at the desirable operational potential of an $0_2/H_2$ fuel cell (+0.99 V vs. SCE) is relatively low ($\leq 10^{-18}$ M), 117 an extremely high reaction rate (i.e., driving force) is required to subsequently reduce the hydrogen peroxide to water. This is why the "direct" four-electron pathway is preferred over the stepwise pathway.

Metalloporphyrins, such as iron porphyrins are essential components of cytochrome c oxidase 120 which is the terminal enzyme in the respiratory redox chain that reduces dioxygen to water. Therefore, metalloporphyrins that are capable of binding oxygen molecules 121 might be expected to constitute potent electrocatalysts for the four-electron reduction of dioxygen to water. This concept has been illustrated by several groups. 113-117 Recently, Collman and Anson 117 demonstrated the remarkable enhancement of the electrocatalysis of the four-electron reduction of dioxygen to water through modification of the pyrolytic graphite surfaces with dicobalt face-to-face porphyrin.

However, the stability and reproducibility of these porphyrinmodified oxygen electrodes as well as the elucidation of the corresponding reaction mechanism still needs attention.

In this work, a number of cobalt porphyrins including eight monomers and three dimers as shown in Figure 6.1 were used to examine the so-called "molecular engineering" of the chemically modified electrodes. The eight monomeric cobalt porphyrins have different substituents on the porphyrin rings, allowing substituent effect to be examined. Two of the three dimeric cobalt porphyrins, $Co-Co-4^{123}$ and C_8-Co- Co-5. 124 that have similar structures to those used in Reference 117 also yield similar results of the electrocatalysis of oxygen reduction. These two dimers are basically different in the length of the chains that connect the pairs of porphyrin rings. Thus, the effect of the distance between the cobalt centers on the electrocatalysis of oxygen reduction can also be examined. The other dimer, "slipped"-Co-Co-4, 123 was prepared by connecting the meso-position of one porphyrin ring with the β -position of another porphyrin ring. Therefore, it will result in an offset in the relative position of the two cobalt atoms, i.e., will form a slipped configuration. It is of interest to inspect the influence of this "offset" 123 on the oxygen reduction kinetics.

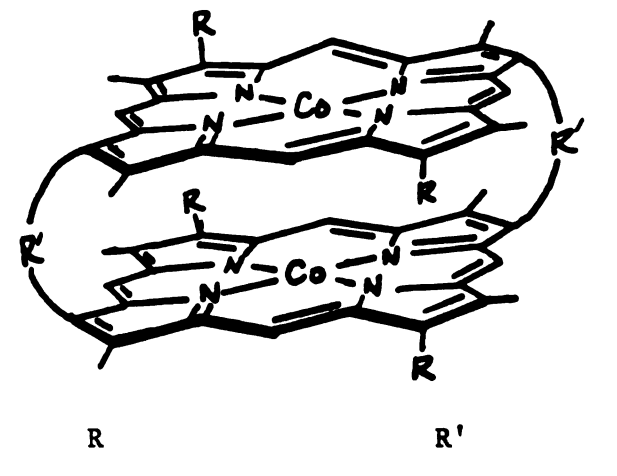
A rotating ring-disc electrode¹²⁵ (RRDE), which has been demonstrated to be a useful tool for the investigation of the formation of the reaction intermediates during electrode reactions, was extensively used in this study. Basically the RRDE consists of a disc and a concentric ring separated by a small Teflon gap as shown

Figure 6.1 Structures of cobalt porphyrins

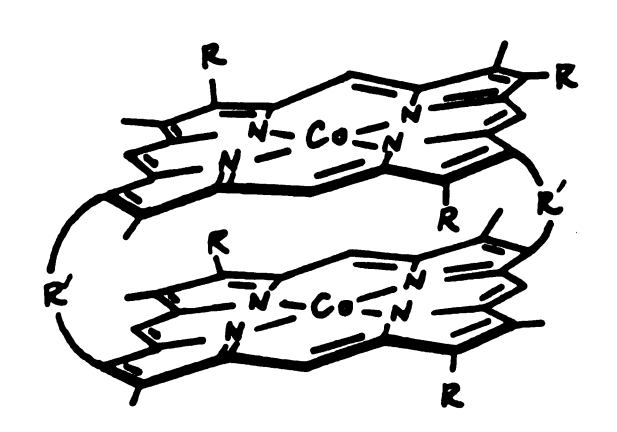
	R ₁	R ₂	R ₃	R ₄	R ₅
Co-OEP	C ₂ H ₅	с ₂ н ₅	н	H	н
Co-Etio	с ₂ н ₅	CH ₃	H	H	н
Co-TPP	Н	Н	^C 6 ^H 5	^C 6 ^H 5	^C 6 ^H 5
Co-TPP(p-OMe)	Н	Н	C ₆ H ₄ (p-OMe)	C_6H_4 (p-OMe)	C ₆ H ₄ (p-OMe)
Co-TPPF ₂₀	Н	H	^C 6 ^F 5	^C 6 ^F 5	^C 6 ^F 5
Co-OEP-C1	C ₂ H ₅	с ₂ н ₅	Cl	Н	н
Co-OEP-C1 ₂	с ₂ н ₅	с ₂ н ₅	Cl	C1	H
Co-OEP-C1 ₄	с ₂ н ₅	с ₂ н ₅	C1	Cl	C1

Figure 6.1

Figure 6.1 (cont.)



C₈-Co-Co-5 C₈H₁₇ -CH₂CON(n-Bu)CH₂CH₂Co-Co-4 C₅H₁₁ -CH₂CONHCH-



$$\begin{array}{ccc} & & & & & R' \\ & & & & & \\ & & & & \\ & & & \\ & & & \\ & & & \\ & & & \\ & & & \\ & & & \\ & & & \\ & & & \\ & & & \\ & \\ & & \\ & & \\ & & \\ & & \\ & & \\ & & \\ & & \\ & & \\ & & \\ & & \\ & & \\ & & \\ & & \\ & &$$

in Figure 6.2. Therefore, the potential of both the disk and the ring can be controlled independently by a bipotentiostat. With the aid of the RRDE, the production of hydrogen peroxide at the disk can be detected at the ring by holding the potential of the ring at a value at which hydrogen peroxide will be oxidized. The resulting ring-disk voltammograms for oxygen reduction at the porphyrinmodified graphite surfaces will be presented and discussed. Furthermore, the corresponding formal potentials of the attached cobalt porphyrins at the graphite surfaces were also determined by conventional cyclic voltammetry. This measurement provides a way to differentiate the electroactivities of these cobalt porphyrins under consideration and allows the reaction mechanism of oxygen reduction to be determined.

There are two possible pathways for oxygen reduction at the porphyrin-modified surfaces, two-electron reduction of dioxygen to hydrogen peroxide and four-electron reduction of dioxygen to water as described. Thus, it is interesting to calculate the number of electrons involved in oxygen reduction which can be evaluated from the corresponding ring-disk voltammograms. There are a number of ways to calculate the number of electrons involved in electrode reactions. The ring current is attributed to the oxidation of the hydrogen peroxide that is produced at the disk during oxygen reduction. Therefore, the ratio of $(-i_R/i_DN)$, where i_R and i_D are diffusion-limited currents at the ring and the disk respectively, and N is the collection efficiency of the RRDE, can be treated as the percentage of the over-reaction of oxygen reduction that follows

Figure 6.2 Diagram of a Rotating Ring-Disc Electrode (RRDE)

ROTATING RING-DISC ELECTRODE (RRDE)

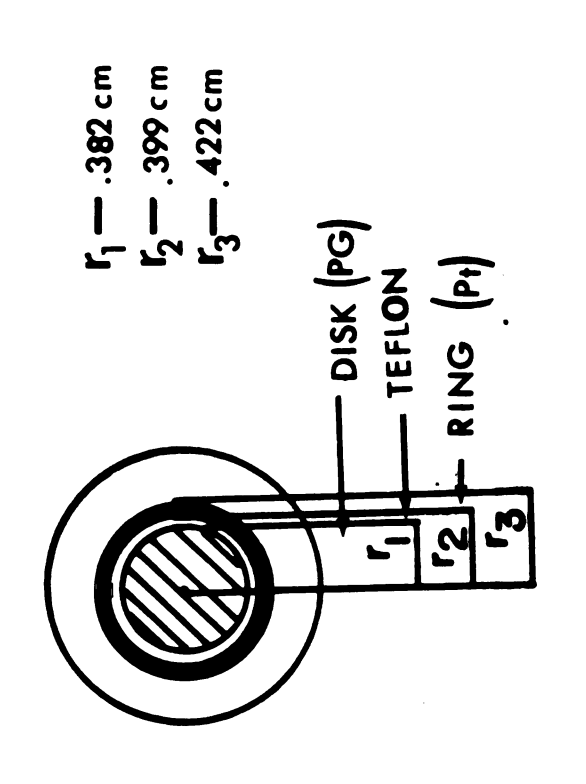


Figure 6.2

two-electron reduction of dioxygen to hydrogen peroxide. Then, the average number of electrons involved in oxygen reduction at the disk can be extracted from the following relation

$$n_{av} = 4 - 2 \left(\frac{-i_R}{i_D N}\right)$$
 (6.4)

If no ring current is detected, $i_R = 0$, then, $n_{av} = 4$. If oxygen reduction at the disk entirely follows two-electron pathway, $-i_R = i_D N$, then $n_{av} = 2$. The values of n can also be directly obtained from the limiting current using the Levich relation 125 or the corresponding slope of the Levich plot ($i_R vs. \sqrt{\omega}$).

2. Experimental

a. <u>Materials</u>

The cobalt porphyrins used in this work were kindly supplied by Professor C. K. Chang of this Department. Their structure are shown in Figure 6.1. Their syntheses and characterization have been discussed in References 123 and 124. Trifluoroacetic acid (HTFA) (MCB Co.) was used without further purification. Dichloromethane was purified by distillation. Highly purified water prepared as described in Chapter III was used to prepare the electrolyte solution (0.5 M HTFA). Tetrabutylammonium perchlorate (TBAP) was prepared by mixing tetrabutylammonium hydroxide and 70% perchloric acid. The addition of water gave a precipitate which was recrystallized from 95% ethanol.

b. Rotating Ring-Disc Electrode (RRDE)

A Pine Instrument Co. Model DT6 rotating ring-disc electrode (RRDE) was extensively used in this work. The RRDE contains a pyrolytic graphite (PG) disk and a platinum (Pt) ring as shown in Figure 6.2. The RRDE has been widely used to examine the formation of the intermediates during the electrode reaction. A certain portion of the materials produced at the disk will diffuse to the ring when the RRDE is rotated. The quantity of the intermediates produced at the disk that can be detected at the ring is dependent on the so-called "collection efficiency", N, of the RRDE. Therefore, the collection efficiency of the RRDE can be simply formulated as

$$N = \frac{-i_R}{i_D} \tag{6.5}$$

where i_R and i_D are the diffusion-limited currents at the ring and the disk of the RRDE respectively. The collection efficiency is determined by the radii of the disk and the ring and the size of the gap between them. The theoretical calculation 126,127 of the collection efficiency utilizes the following equation

$$N = 1 - F(\frac{\alpha}{\beta}) + \beta^{2/3} [1 - F(\alpha)] - (1 + \alpha + \beta)^{2/3} \{1 - F(\frac{\alpha}{\beta})(1 + \alpha + \beta)]\}$$
 (6.6)

where $\alpha = (r_2/r_1)^3 - 1$, $\beta = (r_3/r_1)^3 - (r_2/r_1)^3$, and r_1 , r_2 , and r_3 are defined in Figure 6.2. The function $F(\theta)$ is defined as

$$F(\theta) = (\frac{\sqrt{3}}{4\pi}) \ln \{\frac{(1+\theta^{1/2})^3}{\theta}\} + \frac{3}{2\pi} \arctan(\frac{2\theta^{1/3}-1}{\sqrt{3}}) + \frac{1}{4}$$
 (6.7)

and is tabulated in Reference 127.

c. <u>Instrumentation</u>

A bipotentiostat is required in the performance of the RRDE voltammetry in order to control the potentials of the disk and the ring independently. Generally, the potential of the ring is held constant while scanning the potential of the disk. In this work, a bipotentiostat was constructed by inter-connecting two PAR 174A polarographic analyzers together through their rear panel connectors as suggested by PAR Co. Figure 6.3 presents the diagram used to make the modification. The operation of this bipotentiostat is illustrated by a simplified circuit shown in Figure 6.4. The principle of the performance of this bipotentiostat follows: Working Electrode El (W1): Since electrode El is in a voltage follower configuration, input equals the output

$$E_{ref} = -E_{A} \tag{6.8}$$

Since the Working Electrode 1 is at virtual ground (not shown in this scheme)

$$E_{W1} = 0 \tag{6.9}$$

$$E_{ref} - E_{Wl} = - E_{A} \tag{6.10}$$

therefore $E_1 = -E_A$. Working Electrode 2 (W2): At the summing point

Figure 6.3 Schematic diagram for the connection of the "modified" bipotentiostat

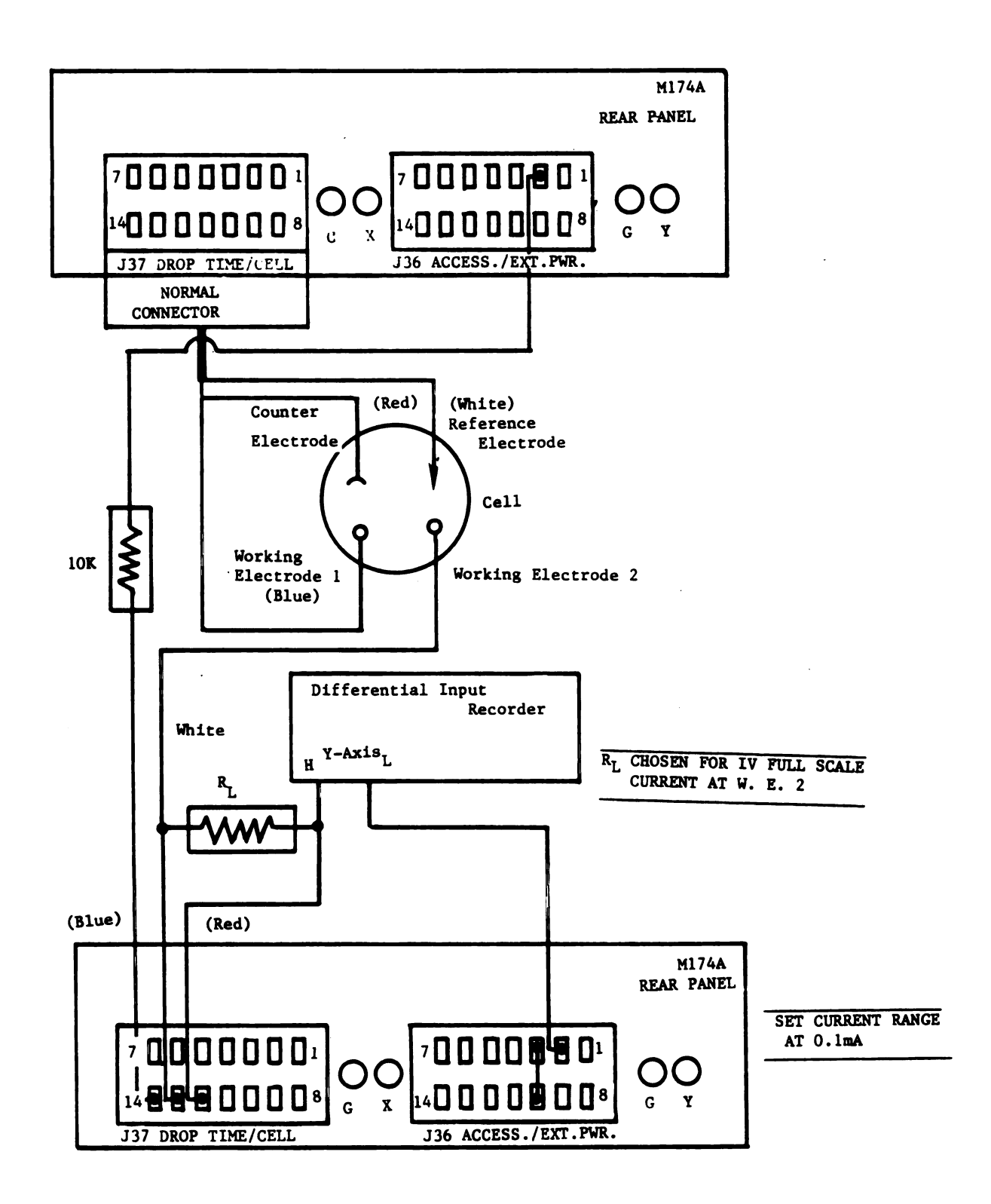


Figure 6.3

Figure 6.4 Schematic diagram for the operation of the "modified" bipotentiostat

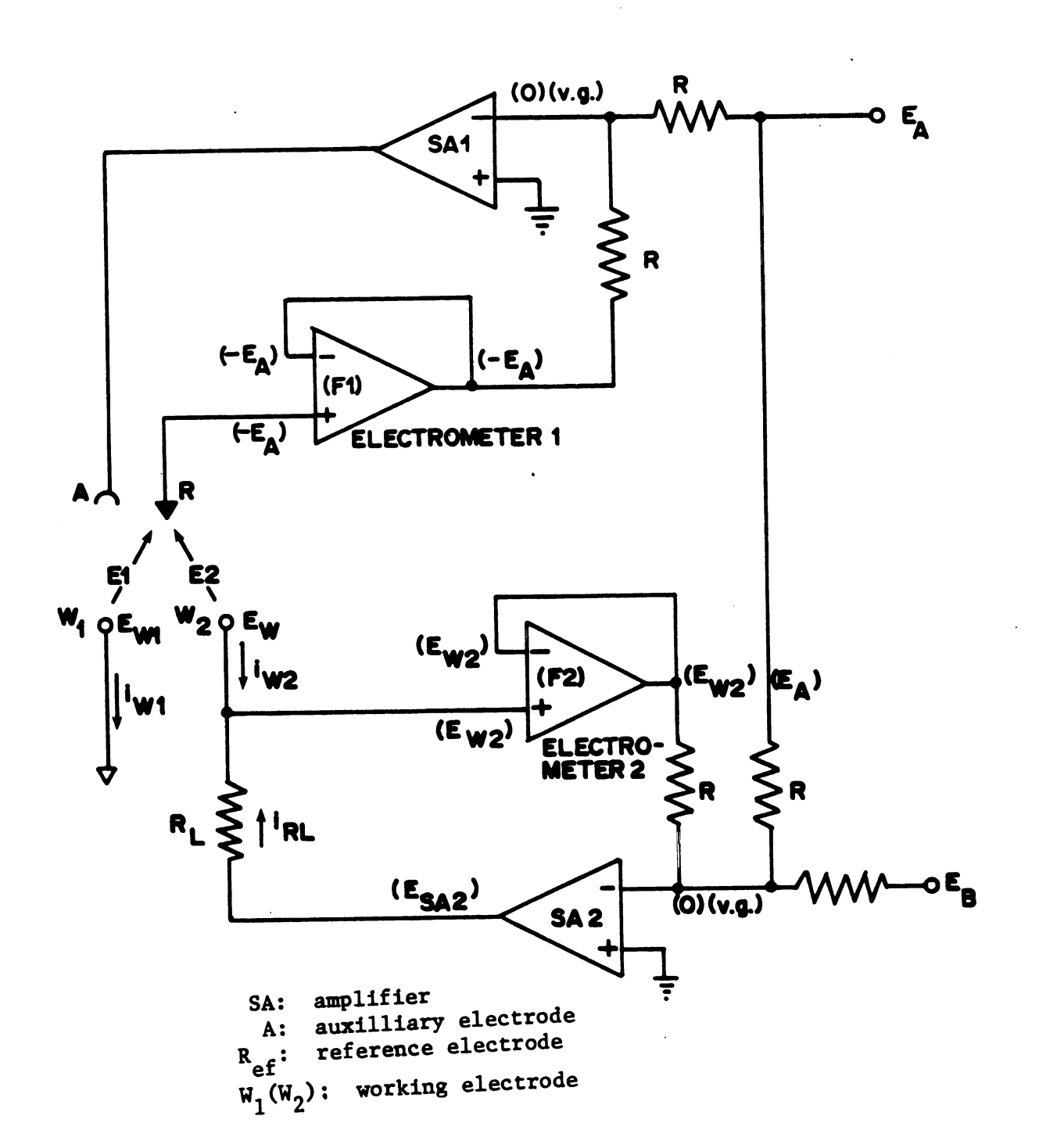


Figure 6.4

of amplifier SA2

$$E_{W2/R} + E_{A/R} + E_{B/R} = 0$$
 (6.11)

$$E_{W2} = -E_A - E_B$$

$$E_2 = E_{ref} - E_B \tag{6.12}$$

therefore $E_2 = E_8$.

Note that the relationship between the polarity of the applied potential and the polarity of the reference electrode vs. working electrode in the case of Working Electrode 1 is opposite that in the case of Working Electrode 2.

A sodium saturated calomel electrode (SCE) (Sargent-Welch Corp.) was used as reference electrode. A platinum wire activated by means of a flame was used as the auxiliary electrode. A PAR Model ASR2 analytical rotator was employed to rotate the RRDE. The electrochemical cell was as described in Chapter III except with larger dimensions in order to fit the larger RRDE.

d. Porphyrin-Modified Electrodes

The procedure 117 used to prepare the modified electrodes is relatively straightforward. The cobalt porphyrin can be irreversibly adsorbed on the pyrolytic graphite surface. First, the RRDE was carefully polished with 0.3 alumina on a polishing wheel as described in Chapter III. After polishing, the electrode was rinsed

with purified water and dichloromethane. Then it was soaked in a dichloromethane solution containing a small amount of cobalt porphyrin (<10⁻⁴ M) for five to ten minutes. ¹²⁹ After the excess solution on the electrode surface was carefully removed and the electrode was rinsed with purified water, yielding the "modified" graphite electrode. With this procedure, the electroactivity for oxygen reduction at these prepared graphite surfaces was relatively reproducible. However, the stability of the limiting current of oxygen reduction at these surfaces was variable and depended on the cobalt porphyrin used.

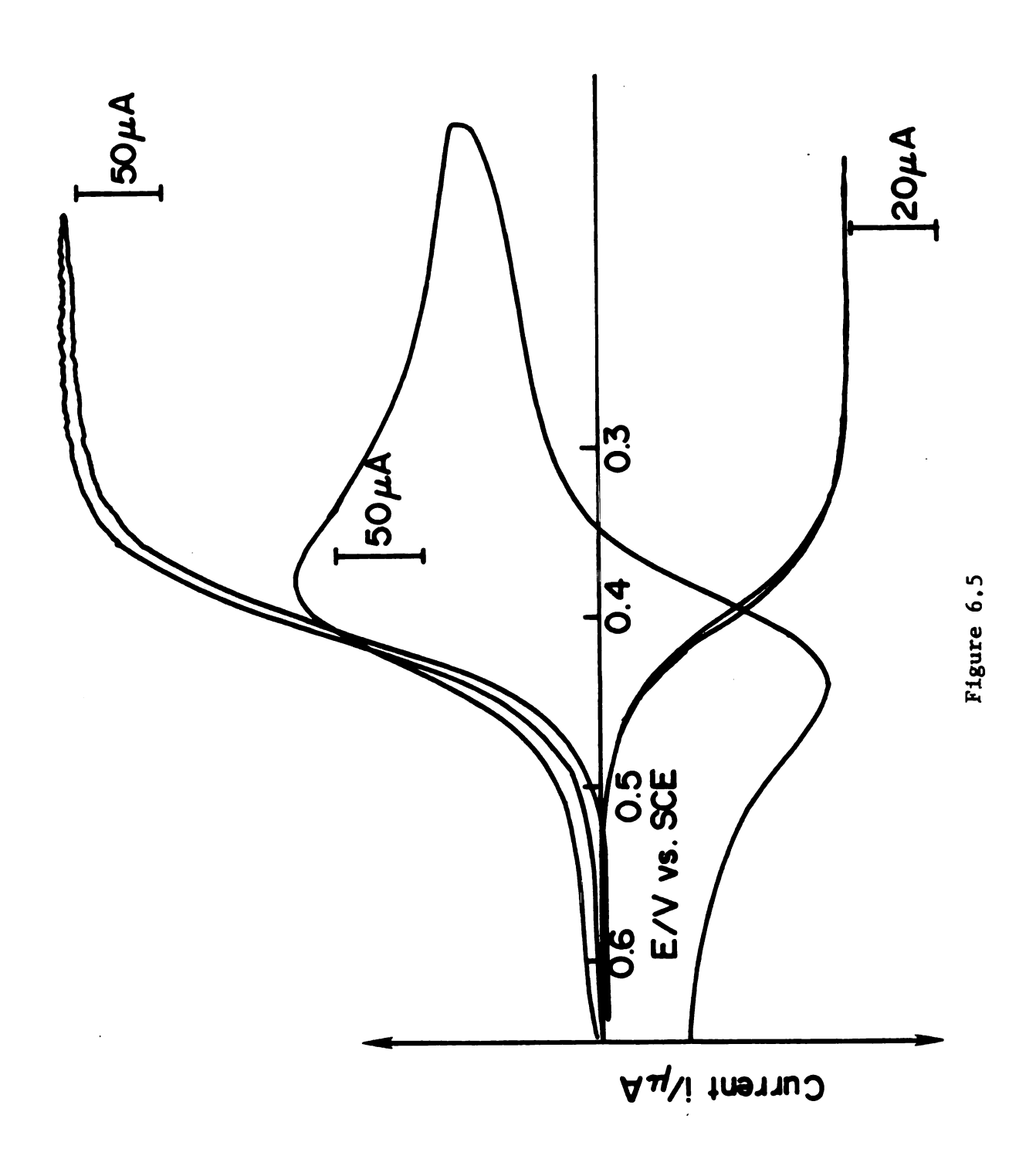
3. Results

a. Characterization of the PG/Pt RRDE

The mechanistically simple redox couple, $Fe(CN)_6^{3-/4-}$, was employed to characterize the PG/Pt RRDE and the modified bipotentiostat. Figure 6.5 shows the typical ring-disk voltammogram of $Fe(CN)_6^{3-/4-}$ at the PG/Pt RRDE in 0.5 M HTFA solution. Figure 6.5 also includes the corresponding cyclic voltammogram measured at the disk. The response of the disk current was not affected by the presence of the ring potential. This verifies the proper function of the bipotentiostat used in this work. From the ring-disk voltammogram, the collection efficiency (0.182) obtained from $N = -i_R/i_D$ is close to the theoretical value (0.177) calculated from Equation 6.6. The validity of the application of the Levich relation on the PG/Pt RRDE used in this work was also tested as follows.

The Levich equation 128 is

Figure 6.5 RRDE voltammogram for $Fe(CN)_6^{-3/-4}$ couple at the PG/Pt electrode. The potential of the Pt ring was held at 0.7 V vs. SCE. The scan rate of the cyclic voltammogram was 0.1 V sec^{-1}



$$i_g = 199 \text{ nAD}^{2/3} \gamma^{-1/6} \omega^{1/2} C_b F$$
 (6.13)

where i_{χ} is the diffusion-limited current (mA), n is the number of electrons involved in reaction, F is the Faraday, A is the electrode area (cm²), D is the diffusion coefficient (cm²/sec), γ is the kinematic viscosity (cm²/sec), ω is the rotation speed (rpm), and C_b is the bulk reactant concentration (moles/cm³). At 22°C, γ = 9.57 x 10 cm/sec, 139 the Levich equation can be simplified to

$$i_{\ell} = 4.18 \times 10^7 \text{ nAD}^{2/3} \omega^{1/2} C_b$$
 (6.14)

According to Equation 6.14, the limiting current is proportional to the square root of the rotation speed; the resulting Levich plot $(i_{\ell} \text{ vs } \sqrt{\omega})$ is shown in Figure 6.6. Furthermore, from the slope of the Levich plot, the number of electrons can be calculated. The value of n (1.05) evaluated from the Levich plot is close to the theoretical value (n = 1) for $Fe(CN)_6^{3-/4-}$.

Figure 6.7 shows the background cyclic voltammogram of the disk of the RRDE that was measured in 0.5 M HTFA deaerated solution. As has been reported, 130,131 the reduction wave (0.28 V vs. SCE) and the oxidation wave (0.37 V vs. SCE) seen in Figure 6.7 are probably due to the reduction of quinone-like group and oxidation of hydroquinone-like group respectively. Those surface groups may be responsible for the irreversible adsorption of cobalt porphyrins at the graphite surface as a result of π - π electron interaction.

Figure 6.6 Plot of the limiting disk current i vs. the square root of rotation rate $(\omega^{1/2})$ for the reduction of Fe(CN) $_6^{3-}$ (1.4 mM) on the PG/Pt electrode

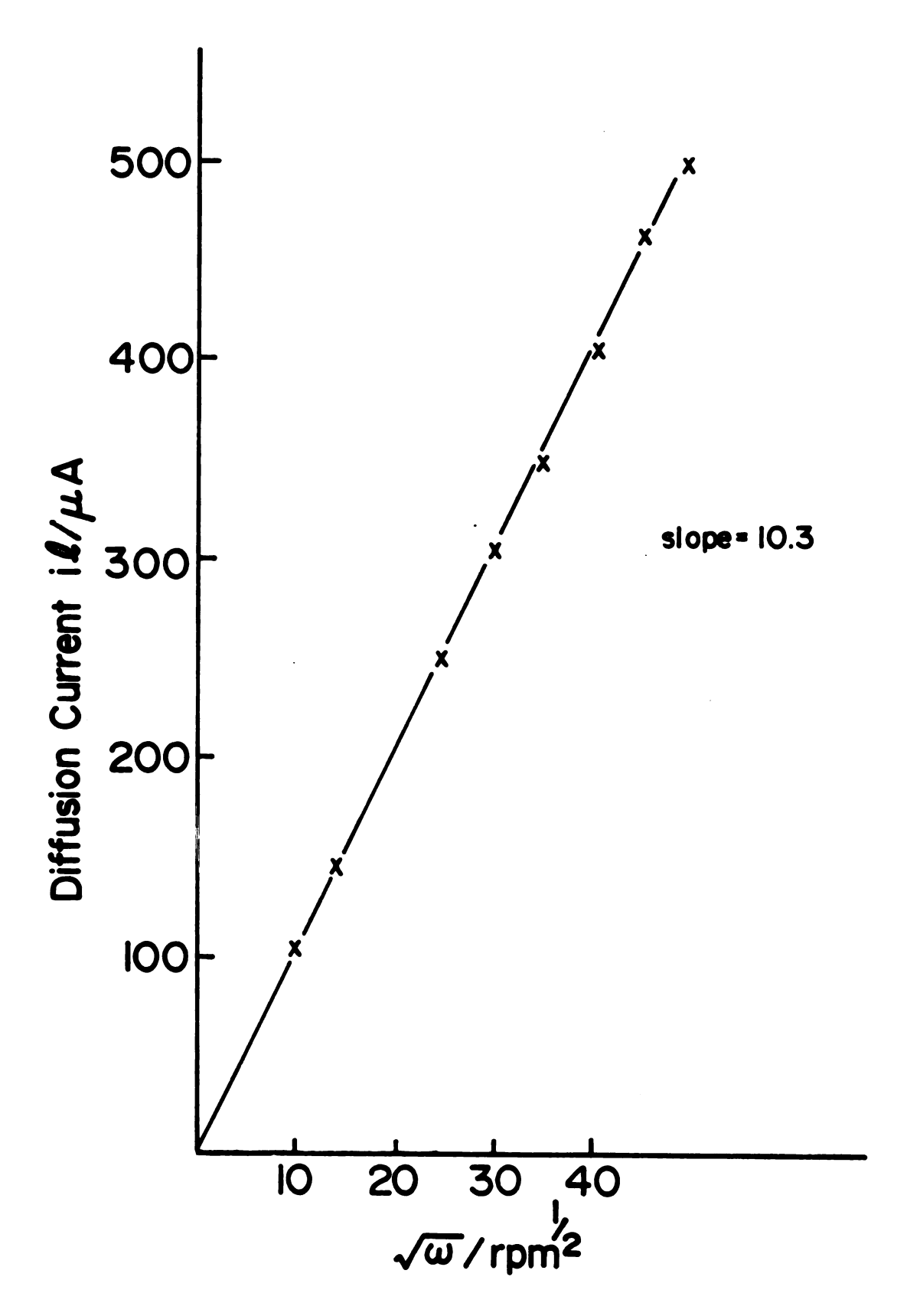
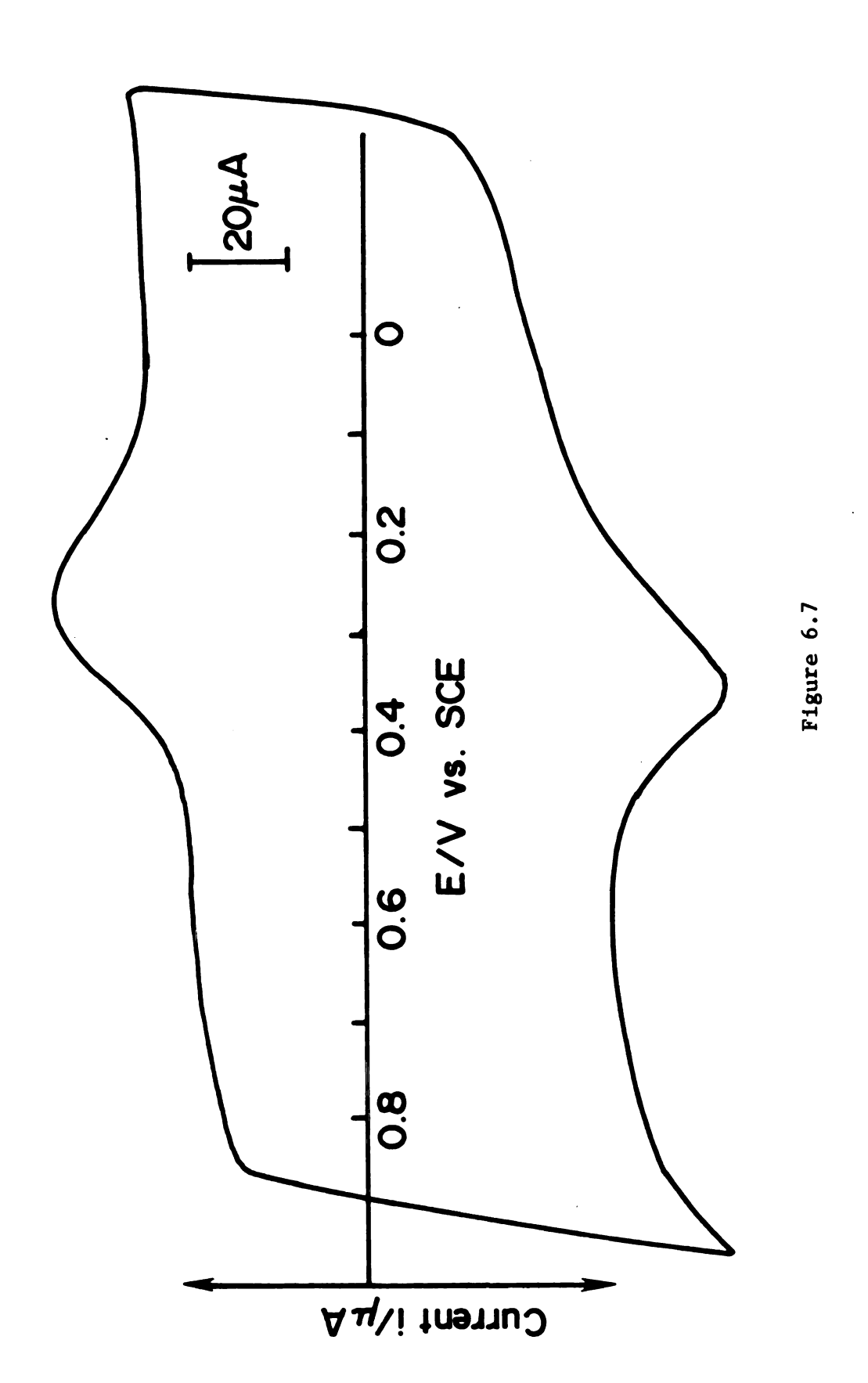


Figure 6.6

Figure 6.7 Cyclic voltammogram at the "blank" graphite electrode of the RRDE at 0.1 V/sec in 0.5 M $\,$ HTFA



b. Oxygen Reduction on the "Blank" Pyrolytic Graphite Surface

Contrary to platinum which is known to be an efficient electrocatalyst for the four-electron reduction of dioxygen to water, the graphite electrode is a very poor catalyst for oxygen reduction. Figure 6.8 shows the voltammograms of oxygen reduction at the PG disk and the Pt ring of the RRDE in a 0.5 M HTFA solution saturated with oxygen. Compared with platinum, curve (b), the reduction potential of oxygen reduction at the graphite disk, curve (a), is relatively negative (-0.35 V vs. SCE). Furthermore, it has been shown late that at the graphite surface the oxygen molecule is reduced via two-electron reduction to hydrogen peroxide. As discussed in the beginning of this chapter, the formation of hydrogen peroxide will block out the desirable four-electron reduction reaction.

c. Redox Properties of the Cobalt Porphyrins

Eleven cobalt porphyrins which are shown in Figure 6.1 were employed to prepare the porphyrin-modified graphite surfaces. The redox properties of some of these cobalt porphyrins have been examined 134,135 in dichloromethane or benzonitrile solution. These are so-called "bulk" properties. In this work, the "bulk" redox potentials of these cobalt porphyrins were determined in 0.1 M TBAP dichloromethane solution deaerated with nitrogen at the graphite disk of the RRDE. A typical voltammogram is shown in Figure 6.9. The derived data are listed in Table 6.1. The agreement of the redox potentials of Co^{III/II} reaction between the reported data and the

Figure 6.8 Cyclic yoltammograms for the reduction of oxygen in 0.5 M HTFA at 0.1 V/sec on (a) the "blank" graphite disk electrode; (b) the platinum ring electrode; (c) the monomeric porphyrin-modified surface; (d) the dimeric porphyrin-modified surface

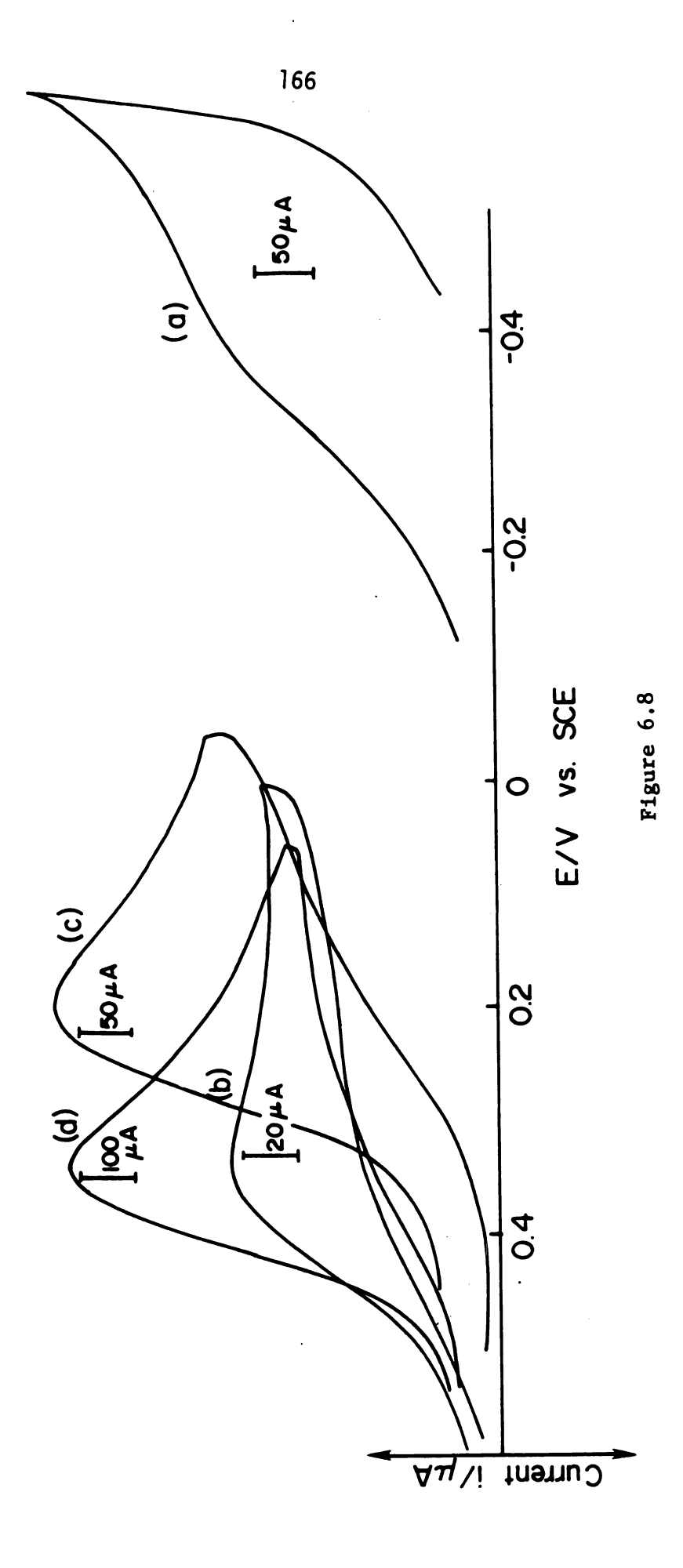


Figure 6.9 Cyclic yoltammogram for the "bulk" redox reaction of Co(III/II) of Co-Co-4 on the graphite disk electrode in 0.1 M TBAP dichloromethane at 0.2 V/sec

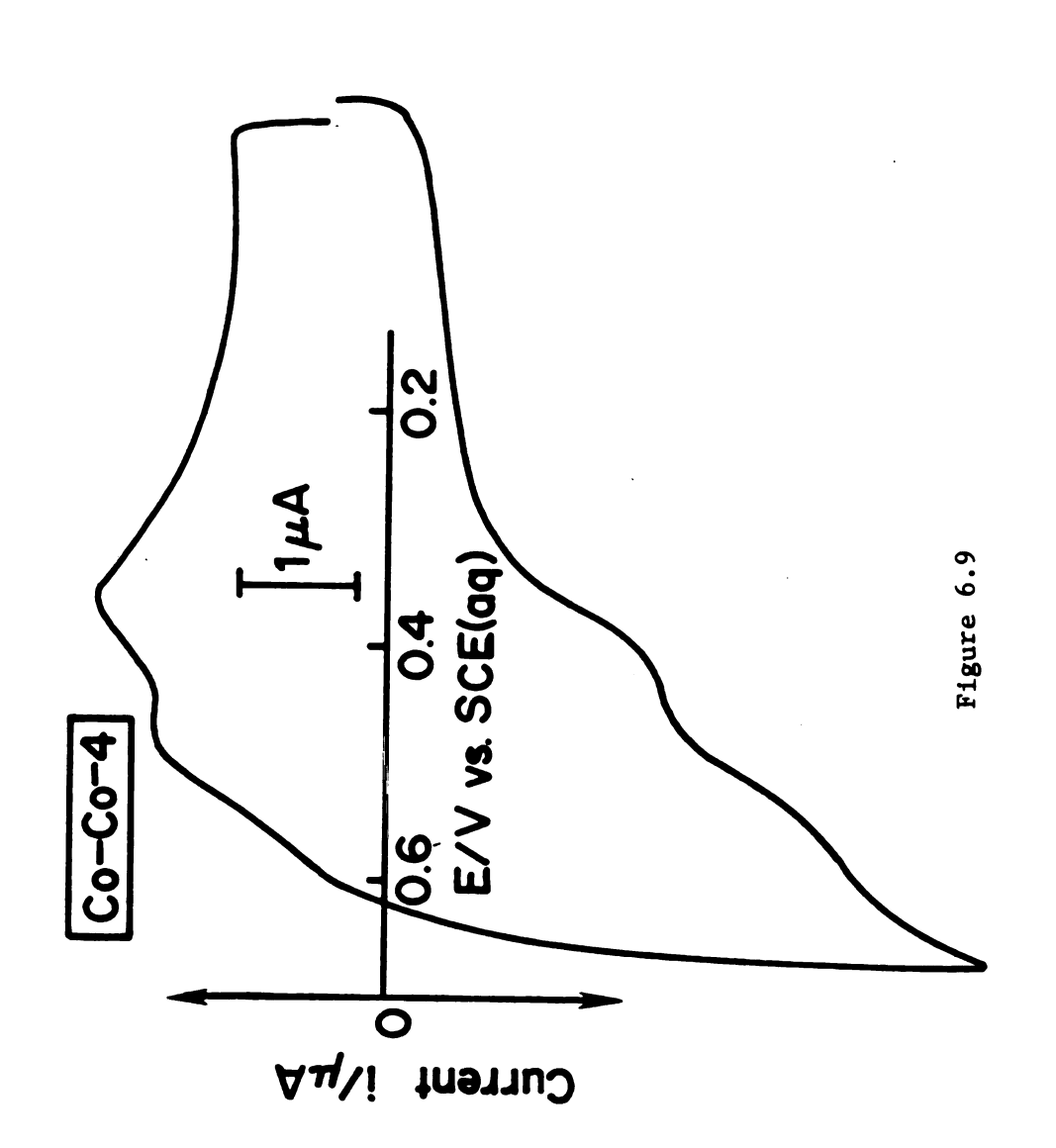


Table 6.1. "Bulk" and "Surface" Redox Potential's for the ${\rm Co}^{2+/3+}$ Couple of Cobalt Porphyrins.

Cobalt Porphyrin	E ^B _{1/2} (vs Fc ⁺ /Fc) ^a E ^S _{1/2}	(vs Fc ⁺ /Fc) ^b	ES (vs SCE aq) C
Co-OEP	0.20	0.46	0.59
Co-Etio	0.20 0.30 ^f	0.45	0.58
Co-TPP	0.22 0.30 ^f 0.29 ^g 0.49 ^h	0.53	0.66
Co-TPP(p-OMe)	0.28 _{0.28} ^g	0.50	0.63
Co-TPPF ₂₀			
Co-OEP-C1	0.23	0.56 ^e	0.69 ^e
Co-OEP-Cl ₂	0.23	0.55 ^e	0.68 ^e
Co-OEP-C14	0.28	0.47 ^e	0.60 ^{d,e}
C ₈ -Co-Co-5	0.19 -0.06	0.50 0.17	0.63 0.30
SIipped- Co-Co-4	0.18 0.05 ^d	0.55 0.15	0.6 <u>8</u> 0.28
Co-Co-4	0.18 0.02	0.53 0.18	0.66 0.31
Co-C ₂ -diester	-0.05 ^k	0.42 ⁱ ,j	0.55 ⁱ
Co ₂ βF5N-H	0.15 ^k -0.01 ^k		
Co ₂ βF4N-H	0.20 <mark>k</mark> -0.01 ^k	0.15 ^{b,k}	0.28 ^{c,k}

^aBulk redox potential of $Co^{3+/2+}$ measured in 0.1 M TBAP CH_2Cl_2 at pyrolytic graphite vs SCE_1 . The potentials were reported vs Fc^+/Fc .

lytic graphite vs SCE_{aq} . The potentials were reported vs Fc^+/Fc . bSurface redox potential of $Co^{3+/2+}$ measured in 0.5 M HFTA solution at porphyrin-modified surfaces. The potentials were reported vs. Fc^+/Fc .

^CSame as b except the potentials were reported vs. SCE(aq).

dOnly reduction wave was observed.

 $^{^{}m e}$ These redox potentials were estimated from ill-defined cyclic voltam-mograms.

f From reference 143 measured in 0.1 M TBAP benzonitrile vs. SCE(aq).

⁹From reference 144 measured in 0.1 M TBAP dichloromethane.

Table 6.1. Continued.

^hFrom reference 134 measured in 0.1 M TEAP benzonitrile.

¹From reference 146 measured in 0.5 M HTFA vs. SCE (aq).

^jSame as i except vs. Fc⁺/Fc.

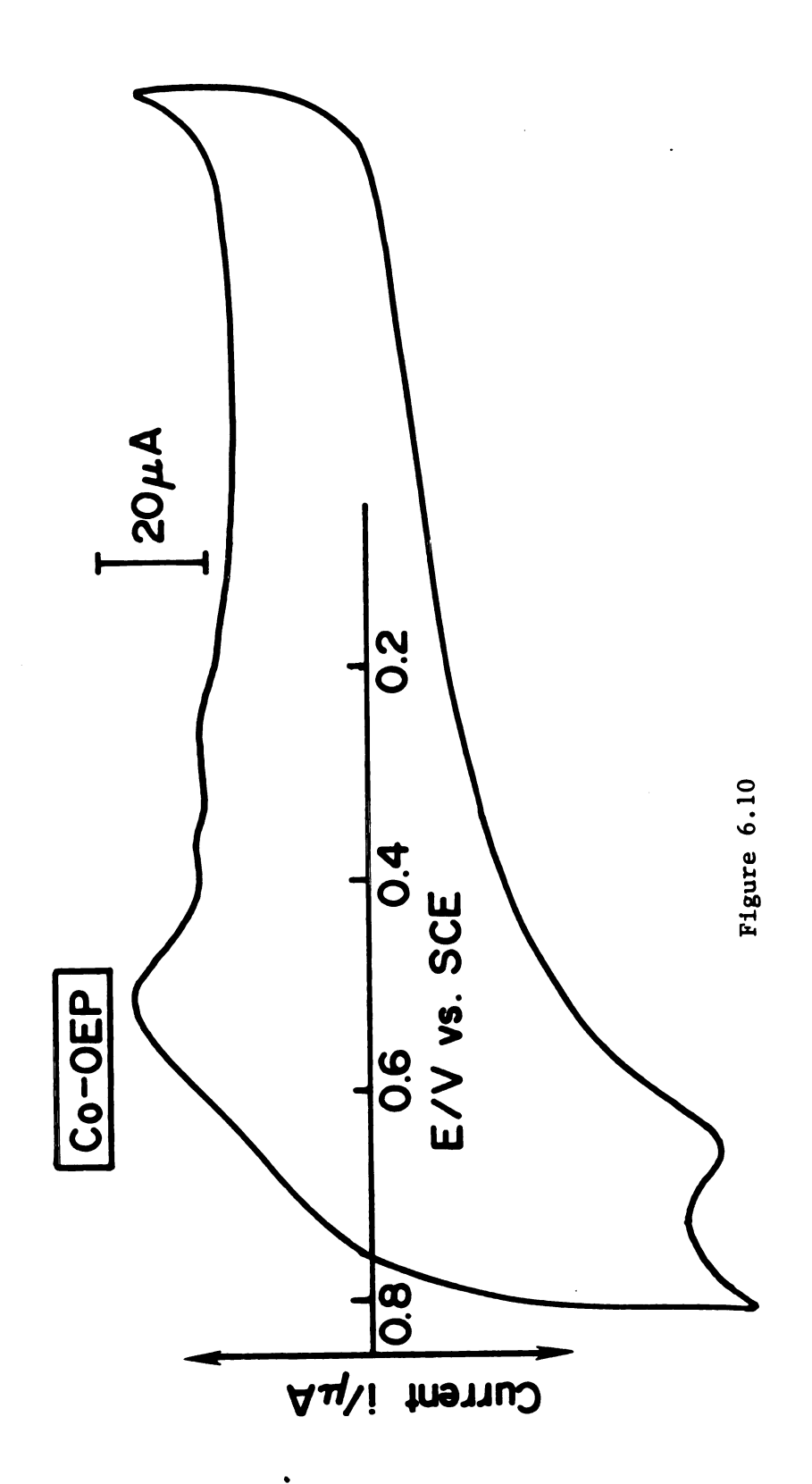
kFrom reference 147 measured in 0.1 M TBAP benzonitrile.

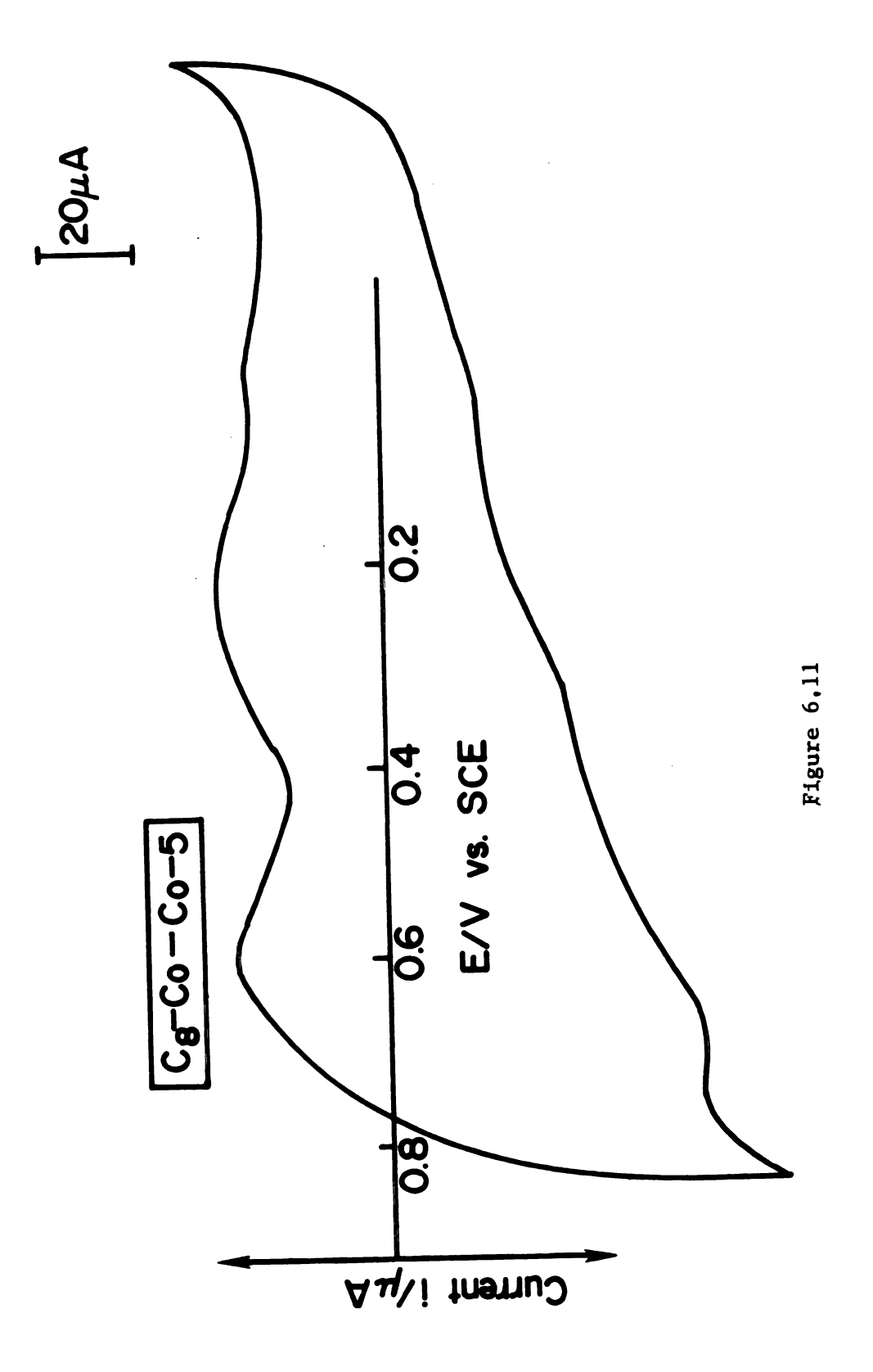
literature data is variable as shown in Table 6.1 which also includes the literature values. This variation may be due to the difference in the arrangement of the electrochemical cell which may cause the variation of the resulting junction potential. In this work, the arrangement of the electrochemical cell was clearly described in Chapter III. The electrode potential was measured with respect to an aqueous SCE, but the potentials listed in Table 6.1 are against the Ferricinium/Ferrocene redox potential (the "Ferrocene assumption"). 136 The Ferrocene assumption is that the absolute standard potential $\phi_{\rm m}^{\rm o}$ of the ferricinium-ferrocene (Fc $^{+}$ /Fc) redox couple is independent of the solvent.

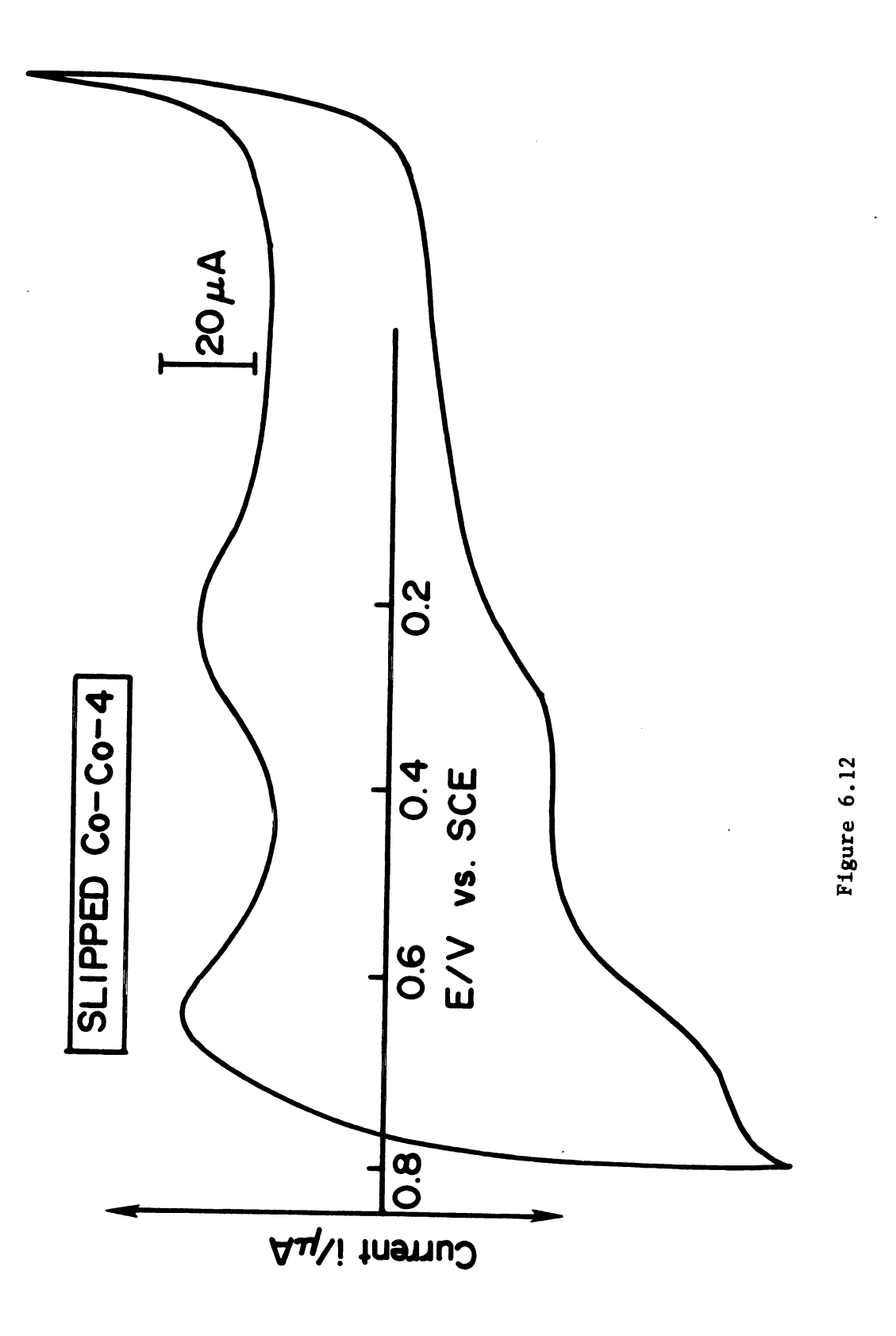
The investigation of the "surface" properties of the attached cobalt porphyrins in aqueous solution is very important in the evaluation of the reaction mechanism of oxygen reduction at the porphyrin-modified surfaces. The "surface" redox potentials of the attached cobalt porphyrins were measured by cyclic voltammetry in 0.5 M HTFA deaerated solution. Figures 6.10 to 6.13 show some typical surface cyclic voltammograms. The derived data of all the surface cyclic voltammograms are listed in Table 6.1. Due to the influence from the twenty fluorine substituents which are strong electron-withdrawing groups on the porphyrin ring, Co-TPPF₂₀ did not yield any detectable redox waves for both the bulk and the surface redox reactions. The assignment of these surface redox waves will be discussed later.

It is difficult to determine quantitatively the surface concentration of the attached cobalt porphyrins by conventional cyclic voltammetry due to the interference of the relatively large

Figure 6.10-6.13 Cyclic voltammograms for the "surface" redox reactions of Co(III/II) (?) at the PG disk electrode in 0.5 M HTFA aqueous solution deaerated with nitrogen at 0.2 V/sec. The porphyrins under consideration are indicated in the corresponding figures







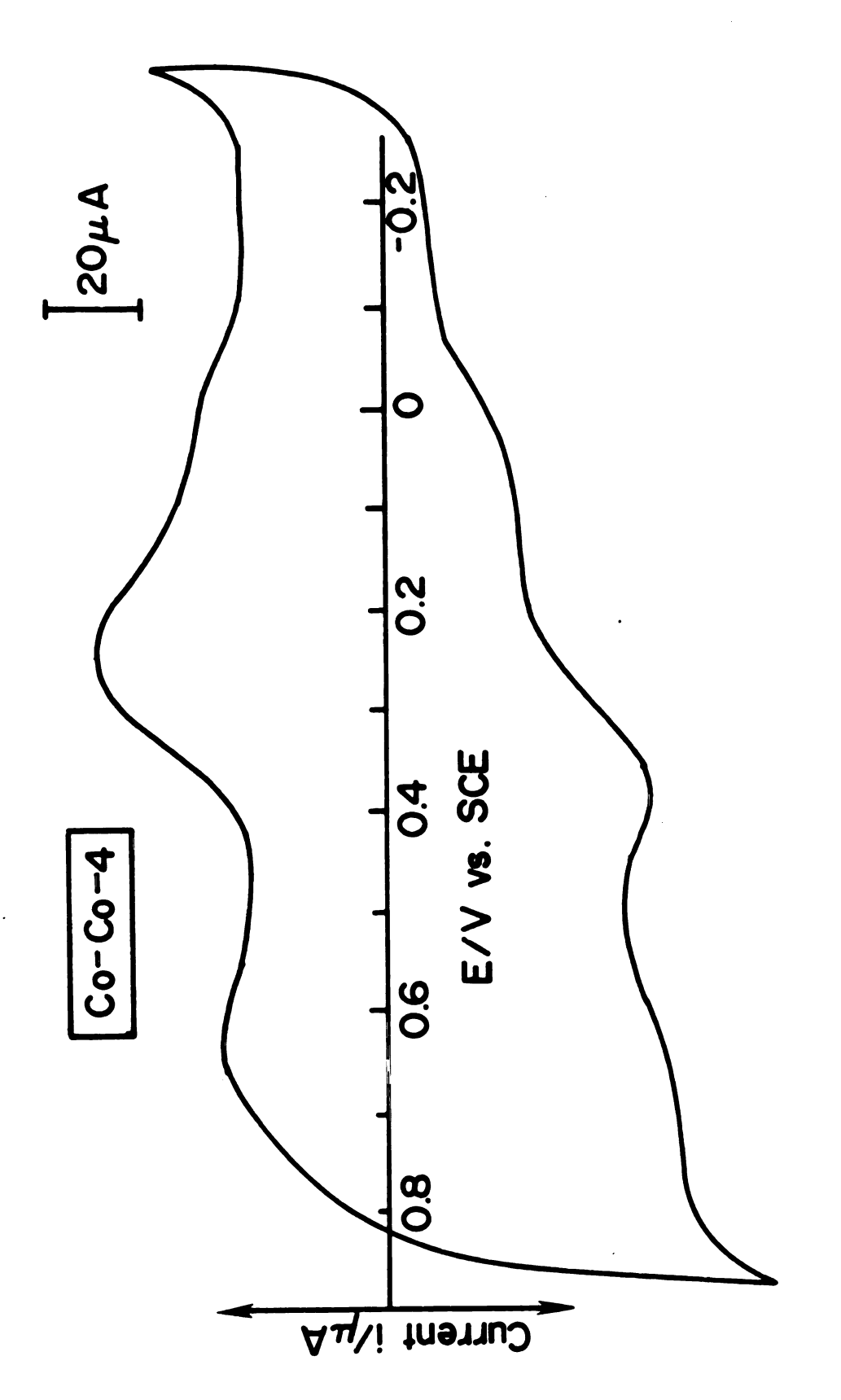


Figure 6.13

background current of the graphite electrode itself. Brown and Anson 137 demonstrated that with modification of the time constant of the PAR 174 the differential pulse voltammetry yielded much better resolution of the surface concentration of weakly adsorbed molecules than with conventional cyclic voltammetry. Nevertheless, in this work the surface concentration of the attached cobalt porphyrins were estimated by integrating the corresponding cyclic voltammograms. The surface concentration of the quinone-like group at the "blank" graphite surface is about $2.3 \times 10^{-10} \text{ mole/cm}^2$, close to a monolayer coverage. For the attached cobalt porphyrins, the values of surface concentration vary between 1.3 and $1.9 \times 10^{-10} \text{ mole/cm}^2$. Thus the coverage of the attached cobalt porphyrins is between 60% and 80% of a monolayer (however, this will be smaller if the roughness factor is included).

d. Oxygen Reduction at the Porphyrin-Modified Graphite Surface

Figure 6.8 presents the cyclic voltammograms of oxygen reduction at the "blank", curve (a), and the porphyrin-modified, curves (c) and (d), graphite electrodes. Note the tremendous improvement of the electrocatalysis of oxygen reduction through modification of the "inert" graphite surface with cobalt porphyrins. Judging from the peak potential of these voltammograms, the cobalt porphyrin can substantially lower the overpotential of oxygen reduction at the "blank" graphite surface.

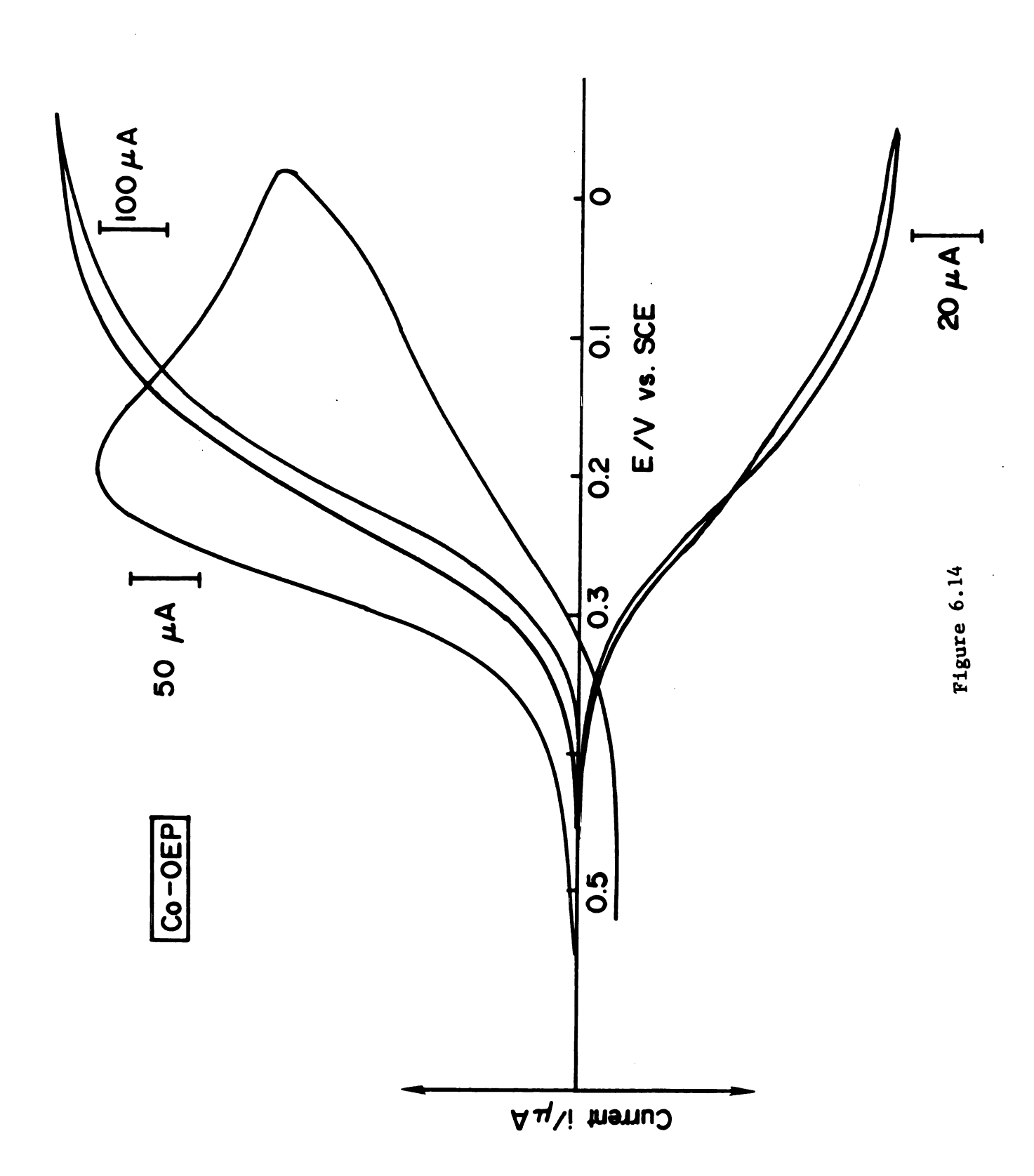
The PG/Pt RRDE with which the formation of hydrogen peroxide can be detected at the ring was used in this work. Representative

ring-disk voltammograms and the corresponding cyclic voltammograms for oxygen reduction measured in 0.5 M HTFA oxygen saturated solution at the porphyrin-modified graphite surfaces are shown in Figure 6.14 to 6.20. These ring-disk voltammograms were obtained by scanning the disk potential between +700 mV and -50 mV vs. SCE to measure oxygen reduction and holding the ring potential constant at +1.0 V vs. SCE to monitor the formation of hydrogen peroxide. The derived data are listed in Table 6.2. Table 6.2 also includes the values of the transfer coefficient for oxygen reduction. The evaluation of the transfer coefficient was described in Chapter II. The values of n calculated using Equation 6.4 are listed in Table 6.2.

There is a special feature of the ring-disk voltammogram of Co-Co-4, a maximum of the disk current i_m was observed as shown in Figure 6.20. A similar result was also obtained by Collman and Anson. 117 Therefore, in Table 6.2 the values of n of Co-Co-4 were calculated according to the diffusion-limited i_{ℓ} as well as maximum i_m currents. In the case of Co-Co-4, the maximum current is much less stable than the limiting current, and the maximum current and the limiting currents decreased about 40% and 20% respectively after thirty minutes. Furthermore, the maximum current would approach the limiting current within about thirty minutes. On the other hand, the limiting currents for oxygen reduction at the monomeric porphyrin-modified surfaces were relatively stable.

Furthermore, upon comparing the surface redox potentials for ${\rm Co}^{\rm III/II}$ and the half-wave potentials for oxygen reduction in the case of monomeric porphyrin-modified surfaces, it is seen that there

Figure 6.14-6.20 Disc (upper- i_D) and ring (lower- i_R) currents for the reduction of oxygen in 0.5 M HTFA on the PG/Pt electrode (ω = 600 rpm). Scan rate for the corresponding cyclic voltammogram for oxygen reduction at the PG disk electrode is at 0.1 V/sec except Figure 6.19 at 0.2 V/sec



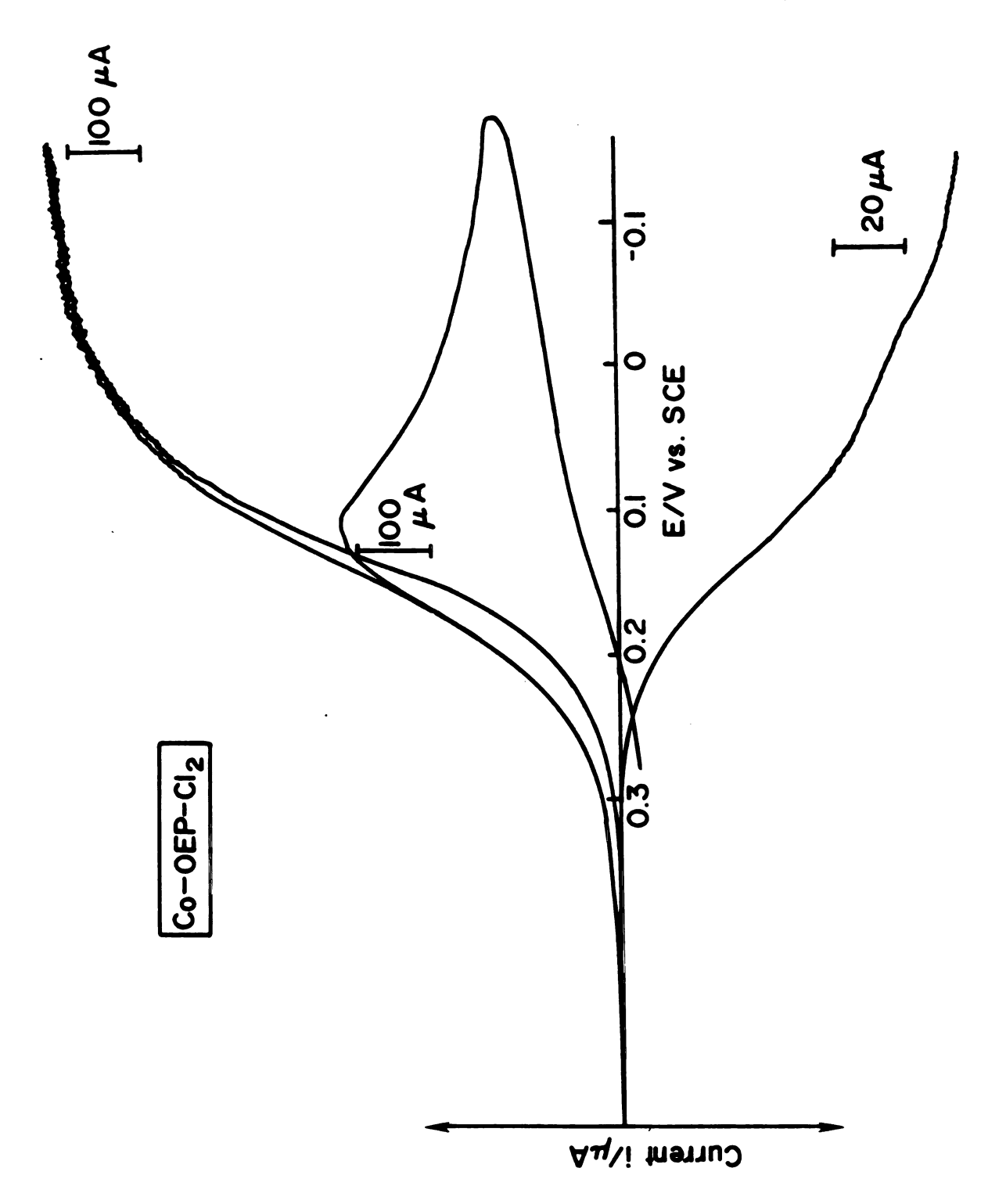
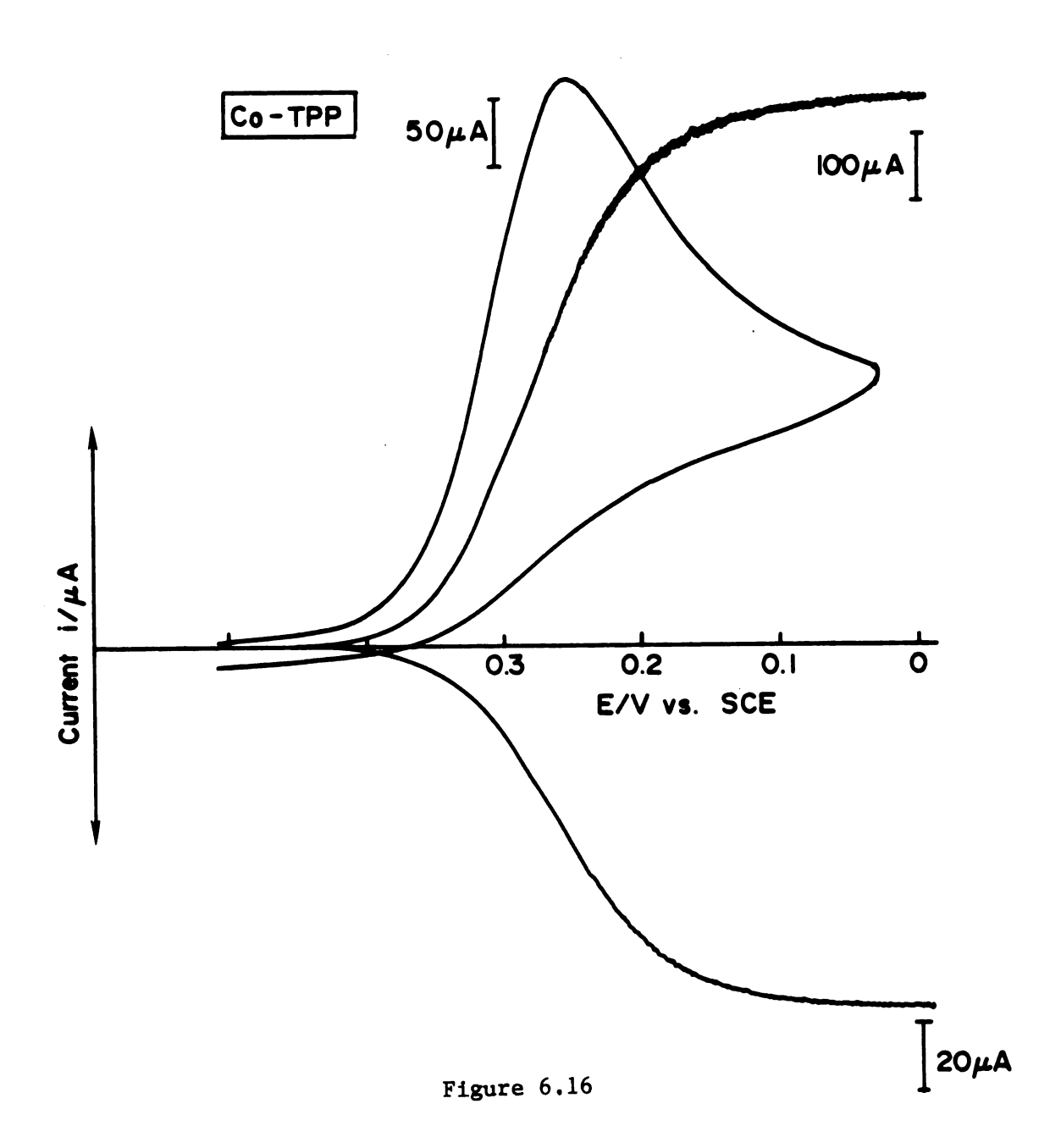
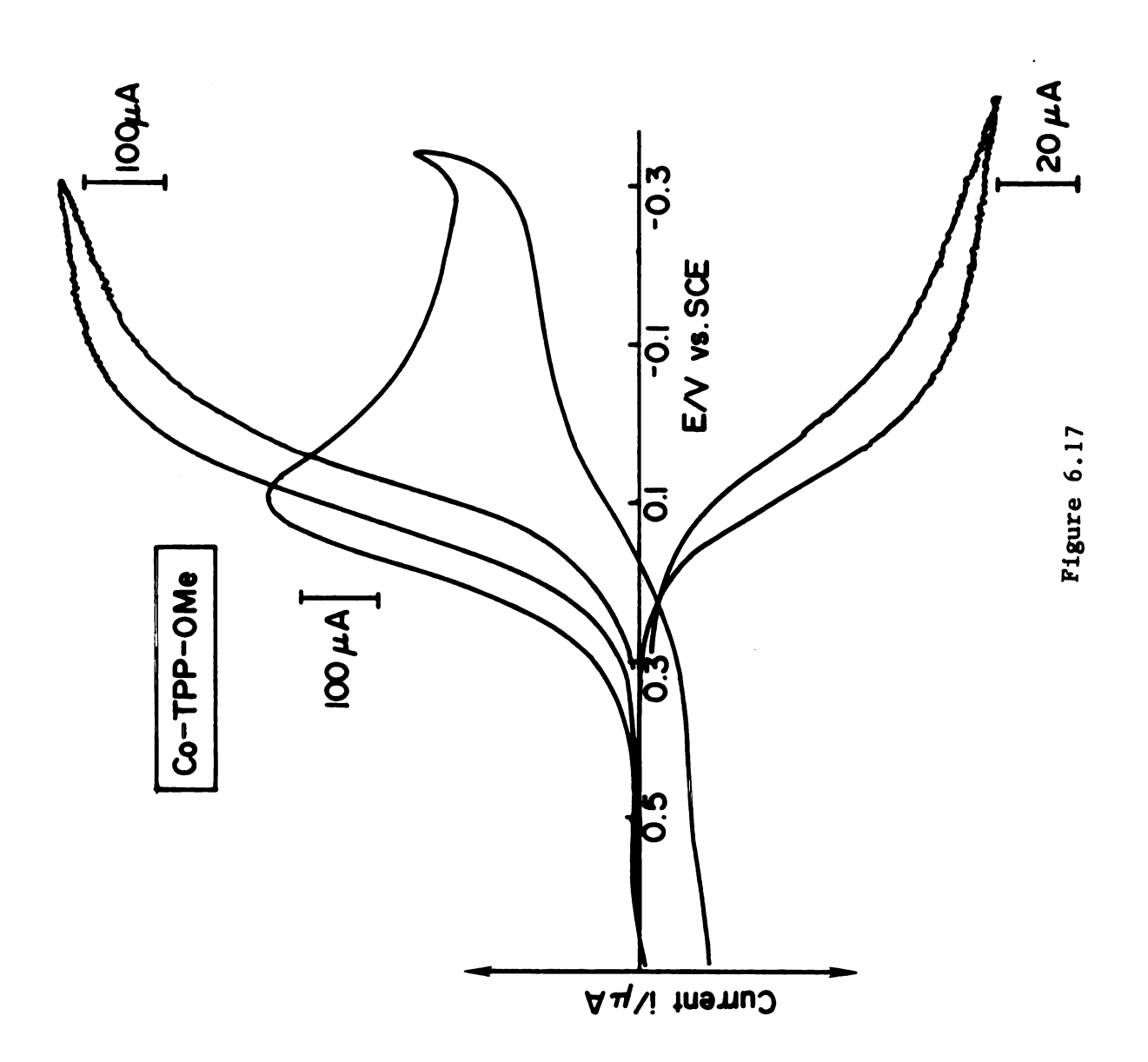
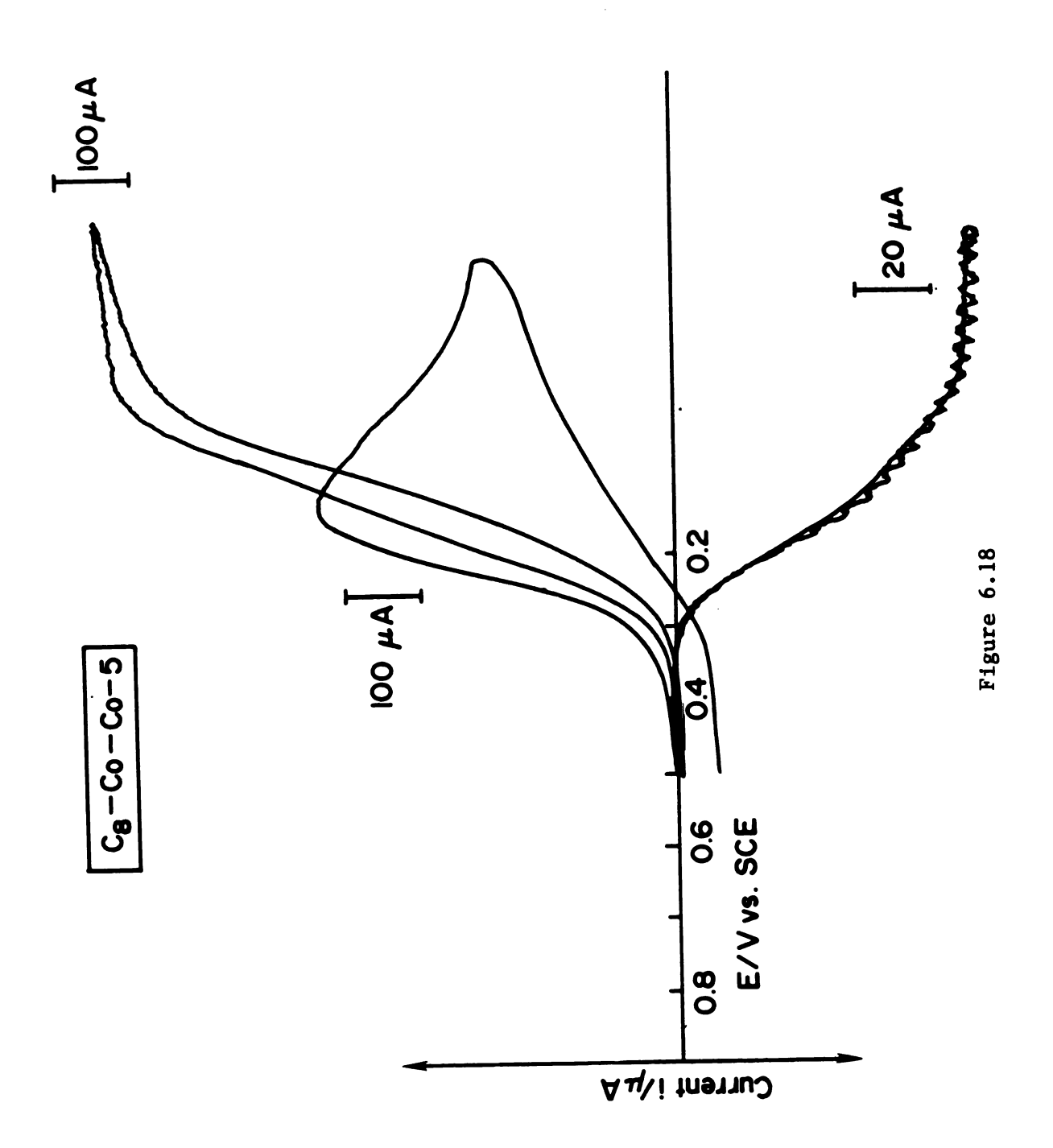
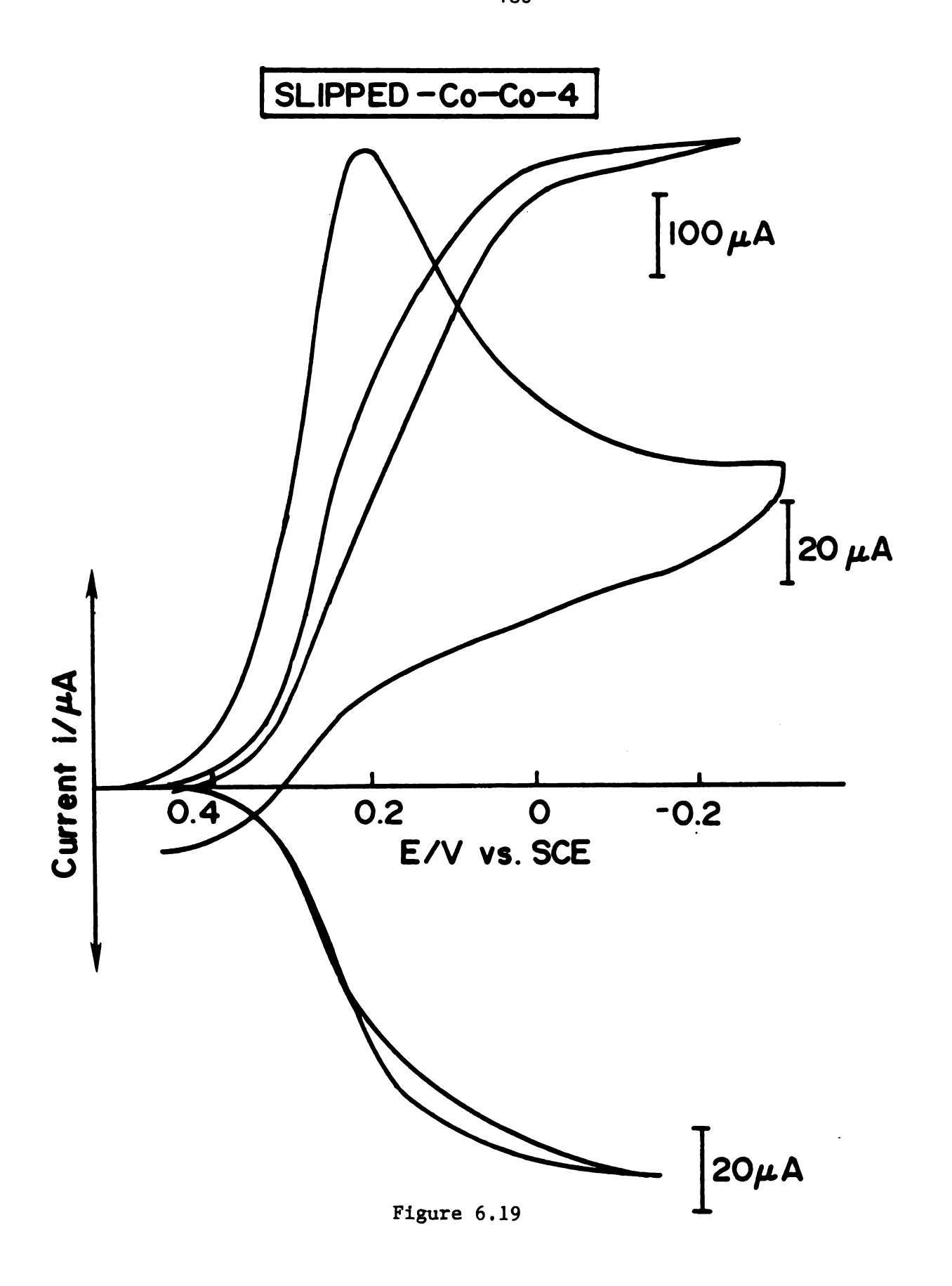


Figure 6.15









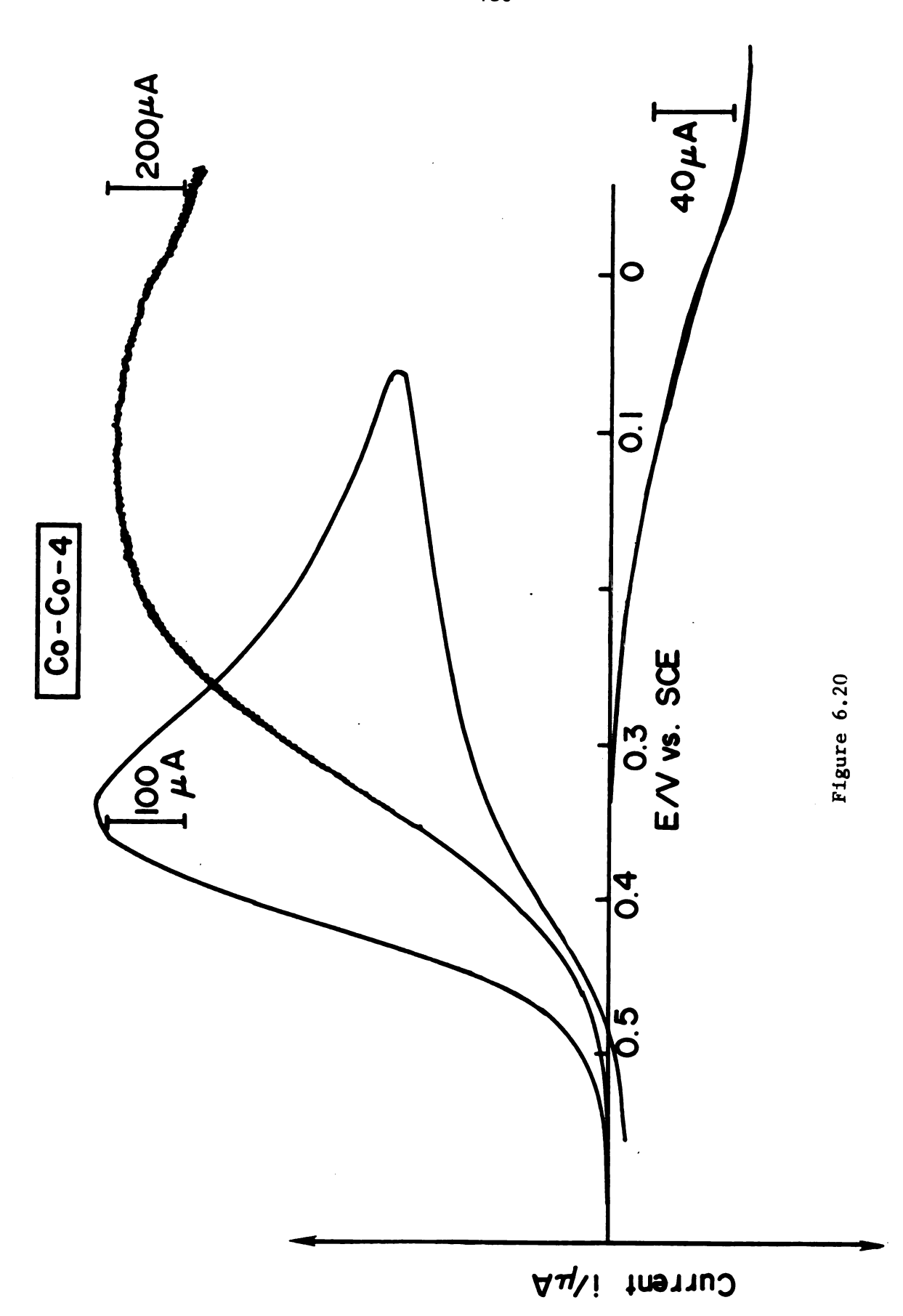


Table 6.2. Kinetic Parameters for Oxygen Reduction at Porphyrin-Modified Surfaces.

Cobalt Porphyrin	E _{1/2} a	lpha app	k ^{250mV^b kapp}	(-i _R /i _D N) ^C 100%	n ^d
"Blank" graphite ⁿ	-0.35		∿10 ⁻⁷		2.0
Co-OEP	0.17	0.53	3.6×10^{-3}	67	2.6
Co-Etio	0.21	0.52	8.8x10 ⁻³	64	2.7
Co-TPP	0.27	0.67	3.2x10 ⁻²	72	2.5
Co-TPP(p-OMe)	0.11	0.42	2.3x10 ⁻³	67	2.6
Co-TPPF ₂₀	0.15	0.35	4.0×10^{-3}	72	2.5
Co-OEP-C1	0.14	0.46	1.7x10 ⁻³	62	2.7
Co-OEP-Cl ₂	0.13	0.55	9.6x10 ⁻⁴	67	2.6
Co-OEP-C1	0.16	0.60	2.5×10^{-3}	69	2.6
C ₈ -Co-Co-5	0.16	0.47	2.5x10 ⁻³	56	2.9
Slipped- Co-Co-4	0.24	0.52	1.4x10 ⁻²	66	2.7
Co-Co-4	0.37	0.67	1.5	{ 9 ^e {19 ^f	(3.8 ^e (3.6 ^f
Co-C ₂ -diester ^g	0.14	0.5	7.2×10^{-31}	75	2.5
Co ₂ F5N-H ^g	0.36	0.5	1.8x10 ⁻²¹	40	3.2
Co ₂ F4N-H ^g	0.48	0.75	3.81	6.7 ^e	3.9 ^e
Co-TSP ^h	0.25	0.36	√5x10 ⁻⁵¹		2.0
Fe-TAPP ⁱ	-0.07				2.2 ^j
Fe(III)TMP ⁺⁵ 5C1 ^{-k}	-0.11	0.56	∿5x10 ⁻⁶¹		2.0 ^j

^aHalf-wave potential of oxygen reduction evaluated from the disk voltammogram (600 rpm). Potential vs. SCE (aq).

 $^{^{\}rm b}$ Rate constant evaluated at 250 mV vs. SCE for oxygen reduction from the disk voltammogram (0.5 M HTFA).

 $^{^{\}text{C}}\text{Ratio}$ of the ring limiting current i_R to the disk limiting current corrected for collection coefficiency $i_\text{D}\text{N}$.

dThe number of electrons involved in oxygen reduction evaluated from Equation 6.4.

 $^{^{\}mathbf{e}}$ Evaluated at the maximum current $\mathbf{i}_{\mathbf{m}}$.

 $^{^{\}rm f}$ Evaluated at the limiting current $^{\rm ii}_{\it L}$.

Table 6.2. Continued.

⁹From reference 117. Measured in 0.5 M HTFA.

 $^{\rm h}$ From reference 113. Measured in 0.05 M $_{\rm 2}$ SO $_{\rm 4}$.

ⁱFrom reference 148. Measured in 0.05 $^{\rm M}$ $^{\rm H}_2$ SO $_4$ at glassy carbon.

jEvaluated from the corresponding cyclic voltammogram.

 $^k\mathrm{From}$ reference 149 in which metal porphyrins employed are watersoluble. Measured in 0.05 M $\mathrm{H_2SO_4}$ at glassy carbon.

Estimated from the corresponding reference 117.

 $^{\mathrm{m}}$ The analysis of transfer coefficient was described in Chapter II.

ⁿEstimated from Figure 6.8 curve a.

is huge potential difference (300 - 400 mV) which is also observed by other authors. 146

4. Discussion

a. An Attempt to ASsign the Surface Redox Waves of the Attached Cobalt Porphyrins

For all the monomeric cobalt porphyrins examined, there is a surface redox wave appearing between +0.5 V and +0.75 V vs. SCE as shown in Figure 6.10. As for the dimeric cobalt porphyrins, there are two distinguishable surface redox waves appearing between +0.5 V and +0.75 V and between +0.2 V and +0.4 V vs. SCE as shown in Figures 6.11 to 6.13. In addition, the free base porphyrin-modified graphite surfaces gave no surface redox waves in 0.5 M HTFA solution. This indicates that the wave observed at the monomeric porphyrin-modified surfaces is not due to the redox reaction of the porphyrin rings. Therefore, it seems reasonable that the surface wave between +0.5 V and +0.75 V vs. SCE can be assigned to the $Co^{III/II}$ redox reaction of the monomers and the first Co^{III/II} redox reaction of the dimers. The redox potential of $Co^{II/I}$ redox reaction will clearly be more negative compared with that of Co^{III/II}. Then, the surface wave appearing between +0.2 V and +0.4 V vs. SCE can be attributed to the second Co^{III/II} redox reaction of the dimers. Collman and Anson¹¹⁷ also made a similar assignment, except they presumed that the first Co^{III/II} surface wave was beyond the limit of the graphite electrode. Thus, according to their presumption the first surface wave (between

+0.5 V and +0.75 V vs. SCE) observed in this work could be due to the oxidation of the porphyrin rings. However, from the measurement of the bulk redox potentials of these porphyrins, the oxidation potential of the porphyrin rings are more positive than those of Co^{III/II}.134,135 This is true for both monomers and dimers. Therefore, the assignment of the surface redox waves for the dimers as described above is still valid. The second surface redox wave of the dimers, however, lies at a similar potential region to that of the surface groups of the "blank" graphite surface. Nevertheless, the peak separation ($\Delta E_p \approx 125 \text{ mV}$) of the second surface redox wave of the dimers is much larger than that of the surface groups ($\Delta E_p \approx 75 \text{ mV}$) of the "blank" graphite surface. This can be attributed to the higher degree of the irreversibility of the second Co^III/II redox reaction of the dimer.

Because of the difficulty in the investigation of the relatively small concentration of the attached cobalt porphyrins in the aqueous solution, the redox potentials of the attached cobalt porphyrins have been assumed to be equivalent to those of the bulk porphyrin in nonaqueous solution in the diagnosis of the reaction mechanism of oxygen reduction at the porphyrin-modified surfaces. Since the environment of the bulk cobalt porphyrins in benzonitrile or dichloromethane solution is very different from that of the attached cobalt porphyrins in aqueous solution, the corresponding redox potentials of the bulk and the attached cobalt porphyrins can be expected to differ. Generally speaking, according to Table 6.1 surface attachment shifts the redox potential positive compared with that for the bulk complexes. This shift can be attributed to the difference in the

equilibrium constants of the precursor and successor states. However, the interaction between the attached cobalt porphyrins and the surface groups at the graphite surface is not fully understood. Furthermore, on the contrary to the bulk reactions, it is extremely difficult to characterize the intermediates of the surface reactions. Thus, the assignment of the surface redox waves as described could be ambiguous.

b. <u>Electrocatalysis of Oxygen Reduction at the Monomeric Por-</u> phyrin-Modified Graphite Surface

Figure 6.8 demonstrates that the electrocatalysis for oxygen reduction at the pyrolytic graphite surface can be improved tremendously by cobalt porphyrins. The improvement of the electrocatalysis can be most simply measured from the positive shift of the peak potential for oxygen reduction ($\Delta E = 500 \sim 600$ mV) using cyclic voltammetry, as mentioned before. In the practical application of fuel cell technology, 112 both the reaction potential (overpotential) and the corresponding current density are important factors determining the efficiency of a fuel cell. As described earlier, two possible pathways for oxygen reduction were examined. Furthermore, it has been shown that the electrocatalysts that yield two-electron reduction of dioxygen to hydrogen peroxide has a less practical application. Therefore, it is of interest to know whether the reaction pathway of oxygen reduction at the graphite surface which is two-electron reduction can be altered by the adsorbed cobalt porphyrins or not. Strictly speaking, the reaction pathway of oxygen reduction at the porphyrinmodified surfaces can be a combination of the two possible pathways. The contribution of each pathway to the overall reaction can be evaluated from the ratio of $-i_R/i_DN$ as shown in Table 6.2. The values of $-i_R/i_DN$ in Table 6.2 shows that for all the monomeric porphyrinmodified surfaces examined the percentage of the overall reaction of oxygen reduction at these surfaces that follows two-electron reduction can be as high as 70%. This implies that monomers are unable to alter entirely the reaction mechanism of oxygen reduction at the graphite surface.

The reaction mechanism of two-electron reduction of dioxygen to hydrogen peroxide at the monomeric porphyrin-modified surfaces has been proposed. The substantial improvement of the electrocatalysis of oxygen reduction can be attributed to the increase of active sites on the graphite surface by the adsorbed cobalt porphyrins that have great affinity for oxygen molecules. Oxygen reduction at the "blank" graphite surface has been shown to follow a similar mechanism to that of monomers. However, the surface groups at the graphite may have less affinity for oxygen molecules.

It is interesting to evaluate the effect of varying the structure of the porphyrin rings on the electrocatalysis of oxygen reduction. In general, according to the values of $-i_R/i_DN$ x 100% in Table 6.2, the reaction mechanism of oxygen reduction seems to be insensitive to the variation of the structure of the porphyrin rings. The electrocatalysis of oxygen reduction at these monomeric porphyrin-modified surfaces is not improved by the substitution of electron-withdrawing groups on the porphyrin rings. This is illustrated by the negative shift of the half-wave potential of oxygen reduction when the cobalt

porphyrin is changed from Co-OEP to Co-OEP-Cl_n where n = 1,2, or 4 or from Co-TPP to Co-TPPF₂₀. Because the affinity of the cobalt center for oxygen molecules could be diminished by the substitution of electron-withdrawing groups. Co-TPP-(p-OMe) that contains electron-donating substituents also yields less electrocatalysis of oxygen reduction than Co-TPP. This may be explained by the presence of the steric effect arising from the four methoxy substituents of Co-TPP-(p-OMe). The difference in electrocatalysis for oxygen reduction between Co-OEP and Co-Etio can also be interpreted by the steric effect arising from the eight ethyl groups of Co-OEP. However, the electrocatalysis for oxygen reduction of Co-TPP which is comparable to that of Co-Etio. This is opposite from what is expected from the steric effect arising from the four phenyl groups of Co-TPP. Nevertheless, the favorable surface redox potential of Co^{III/II} of Co-TPP as shown in Table 6.1 may compensate for the steric effect.

c. <u>Electrocatalysis of Oxygen Reduction at Dimeric Porphyrin-</u> Modified Graphite Surfaces

In the previous section, the monomeric cobalt porphyrins show enormous enhancements of the electrocatalysis of oxygen reduction. However, the monomers can only catalyze two-electron reduction. In order to facilitate the desirable four-electron oxygen reduction, the electrocatalysts may need two nuclear centers (i.e., two cobalts) to bind oxygen molecules simultaneously. Thus, each cobalt might be expected to yield two-electron reductions. In this study, three dimers, C_8 -Co-Co-S, slipped-Co-Co-S, and Co-Co-S were examined.

The ring-disk voltammograms of C_8 -Co-Co-5 and slipped-Co-Co-4, Figure 6.18 and 6.19, respectively, show significant ring current. Nevertheless, C_8 -Co-Co-5 shows better electrocatalysis in terms of the value of $-i_R/i_DN$ than slipped-Co-Co-4 and all the monomers as shown in Table 6.2. The value of $-i_R/i_DN$ of C_8 -Co-Co-5 is around 56% which implies that two- and four-electron reduction pathways contribute about equally to the overall reaction of oxygen reduction. Therefore, the reaction mechanism of oxygen reduction at the graphite surface still cannot be significantly changed by C_8 -Co-Co-5 and slipped-Co-Co-4. Furthermore, it has been shown that four-electron reduction of dioxygen to water is not due to the concerted reduction of hydrogen peroxide. In other words, C_8 -Co-Co-5 will not catalyze two-electron reduction of hydrogen peroxide to water.

However, the behavior of Co-Co-4 is drastically different from those of C₈-Co-Co-5 and slipped-Co-Co-4. The ring current of the ring-disk voltammogram of oxygen reduction of Co-Co-4 shown in Figure 6.20 is negligible compared with the disk current (< 10%). This strongly suggests that Co-Co-4 is able to catalyze greatly four-electron reduction of oxygen reduction of dioxygen to water. Similar results were reported by Collman and Anson¹¹⁷ with a related di-cobalt porphyrin. However, they obtained slightly better electrocatalysis of oxygen reduction in terms of the reduction potential than ours, which may be due to the higher steric effect of the dimer used in this work. They also proposed the reaction mechanism¹¹⁷ for four-electron reduction of dioxygen to water at the dimeric porphyrin-modified surfaces, which is slightly modified and shown in Figure 6.21. The possibility of forming a stable u-superoxo Co-O-O-Co

Figure 6.21 Proposed mechanism for four-electron reduction of oxygen molecule at the dimeric porphyrin-modified graphite surface

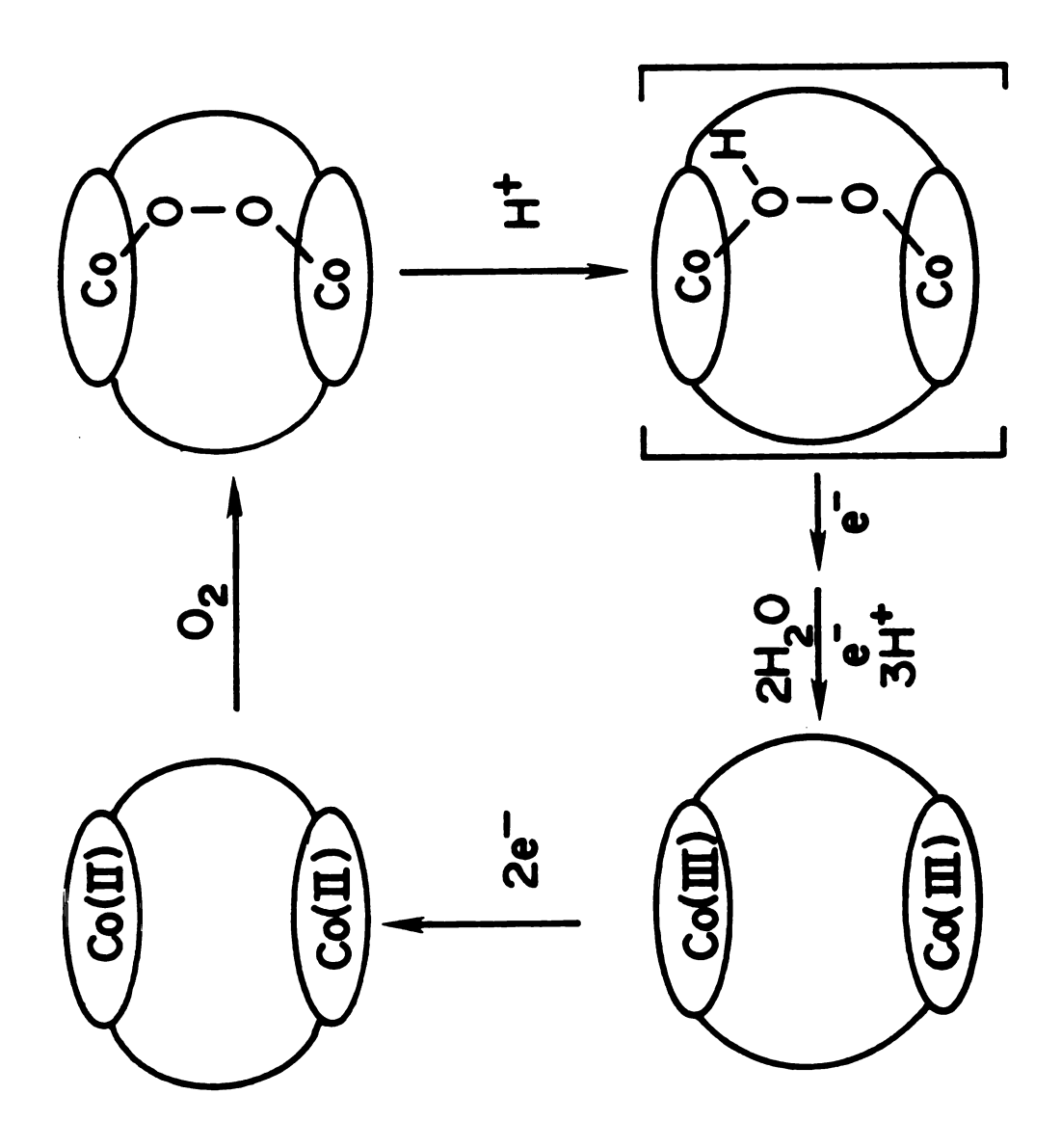


Figure 6.21

complex, which is the required intermediate of the proposed mechanism, has been illustrated by $Chang^{123}$ and $Collman^{117}$ from the study of EPR spectroscopy.

Compared with C_8 -Co-Co-5, the Co-Co distance of Co-Co-4 may be more suitable for binding oxygen molecules simultaneously. Then, this can be responsible for the higher electrocatalysis of Co-Co-4 for oxygen reduction. This is the same reason that slipped-Co-Co-4 has better electrocatalysis in terms of half-potential of oxygen reduction than C_8 -Co-Co-5.

Of these three dimers examined, the EPR spectra of the u-superoxo Co-O-O-Co complexes have been reported by Chang. 123,124 However, a careful comparison of the u-superoxo EPR spectra indicates that there is slight difference between them. Chang suggests that the spectra difference, although small, is indicative of the variation of the cobalt-oxygen bonding in the dimer. Considering the structure of these dicobalt porphyrins, Chang has proposed that the superoxo bridging ligand is bound in a "trans"-configuration in C_8 -Co-Co-5 and slipped-Co-Co-4 but "cis" in Co-Co-4 which are shown in Figure 6.22. To explain the unique electrocatalytic activity of Co-Co-4, perhaps the "cis"-peroxide, being more exposed to solvent, is more accessible to protonation and thus facilitate the cleavage of the stable peroxide bond. This model is consistent with the experimental results 138 as shown in Table 6.2, the electrocatalytic activity of Co-Co-4 for oxygen reduction is relatively larger than those of $C_{\rm R}\text{-}{\rm Co}\text{-}{\rm Co}\text{-}{\rm So}$ and slipped-Co-Co-4. Therefore, the cobalt-oxygen bonding is shown in the "cis"-configuration in Figure 6.21 instead of "trans"-configuration which was proposed by Collman and Anson.

Figure 6.22 Proposed configurations for Co-O-O-Co complexes

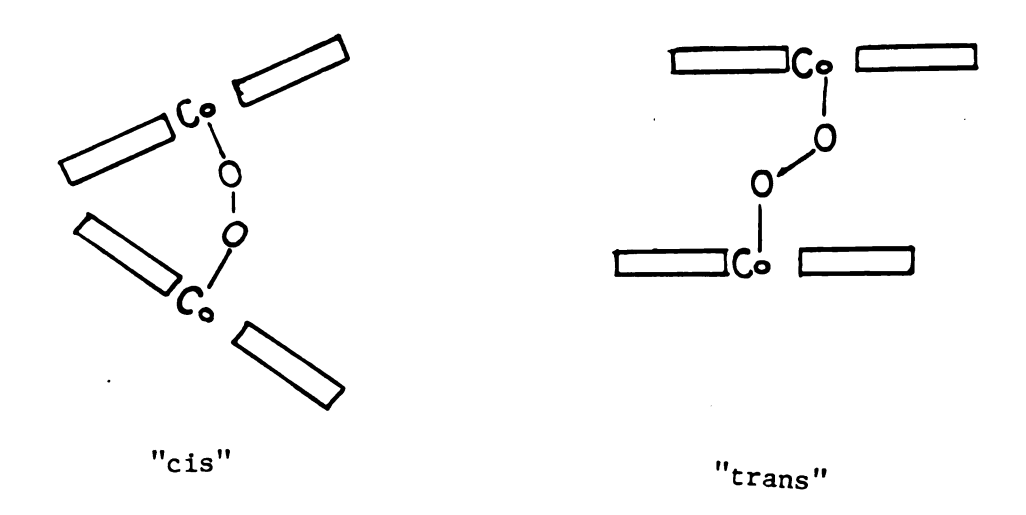


Figure 6.22

Furthermore, the small size of the cavity of slipped-Co-Co-4 make it difficult for oxygen molecules to enter, which may be responsible for the resulting small value of the ratio of $-i_R/i_DN$ compared with that of C_8 -Co-Co-5.

In addition, the proposed four-electron reduction mechanism presumes that the two cobalt centers need to be reduced before binding oxygen molecules to form the u-superoxo Co-O-O-Co complex. In this work, the surface redox potentials of Co^{III/II} of the attached dicobalt porphyrins as shown in Table 6.1 might provide important evidence for this presumption.

CHAPTER VII

CONCLUSIONS AND SUGGESTIONS FOR FUTURE WORK

1. Conclusions

The measurement of the specific adsorption of various anions at the lead-aqueous interface showed that the amount of the specifically adsorbed anions depended significantly on the electrode pretreatment. This could be explained by variations in the degree of the surface inhomogeneity of the polycrystalline lead which resulted from different pretreatments. Compared with mercury and polycrystalline silver surfaces, lead exhibited significantly less tendency to adsorb anions at a given electrode charge. This was probably due to the limitation of the active sites for the adsorption of anions at the lead surface. In addition, the values of the interaction parameter g evaluated from the Frumkin adsorption isotherm at lead surfaces were substantially higher (about one order of magnitude) than those at mercury surfaces. This difference was again attributed to the limitation of the active sites at the lead surface. The comparison of the values of ionic electrosorption valencies at lead and mercury surfaces suggests that the lead-aqueous interface had a thicker inner-layer than mercury, which was consistent with the estimated values of the inner-layer capacitance $(C_{M-2}^{Hg} > C_{M-2}^{Pb})$.

The most significant finding of the present work was to demonstrate a "specific substrate" effect on the energetics of a number of outer-sphere electron-transfer processes involving transition-metal reactants. There were significant differences in the measured rate constants for the electroreduction of a number of mechanistically

simple transition-metal complexes at gallium, polycrystalline lead, and mercury surfaces. These differences could not be accounted for by the conventional ionic double layer effect. For outer-sphere electrode reactions, this discrepency was somewhat unexpected, because there is no direct interaction between the reactant and the electrode surface in the transition state.

From the evaluation of the activation parameters for the electroreduction of several metal complexes, the resulting small or even negative values of the double-layer corrected activation entropies at the lead surface indicated the possibility of nonadiabatic electron-transfer processes. Furthermore, the Marcus theory was shown not to be adequate in the present case. On the other hand, the significant differences in the values of corrected activation enthalpies between lead and mercury surfaces suggested that there were nonelectrostatic work terms involved in bringing the reactant from the bulk to the transition state. Compared with mercury, the gallium surface showed less electroactivity for the electroreduction of Cr(III) aguo complexes than for ammine complexes. Since the water structure in the double layer region at the gallium surface significantly differed from that at mercury and lead surfaces, the water seemed likely to play a very important role in the energetics of electron-transfer at these electrodes.

Graphite is a very poor electrocatalyst for oxygen reduction.

Monomeric porphyrin-modified graphite surfaces dramatically enhance the electrocatalysis. However, they are only moderate electrocatalysts for the four-electron reduction to water. Modification

of the porphyrin structure by adding electron-withdrawing or electrondonating groups on the porphyrin ring had no significant influence on the electrocatalysis.

The dimeric porphyrins, with the exception of Co-Co-4, behaved similarly to the monomeric porphyrins. However Co-Co-4 is an efficient electrocatalyst for the four-electron reduction of dioxygen to water. Since the electroactivity of C_8 -Co-Co-5 was no worse than that of slipped-Co-Co-4, the Co-Co distance of Co-Co-4 therefore, is not the only factor making it unique. From EPR spectra, the configuration of the u-superoxo Co-0-Co, which is the required intermediate of the proposed mechanism, of Co-Co-4 was shown to differ from those of C-Co-Co-5 and slipped-Co-Co-4. The "cis" form of the Co-O-O-Co complex which is more exposed to solvent may be responsible for the better electrocatalysis by Co-Co-4. On the other hand, C_8 -Co-Co-5 and slipped-Co-Co-4 showed "trans" forms of the Co-O-O-Co complex. In addition, there was no direct correlation between the surface redox potentials of the attached cobalt porphyrins and the electroactivities of the corresponding modified surfaces for oxygen reduction.

2. Suggestions for Future Work

Some preliminary results, not reported in this thesis, of electrode kinetics for a number of Cr(III) complexes were obtained at lead-nonaqueous interfaces. The rate constants at lead surfaces corrected for ionic double layer effect were close to those at mercury surfaces. This differs from that observed in aqueous solution

as reported in the present work. This provides additional evidence that the "specific substrate" effect observed here may be due to the specific structure of solvent water between the reacting ions and the electrode surface. Therefore, it is worthwhile to evaluate activation parameters at lead and especially gallium surfaces in nonaqueous solutions. At the same time, it also would be of interest to study the isotopic effect of water as the solvent on electrode kinetics at lead- and gallium-aqueous interfaces.

It would be useful to find a simple metal complex which can adsorb detectably at lead. Then, the study of the corresponding electrode kinetics might provide insight regarding Franck-Condon barriers for elementary electron-transfer process at the lead surface.

Since each single-crystal face of a polycrystalline electrode may possess significantly different electroactivities, it would be very interesting to extend the present study to the single-crystal lead surfaces. However, it has been noted that lead single-crystals are very unstable. 86

Although cobalt porphyrins have been demonstrated to be remarkable electrocatalysts for oxygen reduction, their low stabilities at pyrolytic graphite surfaces in acidic solutions are the main drawback for their practical application. It has been noted that polymer coated graphite surfaces ¹²² showed no improvement in the stabilities of the attached cobalt porphyrins. However, further efforts in this direction may yet be fruitful. It clearly is necessary to improve the stabilities of the porphyrin-modified graphite surfaces. Furthermore, a better understanding of oxygen reduction mechanisms will greatly stimulate

the synthesis of more suitable metalloporphyrins for the electrocatalysis of oxygen reduction.



REFERENCES

- 1. H. Taube, "Electron Reaction of Complex Ions in Solution", Academic Press, New York, 1970.
- 2. N. Sutin, "Inorganic Biochemistry", G. L. Eickhorn, ed., Elsevier, New York, 1973, Chapter 19.
- 3. G. M. Brown and N. Sutin, J. Am. Chem. Soc., <u>101</u>, 883 (1979).
- B. S. Brunschwig, J. Logan, M. D. Newton, and N. Sutin, <u>J. Am.</u> Chem. Soc., <u>102</u>, 5798 (1980).
- 5. P. Sider and R. A. Marcus, J. Am. Chem. Soc., 103, 741 (1981).
- 6. N. Sutin, Acc. Chem. Res., 15, 275 (1982).
- 7. R. A. Narcus and N. Sutin, Inorg. Chem., 14, 213 (1975).
- 8. R. A. Marcus, Can. J. Chem., <u>37</u>, 155 (1959).
- 9. R. A. Marcus, <u>J. Chem. Phys.</u>, <u>43</u>, 679 (1965).
- T. T.-T. Li, M. J. Weaver, and C. H. Brubaker, Jr., J. Am. Chem. Soc., 104, 2381 (1982).
- (a) J. C. Curtis and T. J. Meyer, <u>Inorg. Chem.</u>, <u>21</u>, 1562 (1982).
 (b) K. Reider and H. Taube, J. Am. Chem. Soc., <u>99</u>, 7891 (1977).
- 12. J. Franck, Trans. Faraday Soc., <u>21</u>, 536 (1925).
- 13. E. U. Condon, Physic. Rev., <u>32</u>, 858 (1928).
- 14. S. W. Barr, K. Guyer, and M. J. Weaver, <u>J. Electroanal. Chem.</u>, <u>111</u>, 41 (1980).
- 15. M. Tamkin, Zh. fiz. Khim., 22, 1081 (1948).
- 16. B. E. Conway, "Theory and Principles of Electrode Processes", Ronald Press, New York, 1965, Chapter 6.
- 17. M. J. Weaver, <u>J. Phys. Chem.</u>, <u>80</u>, 2645 (1976).
- 18. For example, see (a) P. Delahay, "Double Layer and Electrode Kinetics", Interscience, New York, 1965, Chapter 7; (b) J. O'M. Bockris, A. K. N. Reddy, "Modern Electrochemistry", Plenum, New York, 1965, Volume 2, Chapter 8.

- 19. P. Delahay, "Double Layer and Electrode Kinetics", Interscience, New York, 1965, Chapter 2-6.
- 20. D. C. Grahame, J. Am. Chem. Soc., 76, 4816 (1954).
- 21. D. C. Grahame, J. Am. Chem. Soc., <u>79</u>, 2093 (1957).
- 22. N. B. Grigoryev, Dalk. Akad. Nauk SSSR., 229, 647 (1976).
- 23. U. V. Palm, M. P. Pyarnoya and N. B. Grigoryev, Sov. Electrochem., 13, 913 (1977).
- 24. L. A. Bgotskaya, B. B. Damaskin, and M. D. Levi, <u>J. Electroanal. Chem.</u>, <u>115</u>, 189 (1980).
- 25. M. D. Leiv, N. V. Fedorovich, and B. B. Damaskin, <u>Sov. Electro-Chem.</u>, <u>17</u>, 159 (1980).
- 26. For reviews, see (a) D. C. Grahame, Chem. Revs. 41, 441 (1947); (b) R. Parsons and M. A. V. Devanathan, Trans. Faraday Soc., 49, 404 (1953); (c) R. Parsons, "Modern Aspects of Electro-Chemistry", J. O'M. Bockris, ed., Volume 1, Butterworths, London, 1954, pp. 103-179.
- 27. G. Lippmann, Ann. Chim. Phys., (5)5, 494 (1857).
- 28. E. Dutkiewicz and R. Parsons, <u>J. Electroanal. Chem.</u>, <u>11</u>, 100 (1966).
- 29. H. D. Hurwitz, J. Electroanal. Chem., <u>10</u>, 35 (1965).
- 30. M. J. Weaver and F. C. Anson, <u>J. Electroanal. Chem.</u>, <u>65</u>, 7373 (1975).
- 31. R. A. Marcus, Ann. Rev. Phys. Chem., 15, 155 (1964).
- 32. M. J. Weaver and F. C. Anson, Inorg. Chem., 15, 1871 (1976).
- 33. M. J. Weaver and F. C. Anson, <u>J. Electroanal. Chem.</u>, <u>58</u>, 81 (1975).
- 34. R. Parsons, <u>Croat. Chem. Acta</u>, <u>42</u>, 281 (1970).
- 35. M. J. Weaver and F. C. Anson, <u>J. Electroanal. Chem.</u>, <u>65</u>, 711 (1975).
- 36. M. J. Weaver and F. C. Anson, <u>J. Electroanal. Chem.</u>, <u>58</u>, 95 (1975).
- 37. (a) A. N. Frumkin, Z. Physik. Chem., 164A, 121 (1933); (b) A. N. Frumkin, Z. Elektrochem., 59, 807 (1955); (c) A. N. Frumkin, in "Advance in Electrochemistry and Electrochemical Engineering", P. Delahay, ed., Interscience, New York, Volume 1, 1961, pp. 1-64.

- 38. S. Arrhenius, Z. Phys. Chem., (Leipzig) 4, 226 (1889).
- 39. E. L. Yee, R. J. Cave, K. L. Guyer, P. D. Tyma, and M. J. Weaver, J. Am. Chem. Soc., 101, 1131 (1979).
- 40. (a) J. N. Agar in "Advance in Electrochemistry and Electrochemical Engineering", P. Delahay, ed., Volume 3, Interscience, New York, 1963, Chapter 2; (b) A. J. deBethune, T. S. Licht, and N. Swendeman, J. Electrochem. Soc., 106, 616 (1959); A. J. deBethune, ibid., 107, 829 (1960); (c) G. Milazzo and J. Chanu, Z. Phys. Chem. (Frankfurt and Main), 68, 250 (1969).
- 41. Estimated from data given in Reference 40a and in G. P. Harnwell, "Principles of Electricity and Magnetism", McGraw-Hill, New York, 1939, p. 187.
- 42. R. A. Marcus, Electrochim. Acta, 13, 995 (1968).
- 43. M. J. Weaver, J. Israel Chem., <u>18</u>, 35 (1979).
- 44. M. J. Weaver, Inorg. Chem., <u>18</u>, 402 (1979).
- 45. M. J. Weaver, in "Inorganic Reactions and Methods", J. J. Zuckerman, ed., Verlag Chemie, 1982, in press.
- 46. M. J. Weaver and T. L. Satterberg, <u>J. Phys. Chem.</u>, <u>81</u>, 1772 (1977).
- 47. M. J. Weaver, J. Phys. Chem., 83, 1748 (1979).
- 48. B. E. Conway, H. Angerstein-Kozlowska, W. B. A. Sharp, and E. E. Criddle, Anal. Chem., 45, 1331 (1973).
- 49. M. Mori, Inorg. Synth., <u>5</u>, 132 (1954).
- 50. D. L. Gay and G. C. Lalor, J. Chem. Soc. A, 1179 (1966).
- 51. M. Linhard and W. Berthod, Z. Anorg. Chem., 279, 173 (1955).
- 52. E. L. King and E. B. Dismukes, <u>J. Am. Chem. Soc.</u>, <u>74</u>, 1674 (1952).
- 53. T. W. Swaddle and E. L. King, <u>Inorg. Chem.</u>, <u>3</u> 234 (1964).
- 54. N. Fogel, et al., <u>J. Am. Chem. Soc.</u>, <u>3</u>, 234 (1964).
- 55. R. S. Nicholson and I. Shain, <u>Anal. Chem.</u>, <u>36</u>, 706 (1964).
- 56. K. L. Guyer, Ph.D. Thesis, Department of Chemistry, Michigan State University, 1981.
- 57. (a) J. Koutecky, Collect. Czech. Chem. Comm., 18, 597 (1953); (b) J. Weber and J. Koutecky, 151d., 20, 980 (1955).

- 58. K. B. Oldham and E. P. Parry, <u>Anal. Chem.</u>, <u>40</u>, 65 (1968) and 38, 867 (1966).
- 59. F. Opekar and P. Beran, <u>J. Electroanal. Chem.</u>, <u>69</u>, 1 (1976).
- 60. J. E. B. Raudles, <u>Can. J. Chem.</u>, <u>37</u>, 238 (1959).
- 61. H. V. Malmstadt, C. G. Enke, and S. R. Crouch, in "Electronics and Instrumentation for Scientist", The Benjamin/Cummings Publishing, Inc., 1981, pp. 213.
- 62. Z. Galus, "Fundamentals of Electrochemical Analysis", E. Horwood, New York, 1976, p. 236.
- 63. K. V. Rybalka and D. I. Leikis, <u>Sov. Electrochem.</u>, <u>3</u>, 332 (1967).
- 64. A. Bewick and J. Robison, J. Electroanal. Chem., 60, 163 (1975).
- 65. J. P. Carr, N. A. Hampson, and R. Taylor, <u>J. Electroanal. Chem.</u>, <u>32</u>, 345 (1971).
- 66. "Comprehensive Treatise of Electrochemistry, I. The Double Layer", J. O'M. Bockris, et al., eds., Plenum Press, New York 1980.
- 67. A. N. Frumkin, <u>Z. Phys. Chem.</u>, <u>166</u>, 466 (1925).
- 68. B. B. Damaskin, Sov. <u>Electrochem.</u>, <u>7</u>, 776 (1971).
- 69. V. S. Krylov and V. A. Myamlin, <u>Sov. Electrochem.</u>, <u>13</u>, 174 (1977).
- 70. G. Valette, <u>J. Electroanal. Chem.</u>, <u>132</u>, 311 (1982).
- 71. A. G. Stromberg and N. P. Pikula, <u>Sov. Electrochem.</u>, <u>17</u>, 1177 (1981).
- 72. K. V. Rybalka and D. I. Leikis, <u>Sov. Electrochem.</u>, <u>3</u>, 1031 (1967).
- 73. J. W. Schultze and K. J. Vetter, <u>J. Electroanal. Chem.</u>, <u>44</u> 63 (1973).
- 74. D. Larkin, K. L. Guyer, J. T. Hupp, and M. J. Weaver, <u>J.</u> <u>Electroanal. Chem.</u>, <u>138</u>, 401 (1982).
- 75. D. M. Mohilner, "Electroanalytical Chemistry", Vol. 1, A. J. Bard, ed., Marcel Dekker, New York, 1966, p. 24.
- 76. D. M. Mohilner and P. R. Mohilner, <u>J. Electrochem. Soc.</u>, <u>115</u>, 261 (1968).

- 77. G. Valette, A. Homelin, and R. Parsons, <u>Z. Phys. Chem. N. F.</u>, 113, 71 (1978).
- 78. K. V. Rybalka, Sov. Electrochem., 8, 387 (1972).
- 79. Chapter 4 of Reference 66.
- 80. D. C. Henry, Philios Mag., 44, 689 (1920).
- 81. A. R. Sears and P. A. Lyons, J. Electroanal. Chem., 42, 69 (1973).
- 82. R. Payne, Trans. Faraday Soc., 64, 1638 (1968).
- 83. E. R. Gonzolez, J. Electroanal. Chem., <u>90</u>, 431 (1978).
- 84. S. Trasatti, J. Electroanal. Chem., <u>33</u>, 351 (1971).
- 85. S. Trasatti, in "Modern Aspects of Electrochemistry", Volume 13, J. O'M. Bockris, B. E. Conway eds., Butterworth, London.
- 86. L. P. Khmelevaya, A. V. Chizhov, and B. B. Damaskin, Sov. Electrochem., 14, 1304 (1978).
- 87. L. P. Khmelevaya, ibid., <u>16</u>, 222 (1980).
- 88. V. F. Ivanov and Z. N. Ushakova, ibid., 9, 753 (1973).
- 89. V. F. Ivanova, B. B. Damaskin, A. N. Frumkin, A. A. Ivashchenko, and N. I. Peshkova, ibid., 1, 239 (1965).
- 90. N. I. Melekhova, V. F. Ivanova, and B. B. Damaskin, <u>Ibid.</u>, <u>5</u>, 613 (1969).
- 91. V. F. Ivanov, N. I. Melekhova, and V. F. Khonina, <u>ibid.</u>, <u>8</u>, 886 (1972).
- 92. D. P. Alexandrova and D. I. Leikis, <u>ibid.</u>, <u>1</u>, No. 2 (1965).
- 93. S. Trasatti, J. Electroanal. Chem., <u>65</u>, 815 (1975).
- 94. A. K. Vijh, J. Phys. Chem., <u>78</u>, 2240 (1974).
- 95. D. J. Barclay, J. Electroanal. Chem., 19, 318 (1968).
- 96. D. J. Barclay, ibid., 28, 443 (1970).
- 97. S. Trasatti, <u>ibid.</u>, <u>123</u>, 121 (1981).
- 98. A. N. Frumkin, N. Polianouskaya, N. Grigoryev, and I. Bagotskaya, Electrochim. Acta., 10, 793 (1965).
- 99. S. Trasatti, <u>J. Electroanal. Chem.</u>, <u>64</u>, 128 (1975).

- 100. J. W. Schultze and K. J. Vetter, <u>J. Electroanal. Chem.</u>, <u>44</u>, 63 (1973).
- 101. N. V. Nikolaeva, N. S. Shapiro, and A. N. Frumkin, <u>Dokl. AN SSSR.</u>, <u>86</u>, 581 (1952).
- 102. N. V. Nikoleava, B. N. Rybalka, and K. A. Radyushkina, Sov. Electrochem., 3,967 (1967).
- 103. B. B. Damaskin and A. N. Frumkin, <u>Electrochim. Acta</u>, <u>19</u>, 173 (1974).
- 104. G. Valette and A. Hamelin, J. Electroanal. Chem., 45, 301 (1971).
- 105. W. R. Fawecett and S. Levine, ibid., <u>43</u>, 175 (1973).
- 106. M. J. Weaver, H. Y. Liu, and Y. Kim, <u>Can. J. Chem.</u>, <u>59</u>, 1944 (1981).
- 107. R. Parsons, J. Electroanal. Chem., 118, 3 (1981).
- 108. J. T. Hupp, D. Larkin, H. Y. Liu, and M. J. Weaver, <u>ibid.</u>, <u>131</u>, 299 (1982).
- 109. (a) R. N. Kestner, J. Logan, and J. Jortner, J. Phys. Chem., 78, 2148 (1974); (b) W. Kauzman, "Quantum Chemistry", Academic Press, New York, 1957, pp. 536-541.
- 110. Suggested by S. Bruckenstein.
- 111. J. P. Badiali, M. L. Rosinberg, and J. Goodisman, <u>J. Electro-anal. Chem.</u>, <u>130</u>, 31 (1973).
- 112. J. O'M Bockris and S. Srinivasan, "Fuel Cells Their Electro-chemistry", McGraw-Hill, New York, 1969, and references therein.
- 113. J. H. Zagal, R. K. Sen, and E. Yeager, <u>J. Electroanal. Chem.</u>, <u>3</u>, 207 (1977).
- 114. M. Savy, C. Bernard and G. Mayer, Electrochim. Acta, 20, 383 (1975).
- 115. M. Berzina, W. Khalil, J. Koryta, and M. Mugilova, <u>J. Electro-anal. Chem.</u>, <u>77</u>, 237 (1977).
- 116. A. P. Brown, C. K. Koval, and F. C. Anson, <u>ibid.</u>, <u>72</u>, 379 (1976).
- 117. J. P. Collman, P. Denisevich, Y. Konai, M. Marrocco, C. Koval, and F. C. Anson, J. Am. Chem. Soc., <u>102</u>, 6027 (1980).
- 118. K. Shigehara and F. C. Anson, <u>J. Electroanal. Chem.</u>, <u>132</u>, 107 (1982).

- 119. J. P. Radin, in "Comprehensive Treatise of Electrochemistry", J. O'M. Bockris et al., eds., Plenum, New York, Volume 4, 1980.
- 120. W. E. Blumberg and J. Peisach, in "Cytochrome Oxidase", T. E. King et al., eds., Elsevier, New York, 1979, pp. 153.
- 121. J. P. Collman, Acc. Chem. Res., <u>10</u>, 265 (1977).
- 122. J. P. Collman, et al., in "Organic Synthesis: Today and Tomorrow", W. B. Trost, ed., pp. 29-45.
- 123. C. K. Chang and C.-B. Wang in "Interaction between Ion and Proteins in Oxygen and Electron Transport", C. Ho ed., Elsevier North Holland, New York, Volume 2, 1982.
- 124. C. K. Chang. J. C. S. Chem. Comm., 800 (1977).
- 125. W. J. Albery and M. L. Hitchman, "Ring-Disc Electrode", Clarendon Press, Oxford, 1971.
- 126. W. J. Albery, Trans. Faraday Soc., <u>62</u>, 1915 (1966).
- 127. W. J. Albery and S. Bruckenstein, ibid., <u>62</u>, 1920 (1966).
- 128. V. G. Leich, "Physicochemical Hydrodynamics", Prentice-Hall, Inc., New York, 1962.
- 129. Depends on the adsorbability of cobalt porphyrin.
- 130. J. V. Hallum and H. V. Drushel, J. Phys. Chem., <u>62</u>, 110 (1958).
- 131. R. E. Panzer and P. J. Elving, Electrochim. Acta, <u>20</u>, 635 (1975).
- 132. F. Z. Sabirov and M. R. Tarasevich, Sov. Electrochem., 5, 564 (1969).
- 133. C. K. Koval, Ph.D. Thesis, Division of Chemistry and Chemical Engineering, California Institute of Technology, 1979.
- 134. J. H. Fuhrhop, K. M. Kadish, and D. G. Davis, <u>J. Am. Chem. Soc.</u>, <u>95</u>, 5140 (1973).
- 135. R. H. Felton and H. Linschitz, <u>J. Am. Chem. Soc.</u>, <u>88</u>, 1113 (1966).
- 136. For a recent review, see O. Popovych, "Treatise on Analytical Chemistry", I. M. Kolthoff and P. J. Elving eds., Part I, Volume 1, Wiley, New York, 1978.
- 137. A. P. Brown and F. C. Anson, Anal. Chem., 49, 1589 (1977).
- 138. H. Y. Liu, M. J. Weaver, C. B. Wang, and C. K. Chang, manuscript in preparation.

- 139. "The Handbook of Chemistry and Physics", 51th edition, The Chemical Rubber Co., Cleveland, Ohio, 1970, pp. F-4, F-36.
- 140. M. V. Stackelburg, M. Pilgrim, and V. Tooms, Z. Elektrochim., 57, 342 (1953).
- 141. K. Grubbin and R. Walker, J. Electroanal. Chem., 112, 469 (1965).
- 142. M. L. Marrocco, Ph.D. Thesis, Department of Chemistry, Stanford University, 1980.
- 143. D. G. Davis, in "The Porphyrins", Volume V, part C, D. Doliphin ed., Academic Press, New York, 1978.
- 144. A. Wolberg, Isr. J. Chem., <u>13</u>, 1031 (1970).
- 145. A. Wolberg and J. Marrassen, J. Am. Chem. Soc., <u>92</u>, 2982 (1970).
- 146. R. Durand and F. C. Anson, <u>J. Electroanal. Chem.</u>, <u>134</u>, 273 (1982).
- 147. P. Denisevich, Ph.D. Thesis, Department of Chemistry, Stanford University, 1979.
- 148. A. Bettelheim, R. Chan, and T. Kuwana, J. Electroanal. Chem., 110, 93 (1980).
- 149. T. Kuwana, M. Fujihira, K. Sunakewa, and T. Osa, J. <u>Electroanal</u>. Chem., <u>88</u>, 299 (1978).